UNIVERSITY OF CALIFORNIA SAN DIEGO

Photophysics of Organic Molecules under the Polariton regime

A dissertation submitted in partial satisfaction of the
requirements for the degree
Doctor of Philosophy

in

Chemistry

by

Luis Ángel Martínez Martínez

Committee in charge:

Professor Joel Yuen-Zhou, Chair
Professor Leonid Butov
Professor Misha Galperin
Professor Amitabha Sinha
Professor Akif Tezcan

2021

The dissertation of Luis Ángel Martínez Martínez is approved, and it is acceptable in quality and form for publication on microfilm and electronically.

University of California San Diego

2021

TABLE OF CONTENTS

Dissertation Approval Page iii

Table of Contents iv

List of Figures vi

List of Tables vii

Acknowledgements viii

Vita x

Abstract of the Dissertation xi

Chapter 1 Introduction 1
1.1 Summary of contents 4

Chapter 2 Theoretical Framework 7
2.1 Few mode approach to the electromagnetic field 7
2.2 Molecules in a confined EM environment 18
2.2.1 Molecular Hamiltonians 18
2.2.2 Interaction with an EM field 20

Chapter 3 Ground-State chemical reactions under the ultrastrong coupling regime . . 26
3.1 Introduction 26
3.2 Theoretical model 28
3.3 Results and discussion 39
3.3.1 Energetic effects 39
3.3.2 Effects on non-adiabatic dynamics 44
3.4 Conclusions 47

Chapter 4 Polariton-assisted Singlet Fission in Acene Aggregates 50
4.1 Introduction 50
4.2 Theoretical model 51
4.3 Discussion of results 56
4.4 Conclusions 61

Chapter 5 Triplet harvesting in the polaritonic regime: a variational polaron approach 63
5.1 Introduction 63
5.2 Theory 64
5.3 Dynamics in the polaron frame and definition of triplet electroluminescence efficiency 72

5.4 Results and discussion 75
5.5 The large N issue 82
5.6 Conclusions 85

Chapter 6 Conclusions 90

Bibliography 94

LIST OF FIGURES

Figure 1.1: Many molecules interacting with a photon mode. 3
Figure 1.2: Dark states scheme. 5

Figure 2.1: Pictorial representation of an organic Fabry-Perot resonator. 8

Figure 3.1: Model organic molecule: adiabatic PESs and transition dipole moment. . . 29
Figure 3.2: Plexciton setup. 30
Figure 3.3: Polariton dispersion and collective couplings. 33
Figure 3.4: PES energy correction and coherent concerted isomerization. 41
Figure 3.5: Energy profile of concerted global isomerization. 43

Figure 4.1: Acenes and dynamics under strong light-matter coupling. 53
Figure 4.2: Time evolution of populations in the singlet and TT electronic states. . . . 57
Figure 4.3: TT yield as a function of Rabi splitting and detuning. 58
Figure 4.4: TT yield of hypotetical molecule. 60

Figure 5.1: Scheme of polaron frame populations. 78
Figure 5.2: Triplet electroluminescence efficiency as a function of cavity detuning and Rabi splitting. 79
Figure 5.3: Partition of triplet electroluminescence efficiencies as a function of Rabi splitting. 80
Figure 5.4: Relative R-ISC rates from triplet manifold to polariton states. 83
Figure 5.5: Ideal scenario to maximize R-ISC. 86
Figure 5.6: Polaritonic R-ISC suppression due to delocalization. 89

LIST OF TABLES

Table 4.1: Summary of bare material-dependent parameters. 55

ACKNOWLEDGEMENTS

I thank my advisor, Professor Joel Yuen-Zhou for his support to carry out the research presented in this dissertation and his genuine interest on the intellectual and professional development of not only myself but all the members of the group. I would also like to thank the mentorship of Dr. Raphael Florentino Ribeiro, Dr. Roberto De J. León-Montiel and Dr. Zixuan Hu. Thank you all for sharing your knowledge and talent that led to many of the accomplishments presented in this dissertation. I am also grateful for Jorge Campos González Angulo, Matthew Du and Gerardo Soriano. Thank you for your helpful insights and friendship.

I acknowledge my parents, Angel Martinez and Araceli Martinez as you taught me that discipline and perseverance are key to reach one's self-proposed goals.

I am also grateful for Ilnett Uzi Garcia, my partner of many years. You have always been there for me when I needed advice and someone to talk to.

I also acknowledge the financial support from the Consejo Nacional de Ciencia y Tecnología and the University of California Institute for Mexico and the United States through scholarship with reference number 293319/410255.

Chapter 3, in full, is adapted from the material as it appears in "Can ultrastrong coupling change ground-state chemical reactions?" Martínez-Martínez L. A., Ribeiro R. F., Campos-González-Angulo J. and Yuen-Zhou J. ACS Photonics, 5, 167 (2018). The dissertation author was the primary investigator and author of this material.

Chapter 4, in full, is adapted from the material as it appears in "Polariton-Assisted Singlet Fission in Acene Aggregates" Martínez-Martínez L. A., Du M., Ribeiro R. F. and Yuen-Zhou J., J. Phys. Chem. Lett., 9, 1951 (2018). The dissertation author was the primary investigator and author of this material.

Chapter 5, in full, is adapted from the material as it appears in "Triplet harvesting in the polaritonic regime: A variational polaron approach" Martínez-Martínez L. A., Eizner E., Kéna-Cohen S. and Joel Yuen-Zhou, J. Chem. Phys., 151, 054106 (2019). The dissertation author

was the primary investigator and author of this material.

VITA

2013	B. Sc. in Chemistry *Mención Honorífica*, Universidad Nacional Autónoma de México
2013-2015	M. Sc. in Chemical Sciencies *Mención Honorífica,* Universidad Nacional Autónoma de México
2015-2016	Graduate Teaching Assistant, University of California San Diego
2021	Ph. D. in Chemistry, University of California San Diego

PUBLICATIONS

Polak D., Jayaprakash R., Lyons T. P., Martínez-Martínez L. A., Leventis A., Fallon K. J., Coulthard H., Bossanyi D. G., Georgiou K., Petty A. J., Anthony J., Bronstein H., Yuen-Zhou J., Tartakovskii A. I., Clark J., & Musser A. J. (2020) "Manipulating molecules with strong coupling: harvesting triplet excitons in organic exciton microcavities.", *Chemical Science, 11*(2), 343-354.

Martínez-Martínez L. A., Eizner E., Kéna-Cohen S. & Yuen-Zhou J., (2019) "Triplet harvesting in the polaritonic regime: A variational polaron approach"*, The Journal of Chemical Physics*, *151*(5), 054106.

Eizner E., Martínez-Martínez L. A., Yuen-Zhou J. & Kéna-Cohen S., (2019) "Inverting singlet and triplet excited states using strong light-matter coupling.", *Science advances, 5*(12), eaax4482.

Du M., Martínez-Martínez L. A., Ribeiro R. F., Hu Z., Menon V. M. & Yuen-Zhou J., (2018) "Theory for polariton-assisted remote energy transfer.", *Chemical science, 9*(32), 6659-6669.

Ribeiro R. F., Martínez-Martínez L. A., Du M., Campos-Gonzalez-Angulo J. & Yuen-Zhou J. (2018) "Polariton chemistry: controlling molecular dynamics with optical cavities.", *Chemical science, 9*(30), 6325-6339.

Martínez-Martínez L. A., Du M., Ribeiro R. F., Kéna-Cohen S. & Yuen-Zhou J., (2018) "Polariton-assisted singlet fission in acene aggregates.", *The Journal of Physical Chemistry Letters, 9*(8), 1951-1957.

Martínez-Martínez L. A. & Yuen-Zhou J., (2018) "Comment on 'Quantum theory of collective strong coupling of molecular vibrations with a microcavity mode."', *New Journal of Physics, 20*(1), 018002.

Martínez-Martínez L. A., Ribeiro R. F., Campos-González-Angulo J., & Yuen-Zhou J. (2017) "Can ultrastrong coupling change ground-state chemical reactions?", *ACS Photonics, 5*(1), 167-176.

Martínez-Martínez L. A., & Amador-Bedolla. (2017) "GPU algorithm for the scaled opposite-spin (SOS) MP2 energy evaluation.", *Journal of the Mexican Chemical Society, 61*(1), 60-66.

ABSTRACT OF THE DISSERTATION

Photophysics of Organic Molecules under the Polariton regime

by

Luis Ángel Martínez Martínez

Doctor of Philosophy in Chemistry

University of California San Diego, 2021

Professor Joel Yuen-Zhou, Chair

The advent of efficient light-confining platforms marked the burgeoning of the field of Cavity Quantum Electrodynamics (Cavity QED), which brought along the realization of exotic phenomena that emerges under extreme light-matter interaction regimes.

On the other hand, in chemistry, the interaction between light and matter is at the core of invaluable spectroscopic techniques and a number of photo-induced chemical processes. From a theoretical standpoint, light-matter interaction in those scenarios can be treated perturbatively, such that molecules and light preserve their individual identity. This picture breaks down when we consider one photonic mode interacting with molecules such that the energy of this interaction surpasses their respective linewidths. This so-called strong coupling (SC) regime has been

accomplished in microsetups which can sustain confinement comparable to the wavelength of light that promotes molecular excitations. Under the SC regime, the excitations sustained by the device are no longer of purely material character but rather exhibit a hybrid molecular and photonic nature, and are usually known as *polaritons*.

The recent observation of the slowing down of chemical reactions in the SC regime has incentivized communities of different backgrounds to converge in order to understand the range of possibilities the regime has to offer on the control of molecular processes.

In this dissertation, a combination of quantum optics and chemical rate theory is used to understand the emergent dynamics of molecules embedded in an strongly confined electromagnetic environment. More specifically, an analysis of the tunability of chemical reactivity of realistic polariton setups in the dark (*i.e.* in the absence of any driving source) is presented. Later on, it is shown that Singlet Fission and Reverse-Intersystem Crossing, two photophysical processes of technological relevance, represent an ideal testing ground to explore the rich dynamics afforded under the polariton regime. In the latter phenomena, special emphasis is cast upon the fleeting nature of the electromagnetic environment, as well as on its implications on the degree of control on molecular processes.

Chapter 1

Introduction

During the 1980s, the technological development of lasers and advances in our understanding of quantum theory introduced unprecedented theoretical perspectives on the leverage of coherent electromagnetic (EM) fields for the manipulation of molecular and atomic processes. The central notion behind the original proposals was to take advantage of the spatial and temporal coherence of the fields afforded by lasers to imprint their features on a material, that ultimately would lead, for instance, to coherently-enhanced photodissociation in molecules, adiabatic population transfer, and molecular deposition and alignment, just to name a few [1].

However, the realization of the numerous schemes proposed for control of molecules with coherent EM fields is hindered to a significant extent by the fact that the molecular and atomic systems are not isolated but rather their information content spreads continuously across their surroundings (decoherence) [1], such that the relative phase-information contained in matter and light (essential for the success of coherent control) can be short-lived, even at room temperature.

As it is usually the case, in the history of chemistry and physics, the emergence of new areas of research is closely related to the existence of technological platforms and/or experimental observations that call out for a confluence of researches of different backgrounds. Similarly to the case with lasers during the 1980s, a myriad of novel perspectives and observations for light-matter

interactions were possible during the 1990s and 2000s [2] due to the development of photonic devices that accomplish an efficient confinement of light within a spatial nanoscale. Those structures placed previously unattainable regimes of light-matter interaction within reach, without the need of very large EM amplitudes. The existence of these platforms, like microresonators that are generically denominated microcavities, has incentivized a deeper understanding of light-matter interaction, and as a result, new areas of research have emerged aiming to the control of a plethora of atomic and photonic phenomena.

Among the most striking phenomena that arises within these devices, we have the experimentally detectable consequences of the non-vanishing variance of EM fields (so-called quantum fluctuations) hosted in the latter, even in the absence of photons. Those manifest as an attractive force between the conducting planes that constitute the microcavity (Casimir-Polder effect) [3], but also can be used to generate photons out of the vacuum by means of non-adiabatic modulation of the spacing between the microcavity [4].

Other counterintuitive picture that can be accomplished by microcavities (and other platforms that allow strong confinement of EM fields) is the possibility to design devices where light can interchange energy with a material inside the resonator at a higher frequency than the one associated to the decay of the excited states of both entities. When this is the case, the usual physical picture of separate and independent identities of the material and light degrees of freedom breaks down, and the excitations sustained by these setups are of hybrid matter-light character, usually called *polaritons* [5].

Theoretical formulations of the aforementioned hybrid states date back to the 1950s and the experimental realization in atomic and solid-state cavity-polaritons ocurred in the 1980s and 1990s, respectively. Surprisingly, probably due to the decoherence problem faced by the coherent-control proponents during the 1980s, the exploration of chemical dynamics within confined EM fields was not a subject of interest until recent reports of modification of molecular photoisomerization rates with the aid of microcavities [6]. Further evidence of cavity-assisted

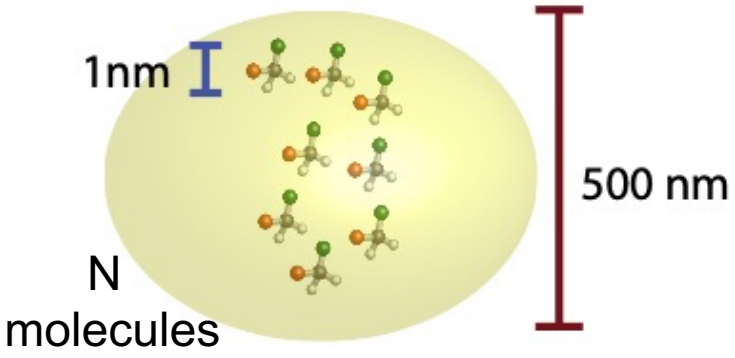

Figure 1.1: Cartoon that illustrates the difference in the spatial extent of molecules and a typical wavelength of the EM modes hosted in an optical microcavity.

modifications of molecular processes, such as nucleophilic substitution reactions [7], and long-range energy transfer [8, 9], ignited the interest of experimentalists and theorist alike.

Those observations revived the efforts of coherent control of molecules with the aid of EM fields [10], and prompted theorists to come up with models to account for the experimental results, as well as to explore the new avenues that these devices have yet to offer on molecular manipulation.

One of the key features of the experiments in organic polaritonic devices is that they afford the polariton regime by confining a macroscopic number of molecules in microcavities, which support EM modes with wavelengths that range usually from the IR to optical frequencies. The need of a large number of molecules can be understood based on the difference in length scales of molecules and the confined EM modes (see Fig. 1.1). This difference permit the latter to couple to a coherently enhanced dipole moment of the molecular ensemble, thus introducing Rabi oscillations between a (superradiant) matter state and a photonic one, whose frequency scales as the square root of the molecular concentration inside the effective volume of the EM mode [11]. Furthermore, the reduced density of photonic states on these platforms (for the case of a planar resonator, we can think of its supported photonic modes as a 2D boson gas) compared with a non-confined scenario, gives room to the feasibility of relatively long-lived Rabi oscillations.

Even though Agranovich and Litinskaya [12, 13] introduced the first works exploring the dynamics of polariton modes in organic microcavities; Galego et. al. [14, 15]and Herrera [16] proposed the first models to understand their implications on photochemical processes. The latter shed light on the collective nature of light-matter coupling and the role of delocalization of the molecular excitations to modify the potential energy surfaces associated to the process of interest.

However, one important drawback on those works is the absence of decoherence mechanisms that must be important for polariton setups, as light confined in these devices can be sustained for timescales as short as a few femtoseconds [17]. The latter is comparable (or even faster) that the timescales of photophysical processes themselves. In this dissertation, the previous facet of the polariton dynamics problem, is addressed.

Another issue that seems to preclude the tunability of cavity-assisted molecular processes is that the vast majority of the excitations hosted by an organic polariton device are of purely molecular character (see Fig. 5.15). Those can be understood as linear combinations of excited molecular states with a non-symmetric spatial permutational symmetry, which turns them into vanishing-dipole-moment states. Dark states may be populated as a result of vibrational relaxation of polariton modes [13], and given their high density of states with respect to the latter [18, 19, 9], the polaritonic excitations tend to be quickly depleted as dark states are entropically favored.

These issues call out for the models that specifically include the mentioned dissipative channels and that would shed light on strategies to mitigate their detrimental effects on molecular-processes manipulation.

1.1 Summary of contents

This dissertation is focused on the development of generic effective models to identify the most significant time and energy scales that come into play in the photophysics and chemical reactivity of organic molecules in highly confined EM environments. A special emphasis is

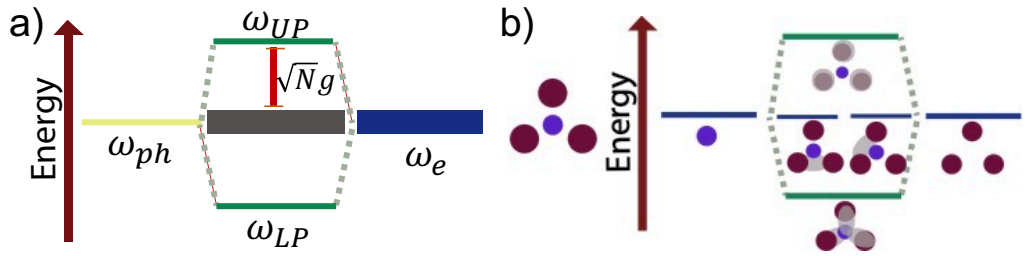

Figure 1.2: a) When a single photonic state interchanges amplitude with a dense manifold of (energy-disorder free) N molecular transitions (assuming N molecules, each treated as a two-level system) and for sufficiently large light-matter coupling strengths, we can spectrally resolve a single lower (upper) polariton with frequency ω_{LP} (ω_{UP}). The rest $N-1$ molecular states do not interchange amplitude with the photonic state, as they feature a vanishing dipole moment (in quantum optics literature, they are usually referred to as subradiant states). b) Dark states can be understood as the analogous of non-bonding orbitals that result from the formulation of symmetry-adapted linear combination of atomic orbitals in molecular orbital theory.

deposited on the dissipative mechanisms that compete with the molecular processes of interest. One of the main advantages of the developed models with respect to an *ab initio* approach is that the former allow an explicit treatment of a macroscopic ensemble of molecules. That is a consequence of the fact that only the most relevant degrees of freedom of realistic setups are included such that the essential physics of the dynamics is captured. Furthermore, this allows us to get an analytical insight of the degree of molecular control that polariton setups can offer.

Chapter 2 presents the general theoretical framework to model light-matter interaction when molecules are spatially confined within an (also spatially constrained) EM field. The most important approximations that permit a few-mode description of the photonic and molecular degrees of freedom are laid out.

Chapter 3 introduces the implications of the so-called ultrastrong coupling regime on chemical reactivity (more precisely, an isomerization processes) in the electronic ground state of organic molecules. The motivation of this exploration relies on the observation that for sufficiently high light-matter energy scales (comparable to that of a typical electronic molecular transition), the global ground state of the hybrid molecular-photonic system is no longer purely material but acquires a non-vanishing photonic character. In this chapter the implications of this dressing on

the isomerization process is discussed.

Chapter 4 elaborates on the importance of the dissipative nature of polariton modes afforded by SC when molecules that undergo the photochemical process known as singlet-fission (SF) [20] are employed. SF is of contemporary technological relevance as it has been shown to significantly enhance the efficiency of organic photovoltaic devices [21]. For that end, the toolkit of open-quantum-systems [22] was used to develop a kinetic model that reveals different kinetic pathways that are absent in a cavity-free scenario [19]. Furthermore, the insight shed by this approach allowed to propose ideal-candidate molecular features to boost SF under strong light-matter coupling (SC).

Chapter 5 follows a similar approach to the previous one, to get insight on the process known as Reverse-Intersystem-Crossing (RISC) under SC. In this photochemical process, an exciton of electronic triplet character undergoes a transition to a singlet-exciton as a result of spin-orbit coupling. RISC, in spite of being a very slow transition in organic materials, can be employed to harvest (non-luminescent) triplet excitons which subsequently transition into singlet excitons that emit light, before the former are lost as heat as a result of radiationless decay. Thus, this chapter explores the benefits of the SC regime for RISC, and strategies to circumvent the delocalized character of polariton modes. For that end, a generalization of a variational approach to the dynamics of open-quantum systems, previously used to describe multichromophoric exciton transport [23] and photoluminescence of polaritons [24], is developed and implemented numerically.

Finally, in Chapter 6 a general perspective of the accomplished results are presented, as well as the likely routes that can be followed to get further insight on the molecular dynamics under SC.

Chapter 2

Theoretical Framework

This chapter describes the theoretical foundations of this dissertation. Firstly, the electromagnetic field sustained by dielectric structures is cast in quantized form. Even though most of the chapters that follow rely on parameters that correspond to typical organic Fabry-Perot resonators (see Fig. 2.1), it is instructive to describe a general framework (valid for any linear isotropic dielectric platform) that introduces a distinction between what we denote as system photon modes (those that exhibit certain degree of confinement under the presence of dielectrics) and the rest of the universe (bath photon modes). The latter approach allows a few-mode approximation for the electromagnetic (EM) field, which is one of the basis for the effective coarse-grained models defined throughout this dissertation.

Later, the coupling of the confined electromagnetic modes with molecular degrees of freedom (DOFs) is introduced, as well as the most important approximations that permit the exploration of the emergent chemical dynamics in these setups.

2.1 Few mode approach to the electromagnetic field

One of the key ingredients to accomplish a strong interaction between light and matter is confinement of EM fields. In practice, this is achieved through a variety of platforms that

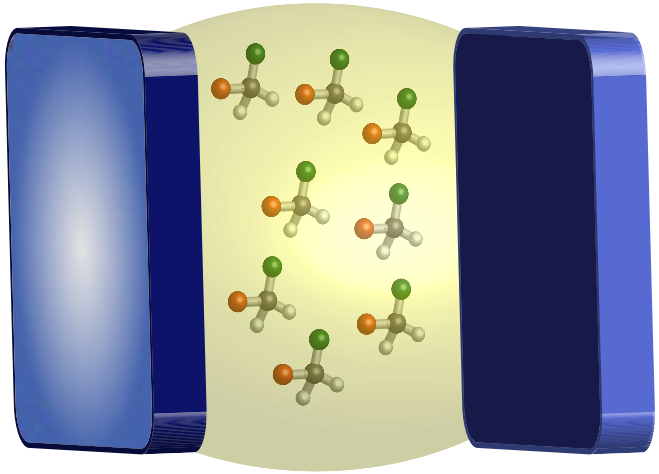

Figure 2.1: Pictorial representation of a molecular ensemble embedded in a Fabry-Perot resonator.

include, for instance, Fabry-Perot resonators and plasmonic nanostructures. Nowadays, devices that feature sharp resonances (*i.e.* with very small linewidths) in their scattering spectra are within reach [25, 17, 26]. When this is the case the system can be modeled as a set of EM modes supported by the device and weakly coupled to external ones. Nevertheless, for platforms operating at optical frequencies (which are the ones usually employed in the systems considered in this dissertation) it is usually the case that they exhibit broad resonances and/or overlapping modes, which precludes an straightforward choice of system modes [17]. Fortunately, this issue has been recently addressed in Ref. [27] and constitutes one of the basis (along Ref. [28]) for the framework outlined below.

Before proceeding to the quantum-mechanical formulation of EM fields, it is worthy to remark the salient analogies between the Maxwell and Schrödinger equations: their solutions feature oscillations in space and time, and in lossless media, they preserve energy. As pointed out in Ref. [29], all wave equations can be written abstractly as

$$\partial_t \mathbf{w} = \hat{D}\mathbf{w} + \mathbf{s} \tag{2.1}$$

where $\mathbf{w}$ is a vector field characterizing the solutions, $\hat{D}$ is a linear operator, and $\mathbf{s}$ is a vector source. The key property of $\hat{D}$ is that it is antihermitian (under a defined inner product), a trait from which follows the oscillatory characteristics of the solutions and energy conservation. To see this, we note that the harmonic mode solutions of Eq. (2.1) are of the form $\mathbf{w}(\mathbf{r},t) = \mathbf{W}(\mathbf{r})e^{-i\omega t}$, such that, in the absence of a source ($\mathbf{s} = \mathbf{0}$) we have

$$\omega\mathbf{W}(\mathbf{r}) = i\hat{D}\mathbf{W}$$

where, if $\hat{D}$ is antihermitian such that $(\mathbf{w}, \hat{D}\mathbf{w}') = (\hat{D}^{\dagger}\mathbf{w}, \mathbf{w}') = -(\hat{D}\mathbf{w}, \mathbf{w}')$, it follows that $i\hat{D}$ is a hermitian operator. The latter conclusion has the consequences that the eigenvalues ω are real (*i.e.* the solutions are lossless) and the harmonic solutions $\mathbf{W}$ constitute a complete basis.

To make the connection with electromagnetic theory, we note that the source-free Maxwell's equations in presence of matter (sometimes called macroscopic Maxwell equations)

$$\nabla \cdot \mathbf{D} = 0$$

$$\nabla \cdot \mathbf{B} = 0$$

$$\partial_t \mathbf{D} = \nabla \times \mathbf{H}$$

$$\partial_t \mathbf{B} = -\nabla \times \mathbf{E}$$

and assuming for simplicity an isotropic and linear dielectric media, such that the constitutive relations

$$\mathbf{D} = \varepsilon(\mathbf{r})\mathbf{E}$$

$$\mathbf{B} = \mu(\mathbf{r})\mathbf{H} = \mathbf{H}$$

are satisfied [$\varepsilon(\mathbf{r}), \mu(\mathbf{r})$ are the relative permittivity and magnetic permeability of the dielectric,

respectively. Hereafter, we will use $\hbar = c = 1$, unless stated otherwise]; can be written in the form

$$\partial_t \begin{bmatrix} \mathbf{E} \\ \mathbf{B} \end{bmatrix} = \begin{bmatrix} 0 & \frac{1}{\varepsilon}\nabla\times \\ -\frac{1}{\mu}\nabla\times & 0 \end{bmatrix} \begin{bmatrix} \mathbf{E} \\ \mathbf{B} \end{bmatrix} \tag{2.2}$$

$$= \hat{O} \begin{bmatrix} \mathbf{E} \\ \mathbf{B} \end{bmatrix} \tag{2.3}$$

We define the inner product as an integral over space at a fixed time ($\mathbf{w} = [\mathbf{E} \quad \mathbf{B}]$)

$$(\mathbf{w}, \mathbf{w}') = \frac{1}{2}\int d\mathbf{r}\left[\mathbf{E}^* \cdot (\varepsilon \mathbf{E}') + \mathbf{B}^* \cdot (\mu \mathbf{B}')\right]$$

and we can verify that $(\mathbf{w}, \hat{O}\mathbf{w}') = -(\hat{O}\mathbf{w}, \mathbf{w}')$. Thus, $i\hat{O}$ is a Hermitian operator, and the harmonic field solutions $\mathbf{w}(\mathbf{r}, t)$ are complete.

The quantization of the EM field is carried out by defining the vector potential, choosing a gauge and later promoting the canonical coordinates to operators. We have

$$\mathbf{B} = \nabla \times \mathbf{A}$$

$$\mathbf{E} = -\nabla\Phi - \partial_t \mathbf{A}$$

where Φ is the scalar potential. Under the absence of free-charges (such that $\Phi = 0$) the gauge can be chosen by requiring $\nabla \cdot [\varepsilon(\mathbf{r})\mathbf{A}] = 0$ which implies a transversality condition on $\mathbf{D}$ [$\nabla \cdot [\varepsilon(\mathbf{r})\partial_t \mathbf{A}] = 0$]. The equation of motion of the potential vector $\mathbf{A}$ is given by

$$\partial_t \mathbf{E} = \varepsilon(\mathbf{r})^{-1}\nabla \times \mathbf{B} = \varepsilon(\mathbf{r})^{-1}\nabla \times \nabla \times \mathbf{A} = -\partial_t^2 \mathbf{A} \implies \varepsilon(\mathbf{r})\partial_t^2 \mathbf{A} + \nabla \times \nabla \times \mathbf{A} = 0 \tag{2.4}$$

From here, we can derive a Lagrangian that reproduces the equation of motion (2.4) and by

carrying out a Legendre transformation of the former we arrive at the Hamiltonian

$$H = \frac{1}{2}\int d\mathbf{r}\left[\frac{\Pi(\mathbf{r},t)^2}{\varepsilon(\mathbf{r})} + (\nabla\times\mathbf{A})^2\right] \tag{2.5}$$

where the canonical momentum

$$\Pi(\mathbf{r},t) = -\mathbf{D}(\mathbf{r},t)$$

is directly related to the displacement field, rather than to the electric one. We can carry out an expansion of the vector potential

$$\mathbf{A}(t,\mathbf{r}) = \sum_k Q_k(t)\mathbf{f}_k(\mathbf{r}) \tag{2.6}$$

and similarly for

$$\Pi(\mathbf{r},t) = \sum_k P_k(t)\varepsilon(\mathbf{r})\mathbf{f}_k^*(\mathbf{r}) \tag{2.7}$$

in terms of vectors $\mathbf{f}_k(\mathbf{r})$ which satisfy

$$\varepsilon(\mathbf{r})\omega_k^2\mathbf{f}_k(\mathbf{r}) - \nabla\times\nabla\times\mathbf{f}_k(\mathbf{r}) = 0 \tag{2.8}$$

as well as $\nabla\cdot[\varepsilon(\mathbf{r})\mathbf{f}_k] = 0$, together with the boundary conditions required for the particular problem.

By introducing $\mathbf{f}_k(\mathbf{r}) = \varepsilon(\mathbf{r})^{-1/2}\mathbf{g}_k(\mathbf{r})$, we note that the previous equation can be cast in the form

$$\omega_k^2\mathbf{g}_k(\mathbf{r}) - \varepsilon(\mathbf{r})^{-1/2}\nabla\times[\nabla\times\varepsilon(\mathbf{r})^{-1/2}\mathbf{g}_k] = 0$$

and in view of the Hermiticity of the operator $\varepsilon(\mathbf{r})^{-1/2}\nabla\times\nabla\times\varepsilon(\mathbf{r})^{-1/2}$, $\{\mathbf{g}_k\}$ are orthonormal fields. It then follows that

$$(\mathbf{f}_k,\mathbf{f}_{k'}) = \int dr^3\varepsilon(\mathbf{r})\mathbf{f}_k^*\cdot\mathbf{f}_{k'} = \delta_{k,k'}. \tag{2.9}$$

Next, we have that by requiring the vector field $\mathbf{A}(t,\mathbf{r})$ to be hermitian (which is due to the

requirement of real magnetic and electric fields) the following must be satisfied

$$\sum_k Q_k \mathbf{f}_k = \sum_k Q_k^\dagger \mathbf{f}_k^*.$$

Introducing a projection on $\varepsilon(\mathbf{r})\mathbf{f}_m^*(\mathbf{r})$ on both sides of the equation and integrating over space, we obtain, by using Eq. (2.9):

$$\begin{aligned}\int dr^3 \varepsilon(\mathbf{r}) \sum_k Q_k \mathbf{f}_m^*(\mathbf{r}) \cdot \mathbf{f}_k(\mathbf{r}) = Q_m &= \sum_k Q_k^\dagger \int dr^3 \varepsilon(\mathbf{r}) \mathbf{f}_m^*(\mathbf{r}) \cdot \mathbf{f}_k^*(\mathbf{r}) \\ &= \sum_k Q_k^\dagger U_{k,m}^*. \end{aligned} \tag{2.10}$$

The matrix $U_{k,m}^*$ satisfies unitarity:

$$\begin{aligned}\sum_{k'} U_{k,k'} U_{k'',k'}^* &= \sum_{k'} \int dr^3 \int dr'^3 \varepsilon^*(r)\varepsilon(r') f_{k',\alpha}(r) f_{k',\beta}^*(r') f_{k,\alpha}(r) f_{k'',\beta}^*(r') \\ &= \int dr^3 \varepsilon^*(r) f_{k,\alpha}(r) f_{k'',\alpha}^*(r) = \delta_{k,k''}\end{aligned}$$

where $f_{n,\alpha}$ denotes the scalar αth component of $\mathbf{f}_n$ and used the Einstein summation convention. Furthermore, we have

$$\delta_{\alpha\beta}^\varepsilon(r,r') = \sum_k f_{k,\alpha}(r) f_{k,\beta}^*(r')$$

which can be though of as a completeness property for the subspace of transverse fields, since it satisfies

$$\begin{aligned}\int dr'^3 \varepsilon(r') \delta_{\alpha\beta}^\varepsilon(r,r') \mathbf{X}_\beta^T(r') &= \mathbf{X}_\alpha^T(r) \\ \int dr'^3 \varepsilon(r') \delta_{\alpha\beta}^\varepsilon(r,r') \mathbf{X}_\beta^L(r') &= 0\end{aligned}$$

$\mathbf{X}^T(r)$ ($\mathbf{X}^L$) being a transverse (longitudinal) vector field, i.e $\nabla \cdot \mathbf{X}^T(r) = 0$ ($\nabla \times \mathbf{X}^L = 0$). We can carry out the previous arguments developed for the vector field $\mathbf{A}$ and apply them to the transverse

electric field $\Pi(\mathbf{r},t)$ in Eq. (2.7) to conclude that

$$P_k^\dagger = \sum_{k'} P_{k'} U_{k'k}^*. \tag{2.11}$$

Importantly, the reason that explains why the matrix $U_{k,k'}^*$ appears in this generalized quantization approach for (linear) dielectric profiles and it is absent in the usual quantization approach in free space, is that in the former case, the harmonic mode fields$\mathbf{f}_k(r)$ are in general not orthonormal to their time-reversal counterparts $\mathbf{f}_{k'}^*(r)$, (in other words, harmonic mode fields with different boundary conditions are not necessarily orthonormal.)

Substitution of Equations (2.6) and (2.7), together with the relations (2.10) and (2.11) in the Hamiltonian (2.5) yields

$$H = \frac{1}{2}\sum_k (P_k^\dagger P_k + \omega_k^2 Q_k^\dagger Q_k)$$

where the Maxwell equations can be recovered from the Heisenberg equations of motion assuming that the usual commutation relations for the canonical variables P_k and Q_k are satisfied:

$$[Q_k, Q_{k'}] = [Q_k, Q_{k'}^\dagger] = [P_k, P_{k'}] = [P_k, P_{k'}^\dagger] = 0$$
$$[Q_k, P_{k'}] = i\hbar\delta_{k,k'}$$

with the important difference with respect to the free-space quantization procedure that

$$[Q_k, P_{k'}^\dagger] = i\hbar U_{k,k'}^*$$

However, this does not preclude the definition of a diagonal Hamiltonian in terms of creation and annihilation operators. By introducing bosonic ladder operators a_k, $a_k^\dagger$ that satisfy $[a_k, a_{k'}^\dagger] = \delta_{k,k'}$,

we have that the definitions

$$Q_k = \left(\frac{\hbar}{2\omega_k}\right)^{1/2}(a_k + \sum_{k'} U^*_{k,k'} a^\dagger_{k'})$$
$$P_k = i\left(\frac{\hbar\omega_k}{2}\right)^{1/2}(a^\dagger_k - \sum_{k'} U_{k,k'} a_{k'})$$

satisfy the relations (2.10) and (2.11):

$$\begin{aligned}\sum_k Q^\dagger_k U^*_{k,m} &= \sum_k \left(\frac{\hbar}{2\omega_k}\right)^{1/2}(a^\dagger_k U^*_{k,m} + \sum_{k'} U^*_{k,m} U_{k,k'} a_{k'}) \\ &= \left(\frac{\hbar}{2\omega_k}\right)^{1/2}\sum_\mu (a^\dagger_\mu U^*_{\mu,m} + \sum_{k'} U^*_{\mu,m} U_{\mu,k'} a_{k'}) \\ &= \left(\frac{\hbar}{2\omega_k}\right)^{1/2}(\sum_\mu a^\dagger_\mu U^*_{\mu,m} + a_m) \\ &= Q_m\end{aligned}$$

where in the first line we made use of the crucial observation that $U_{k,k'} \sim \delta_{k,k'}$ and therefore the index μ runs over the labels of the degenerate manifold at frequency ω_k. Therefore, the quantized form of Eq. (2.6) is given by

$$\mathbf{A}(t,\mathbf{r}) = \sum_k \left(\frac{\hbar}{2\omega_k}\right)^{1/2}[a_k \mathbf{f}_k + \text{h.c.}] \tag{2.12}$$

Which in integral form is given by (2.6)

$$\begin{aligned}\mathbf{A}(t,\mathbf{r}) &= \sum_m \int d\omega \hat{Q}_m(\omega,t)\mathbf{f}_m(\mathbf{r},\omega) \\ &= c\sum_m \int d\omega \left(\frac{\hbar}{2\omega}\right)^{1/2}[a_m(\omega)\mathbf{f}_m(\mathbf{r},\omega) + \text{h.c.}]\end{aligned}$$

where we added a label m to distinguish between the degenerate modes for a given frequency ω.

We also have that $[a_m(\omega), a^\dagger_{m'}(\omega')] = \delta_{m,m'}\delta(\omega-\omega')$, and $(\mathbf{f}_m(\omega), \mathbf{f}_{m'}(\omega')) = \delta_{m,m'}\delta(\omega-\omega')$.

Similarly, from Eq. (2.7) we have

$$\begin{aligned}\blacksquare(\mathbf{r},t) &= \sum_m \int d\omega P_m(\omega,t)\varepsilon(\mathbf{r})\mathbf{f}^*_m(\mathbf{r},\omega) \\ &= i\varepsilon(\mathbf{r})\sum_m \int d\omega \left(\frac{\hbar\omega}{2}\right)^{1/2} (a^\dagger_m(\omega)\mathbf{f}^*_m(\mathbf{r},\omega) - a_m(\omega)\mathbf{f}_m(\mathbf{r},\omega))\end{aligned}$$

Thus, by taking into account the continuum nature of the space of fields $\mathbf{f}_m(\mathbf{r},\omega)$, we rewrite the Hamiltonian in presence of a dielectric medium as

$$\begin{aligned}H_{rad} &= \frac{1}{2}\sum_m \int d\omega \left[\hat{P}^\dagger_m(\omega,t)\hat{P}_m(\omega,t) + \omega^2\hat{Q}^\dagger_m(\omega,t)\hat{Q}_m(\omega,t)\right] \\ &= \sum_m \int d\omega\omega a^\dagger_m(\omega)a_m(\omega) + \mathrm{C}\end{aligned} \tag{2.13}$$

What was outlined here is a formalism that quantizes the electromagnetic field in presence of dielectrics (for instance, mirrors when considering a microcavity). However, as pointed out at the beginning of this chapter, the models described later in this dissertation rely on a definition of EM modes confined spatially within a dielectric structure coupled to a photonic reservoir.

Ref. [27] introduces a powerful approach to perform the aforementioned partition, based on a Feshbach projection [27]on the harmonic modes $\mathbf{f}_m(\mathbf{r},\omega)$ introduced above, by defining an arbitrary system Λ_Q subspace. It is not an intend of this section to provide a detailed account on this approach, but for completeness, the main features of the procedure are summarized below, adopting for simplicity in the notation purposes, the correspondence $\mathbf{f}_m(\mathbf{r},\omega) \to |f_m(r,\omega)\rangle$ [*i.e.* ignoring the vectorial character of the field, and considering a one-dimensional scenario, whose generalization to three dimensions is straightforward]. Under this conditions, we can cast Eq. (2.8) into a Schrödinger-equation-like form

$$\left(-\frac{1}{2}\frac{\partial^2 f_m(r,\omega)}{\partial r^2}\right) + \frac{\omega_k^2}{2}\left[1-\varepsilon(r)\right] f_m(r,\omega) = H_M f_m(r,\omega) = \frac{\omega_k^2}{2} f_m(r,\omega) \tag{2.14}$$

where the potential $V = \frac{\omega_k^2}{2}[1-\varepsilon(r)]$ is frequency dependent and it is only non-zero for regions of space where permittivity is different from that of the vacuum. The close analogy between the stationary Schrödinger equation and the Maxwell-wave equation (2.14) hints the application of a Feshbach projection approach already developed for scattering problems [28] into the problem at hand.

The aforementioned projection scheme relies on the definition of operators P and Q that satisfy:

$$P^2 = P \qquad Q^2 = Q \qquad P+Q = 1$$

where Q corresponds to the projection on what we define as system subspace, and P to the bath subspace. In other words

$$Q = \sum_{\lambda \in \Lambda_Q} |\chi_\lambda\rangle\langle\chi_\lambda|$$

It is further required for the latter states to be eigenstates of the projected total Hamiltonian $H_{QQ} = QHQ$:

$$H_{QQ}|\chi_\lambda\rangle = E_\lambda|\chi_\lambda\rangle. \tag{2.15}$$

In analogy, the bath states as those that are the eigenstates of the Hamiltonian projected on the P subspace:

$$PHP|\psi_m(\omega)\rangle = H_{PP}|\psi_m(\omega)\rangle = E(\omega)|\psi_m(\omega)\rangle \tag{2.16}$$

Furthermore, since both H_{QQ} and H_{PP} are hermitian [under the inner product shown in Eq. (2.9)], their respective non-degenerate eigenstates are orthogonal. The full eigenmodes $f_m(r,\omega)$ of the Hamiltonian H_M can therefore be written as

$$\begin{aligned} |f_m(r,\omega)\rangle &= Q|f_m(r,\omega)\rangle + P|f_m(r,\omega)\rangle \\ &= \sum_{\lambda\in\Lambda_Q} \alpha_{\lambda m}(\omega)|\chi_\lambda\rangle + \sum_{m'} \int d\omega' \beta_{m,m'}(\omega,\omega')|\psi_{m'}(\omega')\rangle \end{aligned}$$

where $\alpha_{\lambda m}(\omega) = \langle \chi_\lambda | f_m(\omega) \rangle$, $\beta_{m,m'}(\omega,\omega') = \langle \psi_{m'}(\omega') | f_m(r,\omega) \rangle$. It can be shown that the hermiticity of H_M in addition to the requirements (2.15) and (2.16) are sufficient conditions to formulate the Hamiltonian of the EM field (2.13) in terms of the system and bath modes as [27]

$$
\begin{aligned}
H_{rad} &= \frac{1}{2}\sum_\lambda \left[P_\lambda^\dagger P_\lambda + \omega_\lambda^2 Q_\lambda^\dagger Q_\lambda \right] + \frac{1}{2}\sum_m \int d\omega \left[P_m^\dagger(\omega) P_m(\omega) + \omega^2 Q_m^\dagger(\omega) Q_m(\omega) \right] \\
&+ \frac{1}{2}\sum_m \sum_\lambda \int d\omega \left[W_{\lambda,m}(\omega) Q_\lambda^\dagger Q_m(\omega) + \text{h.c.} \right] \qquad (2.17) \\
&= \sum_\lambda \omega_\lambda a_\lambda a_\lambda^\dagger + \sum_m \int d\omega \omega b_m^\dagger(\omega) b_m(\omega) \qquad (2.18) \\
&+ \sum_m \sum_\lambda \int d\omega \frac{1}{2\sqrt{\omega_\lambda \omega}} \left[W_{\lambda,m}(\omega) a_\lambda^\dagger b_m(\omega) + V_{\lambda,m}(\omega) a_\lambda b_m(\omega) + \text{h.c.} \right] \qquad (2.19)
\end{aligned}
$$

where $W_{\lambda,m}(\omega) = \langle \chi_\lambda | H_M | \psi_m(\omega) \rangle$, $V_{\lambda,m}(\omega) = \langle \chi_\lambda^* | H_M | \psi_m(\omega) \rangle$, and a_λ [$b_m(\omega)$] is the annihilation operator for the λth system mode (the mth bath mode with frequency ω).

The matrix elements $W_{\lambda,m}(\omega)$, $V_{\lambda,m}(\omega)$ can be conveniently computed by following an orthogonalization procedure of the free-continuum to the Λ_Q subspace as discussed by Domcke [28]. The latter relies on the calculation of the modes $|\psi_m(\omega)\rangle$ as scattering eigenstate solutions of the Hamiltonian $H_{PP} = K_{PP} + V_{PP}$. The latter can be written as

$$
[E(k) - K_{PP}] \, |\psi_m(k)\rangle = V_{PP} |\psi_m(k)\rangle
$$

and its solutions are given by the Lippmann-Schwinger equation

$$
\begin{aligned}
|\psi_m(k)\rangle &= |k^{(\pm)}\rangle + [E(k) - K_{PP} \pm i\eta]^{-1} V_{PP} |\psi_m(k)\rangle \\
&= |k^{(\pm)}\rangle + \hat{G}_0^{(\pm)} V_{PP} |\psi_m(k)\rangle \qquad (2.20)
\end{aligned}
$$

where $K_{PP}|k^{(\pm)}\rangle = E(k)|k^{(\pm)}\rangle$. The calculation of $|\psi_m(k)\rangle$ is eased with the introduction of so-

called separable expansions for the potential $V_{PP} \approx \sum_{i,j} PV|y_i\rangle Y^{-1}_{i,j} \langle y_j|VP$, $Y_{i,j} = \langle y_i|V|y_j\rangle$, where $P|y_i\rangle = |y_i\rangle$, $Q|y_i\rangle = 0$, and becomes exact when the potential is of the form $V = \sum_{j=1}^{M} |y_j\rangle\langle y_j|$. The advantage of this expansion is that the integral problem (2.20) is rendered into an algebraic one:

$$\begin{aligned} V_n^{(m,k)} &= \langle y_n|V|k^{(\pm)}\rangle + \sum_j \left[\sum_i \langle y_n|V\hat{G}_0^{(\pm)}V|y_i\rangle Y^{-1}_{i,j}\right] V_j^{(m,k)} \\ &= \langle y_n|V|k^{(\pm)}\rangle + \sum_j G_{n,j} V_j^{(m,k)} \end{aligned}$$

where we can solve for $V_n^{(m,k)} = \langle y_n|V|\psi_m(k)\rangle$, once we compute the matrix elements $\langle y_n|V|k^{(\pm)}\rangle$ and $G_{n,j}$, which in turn can be conveniently calculated by solving for $K_{PP}|k^{(\pm)}\rangle = E(k)|k^{(\pm)}\rangle$.

2.2 Molecules in a confined EM environment

Having discussed a framework to formulate an EM environment in presence of dielectrics as a sum of a system and bath contributions, a brief account on the theoretical formulation of molecular DOFs is useful. For that end, a short summary of the approximations for the latter, which permit a coarse-grained formulation of the models used throughout this dissertation, is presented. Later, the scenario of molecules interacting with confined EM fields is addressed.

2.2.1 Molecular Hamiltonians

Considering a polyatomic molecule, the Hamiltonian operator of the latter has the general form [20]

$$H_{mol} = T_{el} + V_{el-nuc} + V_{el-el} + T_{nuc} + V_{nun-nuc} \tag{2.21}$$

where T_{el} (T_{nuc}) is the kinetic-energy operator for the electrons (nuclei). The Coulomb electron-electron, electron-nuclei and nuclei-nuclei interaction are included in V_{el-el}, V_{el-nuc} and $V_{nuc-nuc}$, respectively. The specific form of each term is unimportant for the purposes of this dissertation and can be found elsewhere [20].

On the other hand, the so-called Born-Oppenheimer approximation (BOA), which relies on the clear separation of time-scales of motion between electrons an nuclei, is of central relevance. Under this approximation, many-body electronic stationary solutions are changed adiabatically as a function of the nuclear coordinates, which allows us to have

$$|\psi_{a,M}(\mathbf{r};\mathbf{R})\rangle = X_{a,M}(\mathbf{R})\phi_a(\mathbf{r};\mathbf{R}) \qquad H_{mol}|\psi_{a,M}(\mathbf{r};\mathbf{R})\rangle = E_{a,M}|\psi_{a,M}(\mathbf{r};\mathbf{R})\rangle \tag{2.22}$$

where $\mathbf{r}(\mathbf{R})$ denotes the coordinates of all the electrons (nuclei) of the molecule. In Eq. (2.22) $X_{a,M}(\mathbf{R})$ are time-independent solutions of [20]

$$H_a(\mathbf{R})X_{a,M}(\mathbf{R}) = [T_{nuc} + U_a(\mathbf{R})]\, X_{a,M}(\mathbf{R}) = \mathcal{E}X_{a,M}(\mathbf{R}) \tag{2.23}$$

and $\phi_a(\mathbf{r};\mathbf{R})$ are solutions of the electronic Hamiltonian that features a parametric dependence on the nuclear coordinates $\mathbf{R}$:

$$H_{el}(\mathbf{R})\phi_a(\mathbf{r};\mathbf{R}) = [T_{el} + V_{el-nuc} + V_{el-el}]\, \phi_a(\mathbf{r};\mathbf{R}) = E_a(\mathbf{R})\phi_a(\mathbf{r};\mathbf{R}).$$

In Eq. (2.23) $U_a(\mathbf{R})$ is the effective potential generated by the mutual Coulomb interaction of the nuclei and the interaction of the latter with the electronic charge distribution corresponding to configuration $\mathbf{R}$. In other words, the stationary nuclear wavefunctions under the BOA correspond to the solutions of the time-independent Schrödinger Equation where the potential energy term is given by the Potential Energy Surfaces (PESs) $U_a(\mathbf{R})$. In general, it is possible to perform an harmonic approximation and normal mode analysis on the different PESs $U_a(\mathbf{R})$, which consists

on carrying out the expansion

$$U_a(\mathbf{R}) \approx U_a(\mathbf{R}^{(a)}) + \frac{1}{2}\sum_{m,n}^{3N_{nuc}} \kappa_{mn}^{(a)} \Delta R_m^{(a)} \Delta R_n^{(a)}$$

around the global minimum nuclear configuration $\mathbf{R}^{(a)}$, for small deviations $\Delta R_n^{(a)} = R_n^{(a)} - R_n$. The molecular Hamiltonian is thus given by

$$\begin{aligned} H_{mol} &\approx \sum_a \left[U_a(\mathbf{R}^{(a)}) + \hat{T}_{nuc} + \frac{1}{2}\sum_{m,n}^{3N_{nuc}} \kappa_{mn}^{(a)} \Delta R_m^{(a)} \Delta R_n^{(a)} \right] |\phi_a\rangle\langle\phi_a| \\ &= \sum_a \left[U_a(\mathbf{R}^{(a)}) + \frac{1}{2}\sum_{\mathcal{E}} \left(p_{a,\mathcal{E}}^2 + \omega_{a,\mathcal{E}}^2 q_{a,\mathcal{E}}^2 \right) \right] |\phi_a\rangle\langle\phi_a| \\ &= \sum_a H_a(\mathbf{q}_a) |\phi_a\rangle\langle\phi_a| \end{aligned} \tag{2.24}$$

where the second line is obtained after introducing a linear transformation

$$\Delta R_m^{(a)} = \sum_{\mathcal{E}} M_n^{-1/2} A_{n,\mathcal{E}}^{(a)} q_{a,\mathcal{E}},$$

that renders the vibrational Hamiltonian $H_a(\mathbf{R})$ in terms of the normal mode vibrational coordinates $q_{a,\mathcal{E}}$.

2.2.2 Interaction with an EM field

To account for the interaction of molecules with a confined EM environment, the coupling of charged particles (due to the electrons and nuclei of the former) to the latter, must be considered. The discussion that follows is based on Ref. [30].

In the discussion that follows it is worthy to point out that the quantization of the EM field outlined above was carried out within a macroscopic approach, as the microscopic details of the dielectric structure that permits the EM confinement is unimportant. On the other hand,

hereby the coupling between the molecules confined within a dielectric structure and the EM field sustained by the latter, is treated within a microscopic formalism.

Considering an ensemble of identical molecules confined within a dielectric structure like the one depicted in Fig. 2.1, the total Hamiltonian is given by [30]

$$H = \sum_i \frac{1}{2m_i}\left[\mathbf{p}_i - q_i\mathbf{A}(r_i)\right]^2 + \frac{1}{2}\sum_{i\neq j}\frac{q_i q_j}{|r_i - r_j|} + H_{rad} \tag{2.25}$$

$$= \sum_i \frac{1}{2m_i}\left[\mathbf{p}_i - q_i\mathbf{A}(r_i)\right]^2 + H_{rad} + \frac{1}{2}\sum_m \sum_{\alpha\neq\alpha'} \frac{q_{m,\alpha}q_{m,\alpha'}}{|\mathbf{r}_{m,\alpha} - \mathbf{r}_{m,\alpha'}|} + \frac{1}{2}\sum_{m\neq m'}\sum_{\alpha,\alpha'}\frac{q_{m,\alpha}q_{m',\alpha'}}{|\mathbf{r}_{m,\alpha} - \mathbf{r}_{m',\alpha'}|} \tag{2.26}$$

$$= \sum_i \frac{1}{2m_i}\left[\mathbf{p}_i - q_i\mathbf{A}(r_i)\right]^2 + H_{rad} + V_{intra} + V_{inter} \tag{2.27}$$

where $\mathbf{p}_i$, q_i, m_i and r_i denote the momentum, charge, mass and position of particle i; and H_{rad} is the EM Hamiltonian, taking into account the dielectric structure [see Eq. (2.17) for the one-dimensional version]. The material variables satisfy $[r_i^{(\alpha)}, r_j^{(\beta)}] = [p_i^{(\alpha)}, p_j^{(\beta)}] = 0$, $[r_i^{(\alpha)}, p_j^{(\beta)}] = i\delta_{i,j}\delta_{\alpha,\beta}$; $\alpha,\beta = x,y,z$. In the second line of Eq. (2.25) we carried out a partition of the Coulomb interaction between the charged particles that comprise the molecular ensemble, in terms of the individual identities of the molecules which are indexed by the m, m' labels. When this is introduced, an intra- and inter-molecular Coulomb interaction term can be identified.

In view of the partition of the EM modes described above, the vector potential features a system and a bath contribution:

$$\mathbf{A}(r) = \mathbf{A}_{sys}(r) + \mathbf{A}_{bath}(r)$$

$$\mathbf{A}_{sys}(r) = \sum_\lambda \sqrt{\frac{1}{2\omega_\lambda}}\left[a_\lambda \vec{\chi}_\lambda + \text{h.c.}\right]$$

$$\mathbf{A}_{bath}(r) = \sum_m \int d\omega \sqrt{\frac{1}{2\omega}}\left[b_m(\omega)\vec{\psi}_m(r,\omega) + \text{h.c.}\right]$$

where we conferred back the vectorial character to the partitioned EM field described in the section

above. We can partition the Hamiltonian (2.25) in a purely material, field and field-material part. The latter corresponds to

$$\begin{aligned} H_{int} &= \sum_i \frac{1}{2m_i}\left[-q_i\mathbf{p}_i\cdot\mathbf{A} - q_i\mathbf{A}\cdot\mathbf{p}_i + q_i^2\mathbf{A}^2\right] \\ &= \sum_i \frac{1}{2m_i}\left[-2q_i\mathbf{p}_i\cdot\mathbf{A} + q_i^2\mathbf{A}^2\right] \end{aligned}$$

where we used the fact that in the Coulomb gauge, which is the one considered here,

$$\begin{aligned} [\mathbf{p}\cdot\mathbf{A} - \mathbf{A}\cdot\mathbf{p}]\phi(\mathbf{r}) &= -i\hbar\nabla\cdot(\mathbf{A}\phi(\mathbf{r})) + i\hbar\mathbf{A}\cdot\nabla\phi(\mathbf{r}) \\ &= -i\hbar(\nabla\cdot\mathbf{A})\phi(\mathbf{r}) = 0 \end{aligned}$$

and it follows that $\mathbf{p}\cdot\mathbf{A} = \mathbf{A}\cdot\mathbf{p}$. H_{int} can be significantly simplified as a result of the partition of the vector field outlined in the section above. Depending on the platform on which the confinement of molecules and EM fields is carried out, it is possible, as an approximation, to choose a finite number of system modes and disregard the coupling of charges to the continuum of the bath [27], such that

$$H_{int} \approx \sum_i \frac{1}{2m_i}\left[-2q_i\mathbf{p}_i\cdot\mathbf{A}_{sys} + q_i^2\mathbf{A}_{sys}^2\right]$$

However, the interaction in terms of the vector potential is inconvenient given that optical experiments are given in terms of response to electrical fields. One way to represent the Hamiltonian in terms of the latter is accomplished by introducing a canonical transformation to the Hamiltonian $e^{iS}He^{-iS}$, where

$$\hat{S} = \int dr^3\hat{P}(r)\cdot\mathbf{A}_{sys}(r)$$

$\hat{P}(r)$ being the polarization field (which in classical EM theory corresponds to the induced average dipole moment per unit volume upon the application of an external electric field) and it is defined

according to

$$\hat{P}(r) = \sum_m \hat{P}_m(r)$$
$$\hat{\rho}_m(r) = \sum_\alpha q_{m\alpha}\delta(r - r_{m,\alpha}) = \rho_0(m,r) - \nabla\cdot\hat{P}_m(r) \qquad \rho_0(m,r) = \sum_\alpha q_{\alpha m}\delta(r - R_m)$$

where $\hat{\rho}_m(r)$ is the charge-density operator for molecule m, and $\rho_0(m,r)$ is the charge-density at the center of charge of the molecule, which for neutral molecules is zero.

In a quantum mechanical treatment, polarization can be framed in terms of the volume-averaged adiabatic current of a dielectric in response to a slow turning-on of an external perturbation. This current admits a multipolar expansion, and given the difference in length scales of the system EM modes $\overrightarrow{\chi}_\lambda(r)$ (which at optical frequencies it is of the order of 500 nm) and the size of molecules (in the order of tens of Angstroms), it is a good approximation to to keep only the dipole contributions to polarization:

$$\hat{P}_d(r) = \sum_m \mu_m \delta(\mathbf{r} - \mathbf{R}_m) \qquad \mu_m = \sum_\alpha q_{m,\alpha}\left(\hat{\mathbf{r}}_{m,\alpha} - \mathbf{R}_m\right)$$

Under the dipolar approximation, it can be shown [30] that the following relationships hold

$$e^{i\hat{S}}\mathbf{p}_{m,\alpha}e^{-i\hat{S}} = \mathbf{p}_{m,\alpha} - q_{m,\alpha}\mathbf{A}_{sys}(\overline{\mathbf{r}}_{m,\alpha})$$

$$e^{i\hat{S}}a_\lambda e^{-i\hat{S}} = a_\lambda - i\sqrt{\frac{1}{2\omega_\lambda}}\int dr^3 \hat{P}_d(r)\cdot\vec{\chi}_\lambda(r)$$

$$\begin{aligned} e^{i\hat{S}}\Pi_{sys}e^{-i\hat{S}} &= i\Pi_{sys} - \sum_\lambda \int dr^3 \hat{P}_d(r)\cdot\Re\left[\vec{\chi}_\lambda(r)^*\vec{\chi}_\lambda(r)\right] \\ &= \Pi_{sys} - \mathbf{P}^d_\perp \end{aligned}$$

where Π_{sys} and $\mathbf{P}_d$ are the system electric field and the dipolar polarization field operators,

respectively. Thus, the light-matter Hamiltonian upon this unitary transformation can be written as

$$e^{-i\hat{S}}He^{i\hat{S}} = \sum_{m,\alpha}\frac{1}{2m_{m,\alpha}}\mathbf{p}^2_{m,\alpha} + V_{intra} + V_{inter} + H'_{rad}$$

where

$$\begin{aligned}
H'_{rad} &= \frac{1}{2}\int dr^3\left[(\Pi_{sys}+\mathbf{P}^d_\perp(\mathbf{r}))^2+\mathbf{B}^2_{sys}\right] + H^{(B)}_{rad} + \\
&+\frac{1}{2}\sum_m\sum_\lambda\int d\omega\left[W_{\lambda,m}(\omega)Q^\dagger_\lambda Q_m(\omega)+\text{h.c.}\right] \\
&= \frac{1}{2}\int dr^3\left[\Pi^2_{sys}+\mathbf{B}^2_{sys}\right] + \int dr^3 c^{-1}\Pi_{sys}\cdot\mathbf{P}^d_\perp(\mathbf{r}) + \frac{1}{2}\int dr^3|\mathbf{P}^d_\perp|^2 + H^{(B)}_{rad} \\
&+\frac{1}{2}\sum_m\sum_\lambda\int d\omega\left[W_{\lambda,m}(\omega)Q^\dagger_\lambda Q_m(\omega)+\text{h.c.}\right],
\end{aligned}$$

$H^{(B)}_{rad}$ being the continuum photonic bath and its coupling to the system modes were also included [see Eq. (2.17)].

Finally, we can write the total Hamiltonian in this dipolar gauge as

$$\tilde{H} = H_{mol} + H_{mol-light} + H_{rad}$$

where

$$\begin{aligned}
H_{mol} &= \sum_{m,\alpha}\frac{1}{2m_{m,\alpha}}\mathbf{p}^2_{m,\alpha} + V_{inter} + V_{intra} \\
&= \sum_m H^{(m)}_{mol} + V_{inter}
\end{aligned}$$

$$H_{mol-light} = \int dr^3\Pi_{sys}\cdot\mathbf{P}^d_\perp(\mathbf{r}) + \frac{1}{2}\int dr^3|\mathbf{P}^d_\perp|^2 \tag{2.28}$$

and the field-dependent part of the Hamiltonian is given by

$$H_{rad} = \sum_{i=sys,bath} \int dr^3 \left[\Pi_i^2 + \mathbf{B}_i^2\right] + \frac{1}{2}\sum_m \sum_\lambda \int d\omega \left[W_{\lambda,m}(\omega) Q_\lambda^\dagger Q_m(\omega) + \text{h.c.}\right]$$

Further simplifications can be incorporated when we neglect the self-dipole coupling term $\frac{1}{2}\int dr^3 c^{-2} |\mathbf{P}_\perp^d|^2$ in Eq. (2.28), which is relevant for scenarios where retardation effects are important [31]. Furthermore, since this dissertation is focused on polariton platforms operating at optical frequencies (where the energy of electronic transitions of organic molecules with high oscillator strength lie) we can formulate the dipolar field in Eq. (2.28) in the electronic basis of the molecules that constitute the molecular ensemble [see Eq. (2.24)]: $\mu_m = \sum_{a\neq b} \left(\mu_{a,b}^{(m)} |\phi_a\rangle\langle\phi_b| + \text{h.c.}\right)$, (assuming a vanishing permanent dipole moment) to obtain

$$H_{mol-light} \approx \sum_\lambda \sum_m g_m^\lambda \sum_{a\neq b} \left(|\phi_a\rangle\langle\phi_b| + \text{h.c.}\right)\left(a_\lambda^\dagger - a_\lambda\right)$$

where $g_m^\lambda = i\left(\frac{\omega_\lambda}{2}\right)^{1/2}\left[\mu_{a,b}^{(m)} \cdot \overrightarrow{\chi}_\lambda(\mathbf{R}_m)\right] \overrightarrow{\chi}_\lambda(\mathbf{R}_m) \cdot \int dr^3 \overrightarrow{\chi}_\lambda(r) \approx i\left(\frac{\omega_\lambda}{2V}\right)^{1/2} \mu_{a,b}^{(m)} \cdot \mathbf{e}_\lambda$ ($\mathbf{e}_\lambda$ being the polarization vector of the λth system mode), is the single light-matter coupling. The scaling of the latter with $V^{-1/2}$, V being the volume spanned by the system modes $\overrightarrow{\chi}_\lambda \sim V^{-1/2}$, results after assuming that the length scales of the system electric field is such that it can be considered homogeneous from the molecular perspective: $\mu_{a,b}^{(m)} \cdot \overrightarrow{\chi}_\lambda(\mathbf{R}_m) \approx V^{-1/2} \mu_{a,b}^{(m)} \cdot \mathbf{e}_\lambda$; $\overrightarrow{\chi}_\lambda(\mathbf{R}_m) \cdot \int dr^3 \overrightarrow{\chi}_\lambda(r) \approx V^{-1} \int dr^3 = 1$.

Chapter 3

Ground-State chemical reactions under the ultrastrong coupling regime

3.1 Introduction

As introduced in Chapter 1, the advent of nano- and microstructures which enable strong confinement of electromagnetic fields in volumes as small as $1 \times 10^{-7}\lambda^3$ [32], λ being a characteristic optical wavelength, allows for the possibility of tuning light-matter interactions that can "dress" molecular degrees of freedom and give rise to novel molecular functionalities. Several recent studies have considered the effects of strong coupling (SC) between confined light and molecular states, and its applications in exciton harvesting and transport [33, 34], charge transfer [16] and Bose-Einstein condensation [35, 36, 37] among many others.

Organic dye molecules are good candidates to explore SC effects due to their unusually large transition dipole moment [38, 39, 40, 41]. The underlying reason for these effects is that the SC energy scale is comparable to that of vibrational and electronic degrees of freedom, as well as the coupling between them [14]; this energetic interplay nontrivially alters the resulting energetic spectrum and dynamics of the molecule-cavity system. It is important to emphasize that in these

examples, SC is the result of a collective coupling between a single photonic mode and $N \gg 1$ molecules; single-molecule SC coupling is an important frontier of current research [42], but our emphasis in this chapter, and most of this dissertation, will be on the N molecule case. Since the energy scale of this collective coupling is larger than the molecular and photonic linewidths, the resulting eigenstates of the system have a mixed photon-matter character.

While prospects of photochemical control seem promising, it is still a relatively unexplored question whether ground-state chemical reactivity can be altered via polaritonic methods, although recently, George and coworkers have shown a proof of concept of such feasibility using vibrational SC [7].

Along this line, ultrastrong coupling regime (USC) seems to also provide the conditions to tune the electronic ground-state energy landscape of molecules and in turn, modify not only photochemistry, but ground-state chemical reactivity. Roughly speaking, this regime is reached when $\Omega/\hbar\omega_0 \geq 0.1$, Ω being the (collective) SC of the emitter ensemble to the electromagnetic field and $\hbar\omega_0$ the energy gap of the molecular transition [43]. Under USC, the “nonrotating" terms of the light-matter Hamiltonian acquire relevance and give rise to striking phenomena such as the dynamical Casimir effect [4, 44]and Hawking radiation in condensed matter systems [44]. Furthermore, recent experimental advances have rendered the USC regime feasible in circuit QED [45], and molecular systems [46, 47], thus prompting us to explore USC effects on ground-state chemical reactivity.

In this chapter, we address how this reactivity can be influenced in the USC by studying a reactive model system consisting of an ensemble of thiacyanine molecules strongly coupled to the plasmonic field afforded by a metal, where each of the molecules can undergo cis-trans isomerization by torsional motion. The theoretical model for the photochemistry of the single thiacyanine molecule has been previously studied in the context of coherent control [48]. As we will show, the prospects of controlling ground-state chemical reactivity or nonadiabatic dynamics involving the ground state are not promising for this particular model, given that the alterations of

the corresponding PES are negligible on a per-molecule basis. However, we notice the existence of salient quantum-coherent features associated with concerted reactions that might be worth considering in models featuring lower kinetic barriers.

3.2 Theoretical model

To begin with, we consider a thiacyanine derivative molecule (Fig. 3.1c) and approximate its electronic degrees of freedom as a quantum mechanical two-level system. To keep the model tractable, this electronic system is coupled to only one vibrational degree of freedom R, namely, the torsion along the bridge of the molecule (Fig. 3.1c) along which cis-trans isomerization occurs. The mathematical description of the PES of the ground and excited states (Fig. 3.1a) as well as the transition dipole moment as a function of the reaction coordinate (Fig. 3.1b) have been obtained from Ref. [48]. The adiabatic representation of the electronic states is given by,

$$\begin{aligned} |g(R)\rangle &= \cos\left[\theta(R)/2\right]|\text{trans}\rangle + \sin\left[\theta(R)/2\right]|\text{cis}\rangle \\ |e(R)\rangle &= -\sin\left[\theta(R)/2\right]|\text{trans}\rangle + \cos\left[\theta(R)/2\right]|\text{cis}\rangle \end{aligned} \tag{3.1}$$

where $|e(R)\rangle$ and $|g(R)\rangle$ are the R-dependent adiabatic excited and ground state respectively. $|\text{trans}\rangle$ and $|\text{cis}\rangle$ are the (R-independent) crude diabatic electronic states that describe the localized chemical character of each of the isomers. The ground-state PES has a predominant trans (cis) character to the left (right) of the barrier ($\theta(0) = 0$, $\theta(\pi) = \pi$) in Fig. 3.1a.

Our USC model consists of a setup where an orthorhombic ensemble of thyacyanine molecules is placed on top of a thin spacer which, in turn, is on top of a metallic surface that hosts surface plasmons (SPs) [49] (see Fig. 3.2). The coupling between molecular electronic transitions and plasmons in the metal give rise to polaritons that are often called plexcitons [50, 49]. The

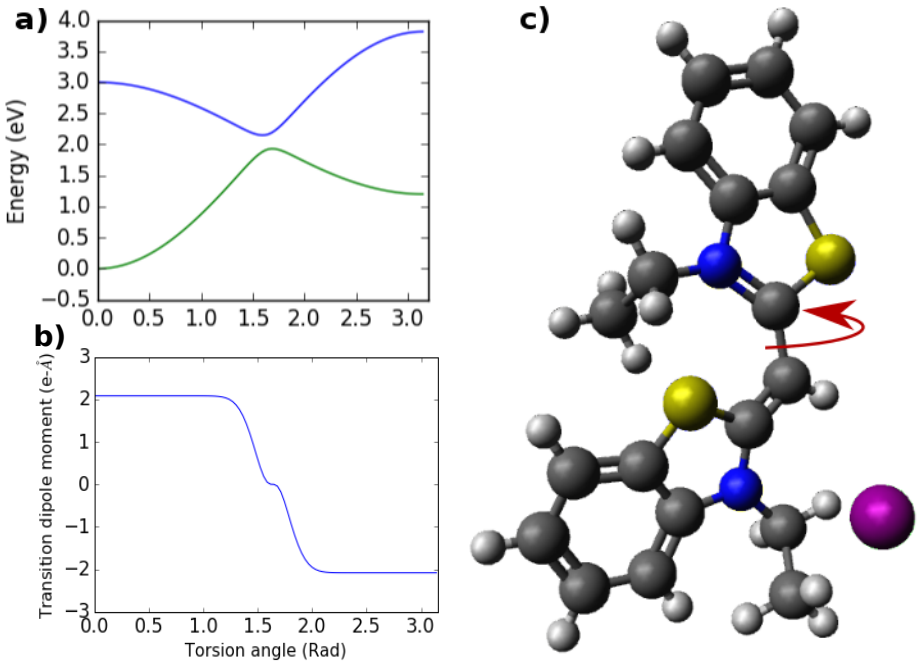

Figure 3.1: a) Adiabatic potential energy surfaces (PESs) of the ground and first excited electronic states of the thyacynine-like model molecule. b) Transition dipole moment ($\mu(R)$) of the model molecule in the adiabatic basis. c) Thiacynine molecule. There exist two geometrical isomers of the molecule, a cis- and a trans-like configuration. The cis-trans isomerization of thiacynine-like molecules occurs via a photo-induced torsion along the bridge which connects the aromatic rings.

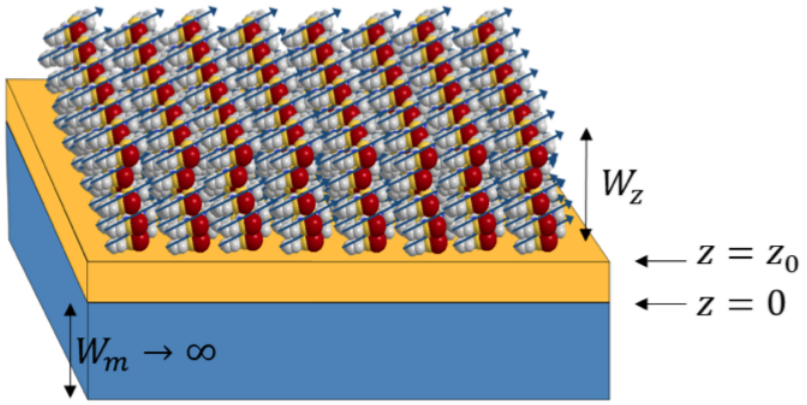

Figure 3.2: *Plexciton setup.* The model consists of a surface-plasmon (SP) metal layer whose width W_m can be considered infinite in comparison with the relevant length scales of the structure. The thiacynine molecular ensemble is separated from the metallic surface by a spacer of width z_0; the balls and sticks represent the molecules, while the arrows denote their transition dipole moments. The molecular layer has a height W_z and is extended along the x and y planes.

ensemble is comprised of N_z single-molecule layers. The location of each molecule can be defined by the Cartesian coordinates $\mathbf{n} + (0,0,z_s)$ where $\mathbf{n} = (\Delta_x n_x, \Delta_y n_y, 0)$ and $z_s = z_0 + \Delta_z s$ for the s-th layer. Here, the spacing between molecules along the i-th direction is denoted by Δ_i, and z_0 is the width of the spacer (see Fig. 3.2). The Hamiltonian of the plexciton setup is given by $H = H_{el} + T_{nuc}$, where $T_{nuc} = \sum_i \frac{\mathbf{P}_i^2}{2M_i}$ is the nuclear kinetic energy operator and

$$\begin{aligned} H_{el}(\mathbf{R}) = &\sum_{\mathbf{k}} \hbar\omega_{\mathbf{k}} a_{\mathbf{k}}^\dagger a_{\mathbf{k}} + \sum_{\mathbf{n},s} \left(\hbar\omega_e(R_{\mathbf{n},s}) - \hbar\omega_g(R_{\mathbf{n},s})\right) b_{\mathbf{n},s}^\dagger(R_{\mathbf{n},s}) b_{\mathbf{n},s}(R_{\mathbf{n},s}) \\ &+ \sum_{\mathbf{k}} \sum_{\mathbf{n},s} g_{\mathbf{k}}^{\mathbf{n},s}(R_{\mathbf{n},s}) \left(a_{\mathbf{k}}^\dagger b_{\mathbf{n},s}(R_{\mathbf{n},s}) + a_{\mathbf{k}} b_{\mathbf{n},s}^\dagger(R_{\mathbf{n},s}) + a_{\mathbf{k}} b_{\mathbf{n},s}(R_{\mathbf{n},s}) + a_{\mathbf{k}}^\dagger b_{\mathbf{n},s}^\dagger(R_{\mathbf{n},s}) \right) \\ &+ \sum_{\mathbf{n},s} \hbar\omega_g(R_{\mathbf{n},s}), \end{aligned} \tag{3.2}$$

corresponds to the Dicke Hamiltonian [51]. Here $a_{\mathbf{k}}^\dagger$ ($a_{\mathbf{k}}$) is the creation (annihilation) operator for the SP mode with in-plane momentum $\mathbf{k}$ which satisfies $[a_{\mathbf{k}}, a_{\mathbf{k}'}^\dagger] = \delta_{\mathbf{k},\mathbf{k}'}$, and $\mathbf{R} = \{R_{\mathbf{n}s}\}$ is an N-dimensional vector that describes the vibrational coordinates of the $N = N_x N_y N_z$ molecules of the ensemble, where N_i is the number of molecules along each ensemble axis. $\hbar\omega_g(R_{\mathbf{n},s})$

accounts for the ground-state energy of the molecule whose location in the ensemble is defined by $\mathbf{n}$ and s. We introduce the (adiabatic R-dependent) exciton operator $b^{\dagger}_{\mathbf{n},s}(R_{\mathbf{n},s})\,(b_{\mathbf{n},s}(R_{\mathbf{n},s}))$ to label the creation (annihilation) of a Frenkel exciton (electronic excitation) with an energy gap $\hbar\omega_e(R_{\mathbf{n},s}) - \hbar\omega_g(R_{\mathbf{n},s})$ on the molecule located at $\mathbf{n} + z_s\hat{\mathbf{z}}$. The coefficients $\hbar\omega_{\mathbf{k}}$ and $g^{\mathbf{n},s}_{\mathbf{k}}(R_{\mathbf{n},s})$ stand for the energy of a SP with in-plane momentum $\mathbf{k}$ and the coupling of the molecule located at $\mathbf{n} + z_s\hat{\mathbf{z}}$ with the latter, respectively. The dipolar SP-matter interaction is described by $g^{\mathbf{n},s}_{\mathbf{k}}(R_{\mathbf{n},s}) = h_{\mathbf{k}}(R_{\mathbf{n},s})f_{\mathbf{k}}(z_s)$, where $h_{\mathbf{k}}(R_{\mathbf{n},s}) = -\mu_{\mathbf{n},s}(R_{\mathbf{n},s})\cdot\mathbf{E}_{\mathbf{k}}(\mathbf{n})$ is the projection of the molecular transition dipole $\mu_{\mathbf{n},s}(R_{\mathbf{n},s})$ onto the in-plane component of the SP electric field $\mathbf{E}_{\mathbf{k}}(\mathbf{n})$ and $f_{\mathbf{k}}(z_s) = e^{-\eta_{\mathbf{k}}z_s}$ is the evanescent field profile along the z direction, with $\eta_{\mathbf{k}}$ being the decay constant in the molecular region ($z > 0$). The quantized plasmonic field $\hat{\mathbf{E}}_{\mathbf{k}}f_{\mathbf{k}}(\mathbf{z}_s)$ has been discussed in previous works [50, 49, 52] and reads $\hat{\mathbf{E}}_{\mathbf{k}}(\mathbf{n})f_{\mathbf{k}}(\mathbf{z}_s) = \sqrt{\frac{\hbar\omega_{\mathbf{k}}}{2\varepsilon_0 S L_{\mathbf{k}}}}a_{\mathbf{k}}\hat{\chi}_{\mathbf{k}}e^{i\mathbf{k}\cdot\mathbf{n}}e^{-\eta_{\mathbf{k}}z} + h.c.$ where ε_0 is the free-space permittivity, S is the coherence area of the plexciton setup, $\hat{\chi}_{\mathbf{k}} = \hat{\mathbf{k}} + i\frac{|\mathbf{k}|}{\eta_{\mathbf{k}}}\hat{\mathbf{z}}$ is the polarization and $L_{\mathbf{k}}$ is the quantization length. This last quantity determines the plasmonic confinement length scale in the molecular region of the plexciton setup: for $|\mathbf{k}| \approx 0$ the plasmon field is light-like and spatially spans the whole molecular slab; on the other hand it monotonically decreases for higher $|\mathbf{k}|$ values and the field is effectively coupled to a smaller number of molecules.

Note that the parametric dependence of the exciton operators on $R_{\mathbf{n},s}$ yield residual non-adiabatic processes induced by nuclear kinetic energy that may be relevant to the isomerization in question. We also highlight the fact that Eq. (3.2) includes both rotating ("energy conserving") terms ($a^{\dagger}_{\mathbf{k}}b_{\mathbf{n},s}$ and $a_{\mathbf{k}}b^{\dagger}_{\mathbf{n},s}$) where a photon creation (annihilation) involves the concomitant annhilation (creation) of an exciton; and counterrotating ("non-energy conserving") terms ($a_{\mathbf{k}}b_{\mathbf{n},s}$ and$a^{\dagger}_{\mathbf{k}}b^{\dagger}_{\mathbf{n},s}$) where there is a simultaneous annhilation (creation) of photon and exciton. These latter terms are ignored in the widely used Rotating Wave Approximation (RWA) [53], where light-matter coupling is weak compared to the transition energy. Since we are interested in the USC, we shall keep them throughout.

For simplicity, we assume that all the transition dipoles are equivalent and aligned along x, $\mu_{\mathbf{n},s}(R_{\mathbf{n},s}) = \mu(R_{\mathbf{n},s}) = \mu(R_{\mathbf{n},s})\hat{\mathbf{x}}$; a departure of this perfect crystal condition does not affect the conclusions of this chapter. Furthermore, it is convenient to first restrict ourselves to the cases where all nuclei are fixed at the same configuration ($\mathbf{R} = \tilde{\mathbf{R}}$, which denotes $R_{\mathbf{n},s} = R$ for all $\mathbf{n}$ and s), so that we can take advantage of the underlying translational symmetry to introduce a delocalized exciton basis where the in-plane momentum $\mathbf{k}$ is a good quantum number. The creation operator of this delocalized state is defined by $b^\dagger_{\mathbf{k}}(R) = \frac{1}{\sqrt{\mathcal{N}_{\mathbf{k}}(R)}} \sum_{\mathbf{n}} \sum_s f_{\mathbf{k}}(z_s) h_{\mathbf{k}}(R) b^\dagger_{\mathbf{n},s}(R)$, and the normalization squared is given by $\mathcal{N}_{\mathbf{k}}(R) = \sum_{\mathbf{n}} \sum_s |h_{\mathbf{k}}(R)|^2 |f_{\mathbf{k}}(z_s)|^2$ which, in the continuum limit, can be seen to be proportional to ρ, the number density of the molecular ensemble. In this collective basis, the previously introduced $H_{el}(\mathbf{R})$ reads

$$\begin{aligned} H_{el}(\tilde{\mathbf{R}}) &= \sum_{\mathbf{k}} \hbar\Delta(R) b^\dagger_{\mathbf{k}}(R) b_{\mathbf{k}}(R) + \sum_{\mathbf{k}} \hbar\omega_{\mathbf{k}} a^\dagger_{\mathbf{k}} a_{\mathbf{k}} \\ &\quad + \sum_{\mathbf{k}} \sqrt{\mathcal{N}_{\mathbf{k}}(R)} \left(a^\dagger_{\mathbf{k}} b_{\mathbf{k}}(R) + a_{\mathbf{k}} b^\dagger_{\mathbf{k}}(R) + a_{\mathbf{k}} b_{-\mathbf{k}}(R) + a^\dagger_{\mathbf{k}} b^\dagger_{-\mathbf{k}}(R) \right) \\ &\quad + \sum_{\mathbf{k}} H_{\text{dark},\mathbf{k}}(R) + \sum_{\mathbf{k}} H_{\text{unklapp},\mathbf{k}}(R) + N\hbar\omega_g(R) \\ &= \sum_{\mathbf{k}} H_{\mathbf{k}}(R) + \sum_{\mathbf{k}} H_{\text{dark},\mathbf{k}}(R) + \sum_{\mathbf{k}} H_{\text{unklapp},\mathbf{k}}(R) + N\hbar\omega_g(R), \end{aligned} \tag{3.3}$$

where $\Delta(R) = \omega_e(R) - \omega_g(R)$ is the exciton transition frequency.

$$H_{\text{dark},\mathbf{k}}(R) = \hbar\Delta(R) \mathbf{P}_{\text{dark},\mathbf{k}}(R) \tag{3.4}$$

accounts for the energy of the $(N_z - 1)$-degenerate exciton states with in-plane momentum $\mathbf{k}$ that do not couple to SPs, and are usually known as *dark states*. The latter are orthogonal to the bright exciton $b^\dagger_{\mathbf{k}}(R)|G_m(\tilde{\mathbf{R}})\rangle$ that couples to the SP field, where $|G_m(\tilde{\mathbf{R}})\rangle$ is the bare molecular ground-state ($b_{\mathbf{k}}(R)|G_m(\tilde{\mathbf{R}})\rangle = 0$). More specifically, $\mathbf{P}_{\text{dark},\mathbf{k}}(R) = \mathbf{I}_{\text{exc},\mathbf{k}}(R) - b^\dagger_{\mathbf{k}}(R) b_{\mathbf{k}}(R)$ is a projector operator onto the $\mathbf{k}$-th dark-state subspace, with $\mathbf{I}_{\text{exc}}(R) = \sum_{\mathbf{n},s} b^\dagger_{\mathbf{n},s}(R) b_{\mathbf{n},s}(R) = \sum_{\mathbf{k},s} b^\dagger_{\mathbf{k},s}(R) b_{\mathbf{k},s}(R) =$

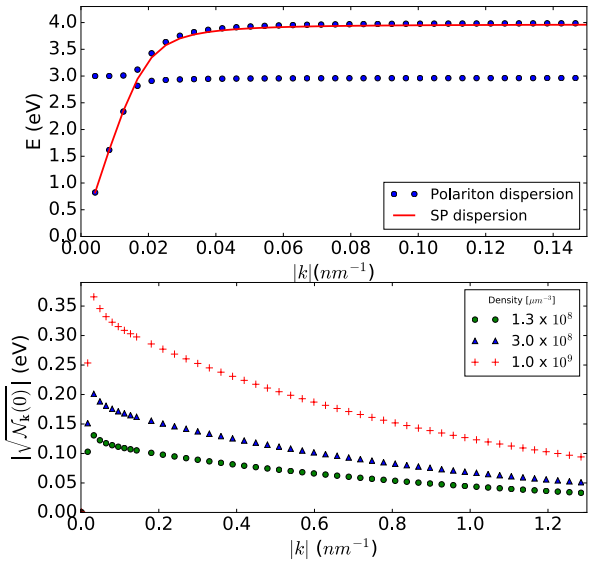

Figure 3.3: *Upper*: Polariton dispersion that results from the interaction of a molecular ensemble with the plasmonic field; we chose $\rho = 1.0 \times 10^9 \mu m^{-3}$. *Lower*: Collective SP-exciton coupling at equilibrium geometry $\sqrt{\mathcal{N}_{\mathbf{k}}(0)}$ as a function of $|\mathbf{k}|$, assuming $\mu(R=0)$ and $\mathbf{k}$ are parallel to the x axis. We consider a slab with $W_z = 120$ nm and compute couplings as a function of varying molecular densities ρ. The range of the resulting couplings is well above the plasmonic linewidth of the order of 10 *meV* [50], indicating the polaritonic onset of strong and ultrastrong light-matter coupling.

$\sum_{\mathbf{k}} \mathbf{I}_{\text{exc},\mathbf{k}}(R)$ being the identity on the exciton space, and $b^{\dagger}_{\mathbf{k},s}(R) = \frac{1}{\sqrt{N_x N_y}} \sum_{\mathbf{n}} e^{-i\mathbf{k}\cdot\mathbf{n}} b^{\dagger}_{\mathbf{n},s}(R)$. Finally,

$$H_{\text{unklapp},\mathbf{k}}(R) = \sum_{\mathbf{q}=(\frac{2\pi q_x}{\Delta_x}, \frac{2\pi q_y}{\Delta_y})} \sqrt{\mathcal{N}_{\mathbf{k}+\mathbf{q}}(R)} \left(a^{\dagger}_{\mathbf{k}+\mathbf{q}} b_{\mathbf{k}}(R) + a^{\dagger}_{\mathbf{k}+q} b^{\dagger}_{-\mathbf{k}}(R) + h.c. \right) \tag{3.5}$$

stands for the coupling of excitons with momentum $\mathbf{k}$ to SP modes with momentum beyond the first excitonic Brillouin zone. We also note that the normalization constant $\sqrt{\mathcal{N}_{\mathbf{k}}(R)}$ in Eq. 3.3 is precisely the collective SP-exciton coupling. As mentioned in the introduction, the condition $\sqrt{\mathcal{N}_{\mathbf{k}}(R)}/\hbar\Delta(R) > 0.1$ is often used to define the onset of USC [43], and it is fulfilled with the maximal density considered in our model (see Fig. 3.3) taking into account that the largest $\hbar\Delta(R)$ is 3 eV (See Fig. 3.1a). We note, as will be evident later, that our main results do not vary significantly by considering ratios $\sqrt{\mathcal{N}_{\mathbf{k}}(R)}/\hbar\Delta(R)$ below the aforementioned threshold.

A Bogoliubov transformation [54] permits the diagonalization of the Bloch Hamiltonian

$H_{\mathbf{k}}$ in Eq. 3.3 by introducing the polariton quasiparticle operators

$$\xi^{j}_{\mathbf{k}}(R) \approx \alpha^{j}_{\mathbf{k}} a_{\mathbf{k}} + \beta^{j}_{\mathbf{k}} b_{\mathbf{k}}(R) + \gamma^{j}_{\mathbf{k}} a^{\dagger}_{-\mathbf{k}} + \delta^{j}_{\mathbf{k}} b^{\dagger}_{-\mathbf{k}}(R), \tag{3.6}$$

where $j = U, L$ and U (L) stands for the upper (lower) Bogoliubov polariton state. Notice that this canonical transformation is valid for a sufficiently large number of molecules N, where the collective exciton operators $b_{\mathbf{k}}(R)$, $b^{\dagger}_{\mathbf{k}}(R)$ are well approximated by bosonic operators [55]. We also stress that Eq. (3.6) is formally an approximate definition since it does not take into account mixing with photonic modes beyond the exciton first Brillouin zone, as described in Eq. (3.5). However, given the large off-resonance between the SP energy and the exciton states for high $|\mathbf{k}|$, Eq. (3.6) is a good approximation.

The bare molecular ground-state with no photons in the absence of light-matter coupling $|G_m(\tilde{\mathbf{R}});0\rangle$, ($a_{\mathbf{k}}|G_m(\tilde{\mathbf{R}});0\rangle = b_{\mathbf{k}}(R)|G_m(\tilde{\mathbf{R}});0\rangle = 0$ for all $\mathbf{k}$) has a total extensive energy with molecular contributions only $\langle G_m(\tilde{\mathbf{R}});0|H_{el}(\tilde{\mathbf{R}})|G_m(\tilde{\mathbf{R}});0\rangle = N\hbar\omega_g(R)$. Upon inclusion of the counterrotating terms, the ground-state becomes the dressed Bogoliubov vacuum $|G(\tilde{\mathbf{R}})\rangle_d$, characterized by $\xi^{j}_{\mathbf{k}}(R)|G(\tilde{\mathbf{R}})\rangle_d = 0$ for all $\mathbf{k}$ and j, with total energy ${}_d\langle G(\tilde{\mathbf{R}})|H_{el}(\tilde{\mathbf{R}})|G(\tilde{\mathbf{R}})\rangle_d = E_0(\tilde{\mathbf{R}})$, where the zero-point energy is given by

$$E_0(\tilde{\mathbf{R}}) = N\hbar\omega_g(R) + \frac{1}{2}\sum_{\mathbf{k}}\left(\sum_{j=U,L}\hbar\omega_{j,\mathbf{k}}(R) - \hbar\omega_{\mathbf{k}} - \hbar\Delta(R)\right), \tag{3.7}$$

$\{\hbar\omega_{j,\mathbf{k}}(R)\}$ being the eigenvalues of the Bogoliubov polariton branches given by

$$\omega_{\substack{U\\L},\mathbf{k}}(R) = \sqrt{\frac{(\Delta(R))^2 + \omega^2_{\mathbf{k}} \pm \sqrt{\left(\omega^2_{\mathbf{k}} - \Delta(R)^2\right)^2 + 16\mathcal{N}^2_{\mathbf{k}}(R)\Delta(R)\omega_{\mathbf{k}}}}{2}}. \tag{3.8}$$

The sum in Eq. 3.7 accounts for the energy shift from the bare molecular energy $N\hbar\omega_g(R)$ due to interaction with the SP modes of the different photonic Brilloun zones of the setup. Using Eq.

(3.8), it is illustrative to check that this shift vanishes identically when the non-RWA terms are ignored.

In order to obtain converged quantities in our calculations of Eq. (3.7), we captured the energetic effects due to $H_{unklapp,\mathbf{k}}(R)$ by summing over SP modes beyond the first Brillouin zone. This approach is justified in view of the large off-resonance between the bare molecular energy and the double excited manifold of the system compared to the $\sqrt{\mathcal{N}_{\mathbf{k}}(R)}$ magnitudes, which allows for a perturbative treatment of the light-matter interaction part of Eq. (3.3). In the Appendix we show that $Eq.(3.7)$ can be approximated as a second order energy correction to the molecular vacuum, non restricted to the first Brilloun zone.

A hallmark of the SC and USC regimes is the anticrossing splitting of the polariton energies at the $\mathbf{k}$ value where the bare excitations are in resonance, $\Delta(R) = \omega_{\mathbf{k}}$ [56] (see Fig. 3.3).

It is worth describing some of the physical aspects of the Bogoliubov ground-state $|G(\tilde{\mathbf{R}})\rangle_d$. With the numerically computed wavefunctions, we can use the inverse transformation of Eq. 3.6 to explicitly evaluate its SP and exciton populations [54],

$$n_{\mathbf{k}}^{SP} = {}_d\langle G(\tilde{\mathbf{R}})|a_{\mathbf{k}}^{\dagger}a_{\mathbf{k}}|G(\tilde{\mathbf{R}})\rangle_d = \sum_j |\gamma_{\mathbf{k}}^j|^2, \tag{3.9a}$$

$$n_{\mathbf{k}}^{exc} = {}_d\langle G(\tilde{\mathbf{R}})|b_{\mathbf{k}}^{\dagger}b_{\mathbf{k}}|G(\tilde{\mathbf{R}})\rangle_d = \sum_j |\delta_{\mathbf{k}}^j|^2, \tag{3.9b}$$

which give rise to humble $O(10^{-3})$ values per mode $\mathbf{k}$, considering a molecular ensemble with $\rho = 3\times 10^8 \mu m^{-3}$ and W_z =120 nm; this calculation is carried out using $N = 8\times 10^7$, although results are largely insensitive to this parameter as long as it is sufficiently large to capture the thermodynamic limit. The consequences of the dressing partially accounted for by Eq. (3.9) (partially since there are also correlations of the form ${}_d\langle G(\tilde{\mathbf{R}})|b_{\mathbf{k}}a_{-\mathbf{k}}|G(\tilde{\mathbf{R}})\rangle_d$) are manifested as energetic effects on $|G_m(\tilde{\mathbf{R}});0\rangle$: $E_0(\tilde{\mathbf{R}}) - N\hbar\omega_g(R)$ can be interpreted as the energy stored in $|G(\tilde{\mathbf{R}})\rangle_d$ as a result of dressing; it is an extensive quantity of the ensemble, but becomes negligible

when considering a per-molecule stabilization. For instance, in molecular ensembles with the aforementioned parameters we find $E_0(\tilde{\mathbf{0}}) - N\hbar\omega_g(0) = O(10^2)$ eV, which implies a $O(10^{-5})$ eV value per molecule; our calculations show that this intensive quantity is largely insensitive to total number of molecules. This observation raises the following questions: to what extent does photonic dressing impact ground-state chemical reactivity? What are the relevant energy scales that dictate this impact?

With these questions in mind, we aim to study the polaritonic effects on ground-state single-molecule isomerization events. To do so, we map out the PES cross section where we set one "free" molecule to undergo isomerization while fixing the rest at $R_{\mathbf{n},s} = 0$. This cross section, described by $E_0(R_{\mathbf{n}_0,0}, 0, \cdots, 0) \equiv E_0(R_{\mathbf{n}_0,0}, \tilde{\mathbf{0}}')$ ($R_{\mathbf{n}_0,0}$ being the coordinate of the unconstrained molecule), should give us an approximate understanding of reactivity starting from thermal equilibrium conditions, since the molecular configuration $\tilde{\mathbf{R}} = \tilde{\mathbf{0}}$ still corresponds to the global minimum of the modified ground-state PES, as will be argued later. By allowing one molecule to move differently than the rest, we weakly break translational symmetry. Rather than numerically implementing another Bogoliubov transformation, we can, to a very good approximation, account for this motion by treating the isomerization of the free molecule as a perturbation on $H_{el}(\tilde{0})$. More precisely, we write $H_{el}(R_{\mathbf{n}_0,0}, \tilde{\mathbf{0}}')|G(R_{\mathbf{n}_0,0}, \tilde{\mathbf{0}}')\rangle_d = E_0(R_{\mathbf{n}_0,0}, \tilde{\mathbf{0}}')|G(R_{\mathbf{n}_0,0}, \tilde{\mathbf{0}}')\rangle_d$, where $H_{el}(R_{\mathbf{n}_0,0}, \tilde{\mathbf{0}}')$ is the sum of a translationally invariant piece $H_{el}(\tilde{\mathbf{0}})$ plus a perturbation due to the free molecule,

$$H_{el}(R_{\mathbf{n}_0,0}, \tilde{\mathbf{0}}') = H_{el}(\tilde{\mathbf{0}}) + V(R_{\mathbf{n}_0,0}). \tag{3.10}$$

The perturbation is explicitly given by

$$V(R_{\mathbf{n}_0,0}) = H_{el}(R_{\mathbf{n}_0,0},\tilde{\mathbf{0}}') - H_{el}(\tilde{\mathbf{0}}) \tag{3.11a}$$

$$= \hbar\Delta(R_{\mathbf{n}_0,0}) b^{\dagger}_{\mathbf{n}_0,0}(R_{\mathbf{n}_0,0}) b_{\mathbf{n}_0,0}(R_{\mathbf{n}_0,0}) - \hbar\Delta(0) b^{\dagger}_{\mathbf{n}_0,0}(0) b_{\mathbf{n}_0,0}(0) \tag{3.11b}$$

$$+ \sum_{\mathbf{k}} \left\{ g^{\mathbf{n}_0,0}_{\mathbf{k}}(R_{\mathbf{n}_0,0}) \left[b_{\mathbf{n}_0,0}(R_{\mathbf{n}_0,0}) + b^{\dagger}_{\mathbf{n}_0,0}(R_{\mathbf{n}_0,0}) \right] \right. \tag{3.11c}$$

$$\left. - g^{\mathbf{n}_0,0}_{\mathbf{k}}(0) \left[b_{\mathbf{n}_0,0}(0) + b^{\dagger}_{\mathbf{n}_0,0}(0) \right] \right\} \left[a_{\mathbf{k}} + a^{\dagger}_{\mathbf{k}} \right] \tag{3.11d}$$

$$+ \hbar\omega_g(R_{\mathbf{n}_0,0}) - \hbar\omega_g(0). \tag{3.11e}$$

Notice that we have chosen the free molecule to be located at an arbitrary in-plane location $\mathbf{n}_0$ and at the very bottom of the slab at $s = 0$, where light-matter coupling is strongest as a result of the evanescent field profile along the z direction.

Before showing the details of our calculation approach, we remark that a perturbative treatment of the terms in Eq. (3.11b) is expected to fail in view of the dramatic change in character of the ground state with R after the avoided crossing featured in the molecular energy landscape. Fortunately, we can take advantage of the symmetries of the system which permit a perturbative treatment in completely different electronic-character regions as long as we change the zeroth order Hamiltonian properly. More specifically, we compute the energetic changes perturbatively in the region $R \in [0,\pi/2]$ ($R \in [\pi/2,\pi]$) pertaining to the reactant (product) by considering $H_{el}(\tilde{\mathbf{0}})$ ($H_{el}(\tilde{\pi})$) as the zeroth order Hamiltonian. In the Appendix, we provide a more detailed analysis of this symmetries and the validity of our approach.

$$V_0(R_{\mathbf{n_0},0} \in [\pi/2,\pi]) = V_{\pi}(R_{\mathbf{n_0}}, 0 \in [0,\pi/2]), \tag{3.12}$$

under the permutation $|trans\rangle \leftrightarrow |cis\rangle$, where $V_0(R_{\mathbf{n_0},0})$ is

We write an expansion of the PES cross section as

$$E_0(R_{\mathbf{n}_{0,0}},\tilde{\mathbf{0}}') = \sum_{q=0}^{\infty} E_0^{(q)}(R_{\mathbf{n}_{0,0}},\tilde{\mathbf{0}}'),$$

where q labels the $O(V^q)$ perturbation correction. The zeroth order term is the Bogoliubov vacuum energy associated to every molecule being at the equilibrium geometry $E_0^{(0)}(R_{\mathbf{n}_{0,0}},\tilde{\mathbf{0}}') = E_0(\tilde{\mathbf{0}})$ as in Eq. (3.7). The $O(V)$ correction corresponds to $\hbar\omega_g(R_{\mathbf{n}_{0,0}}) - \hbar\omega_g(0)$, merely describing the PES of the isomerization of the bare molecule in the absence of coupling to the SP field. The contribution of the SP field on the PES cross-section of interest appears at $O(V^2)$, and it is given by

$$E^{(2)}(R_{\mathbf{n}_{0,0}},\tilde{\mathbf{0}}') \approx \sum_{\substack{\mathbf{k}_1\leq\mathbf{k}_2 \\ i,j=UP,LP}} \frac{|\langle \mathbf{k}_1,i;\mathbf{k}_2,j|V(R_{\mathbf{n}_{0,0}})|G(\tilde{\mathbf{0}})\rangle_d|^2}{E_0(\tilde{\mathbf{0}}) - E^{(0)}_{\mathbf{k}_1,\mathbf{k}_2,i,j}}, \tag{3.13}$$

where $|\mathbf{k}_1,i;\mathbf{k}_2,j\rangle \equiv \xi^{i\dagger}_{\mathbf{k}_1}(0)\xi^{\dagger j}_{\mathbf{k}_2}(0)|G(\tilde{\mathbf{0}})\rangle_d$ and $E^{(0)}_{\mathbf{k}_1,\mathbf{k}_2,i,j} = \hbar(\omega_{i,\mathbf{k}_1}(0) + \omega_{j,\mathbf{k}_2}(0))$. As shown in the Appendix, the approximation in Eq. (3.13) consists of ignoring couplings between $|G(\tilde{\mathbf{0}})\rangle_d$ and states with three and four Bogoliubov polariton excitations, since their associated matrix elements become negligible in the thermodynamic limit compared to their double excitation counterparts. The remaining matrix elements can be calculated by expressing the operators $a_{\mathbf{k}}$, $a^{\dagger}_{\mathbf{k}}$, $b_{\mathbf{n}_{0,0}}(R_{\mathbf{n}_{0,0}})$, $b^{\dagger}_{\mathbf{n}_{0,0}}(R_{\mathbf{n}_{0,0}})$ in Eq. (3.11) in terms of the Bogoliubov operators $\xi^{j}_{\mathbf{k}}(0)$, $\xi^{\dagger j}_{\mathbf{k}}(0)$ (see Eq. (3.6)), leading to

$$\begin{aligned}\langle \mathbf{k}_1,i;\mathbf{k}_2,j|V(R_{\mathbf{n}_{0,0}})|G(\tilde{\mathbf{0}})\rangle_d = {} & F^{\mathbf{k}_2}(R_{\mathbf{n}_{0,0}})D_{\mathbf{k}_1}\left(-\delta^i_{-\mathbf{k}_1}\alpha^j_{\mathbf{k}_2} + \delta^i_{-\mathbf{k}_1}\gamma^j_{-\mathbf{k}_2} - \beta^i_{\mathbf{k}_1}\gamma^j_{-\mathbf{k}_2} + \beta^i_{\mathbf{k}_1}\alpha^j_{\mathbf{k}_2}\right) \\ & + F^{\mathbf{k}_1}(R_{\mathbf{n}_{0,0}})D_{\mathbf{k}_2}\left(-\delta^j_{-\mathbf{k}_2}\alpha^i_{\mathbf{k}_1} + \delta^j_{-\mathbf{k}_2}\gamma^i_{-\mathbf{k}_1} - \beta^j_{\mathbf{k}_2}\gamma^i_{-\mathbf{k}_1} + \beta^j_{\mathbf{k}_2}\alpha^i_{\mathbf{k}_1}\right),\end{aligned} \tag{3.14}$$

where $F^{\mathbf{k}}(R) = \cos(\theta(R))g^{\mathbf{n}_{0,0}}_{\mathbf{k}}(R) - \cos(\theta(0))g^{\mathbf{n}_{0,0}}_{\mathbf{k}}(0)$ depends on the mixing angle that describes

the change of character of $b^{\dagger}_{\mathbf{n}_{0,0}}(R)$ as a function of R (see Equation (3.1)); it emerges as a consequence of coupling molecular states at different configurations. The prefactor

$$D_{\mathbf{k}} = \langle G_m(\tilde{\mathbf{R}});0\rangle | b_{\mathbf{n}_{0,0}}(0) b^{\dagger}_{\mathbf{k}}(0) | G_m(\tilde{\mathbf{R}});0\rangle = \frac{1}{\sqrt{N_x N_y}} \sqrt{\frac{1-e^{-2\eta_{\mathbf{k}}\Delta_z}}{1-e^{-2\eta_{\mathbf{k}}\Delta_z N_z}}}$$

accounts for the weight of a localized exciton operator in a delocalized one, such as the participation of $b^{\dagger}_{\mathbf{n}_{0,0}}(0)$ in $b^{\dagger}_{\mathbf{k}}(0)$. Eq. (3.14) reveals that the maximal contribution of each double-polariton Bogoliubov state to the energetic shift of the considered PES cross section $E(R_{\mathbf{n}_{0,0}}, \tilde{\mathbf{0}}')$ is of the order of $\frac{g_{\mathbf{k}}^{\mathbf{n}_{0,0}}(0)}{\sqrt{N_x N_y}}$. Considering macroscopic molecular ensembles with large $N \approx 10^7$, we computed Eq. 3.13 by means of an integral approximation over the polariton modes $\mathbf{k}$.

3.3 Results and discussion

3.3.1 Energetic effects

We carry out our calculations with ρ in the range of 10^6 to 10^9 molecules μm^{-3} keeping $W_z = 120\,\text{nm}$ (see Fig. 3.4); to obtain results in the thermodynamic limit, our calculations take $N = 8 \times 10^7$, even though the exact value is unimportant as long as it is sufficiently large to give converged results. The results displayed in Fig. 3.4 show that the second order energy corrections to the isomerization PES $E^{(2)}(R_{\mathbf{n}_{0,0}}, \tilde{\mathbf{0}}')$, and in particular $E^{(2)}(R_{\mathbf{n}_{0,0}} = R^*, \tilde{\mathbf{0}}') \approx -0.25\,\text{meV}$, are negligible in comparison with the bare activation barrier $E_a = \hbar\omega_g(R^*) - \hbar\omega_g(0) = \hbar\omega_g(R^*) \approx 1.8$ eV, where $R^* \approx 1.64$ rad corresponds to the transition state. From Fig. 3.1b, we notice that there is a substantial difference in SP-exciton coupling between the equilibrium ($R_{\mathbf{n}_{0,0}} = 0$) and transition state geometries ($R_{\mathbf{n}_{0,0}} = R^*$). Since the perturbation in Eq. (3.11) is defined with respect to the equilibrium geometry, $|E^{(2)}(R_{\mathbf{n}_{0,0}}, \tilde{\mathbf{0}}')|$ maximizes at the barrier geometry.

To get some insight on the order of magnitude of the result, we note that the sum shown in Eq.

3.13 can be very roughly approximated as

$$\begin{aligned} E^{(2)}(R_{\mathbf{n}_0,0},\tilde{\mathbf{0}}') &= O\left[-\sum_{\mathbf{k}_1\leq\mathbf{k_2}}\frac{[g^{\mathbf{n}_0,0}_{\mathbf{k}_1}(R_{\mathbf{n}_0,0})]^2D^2_{\mathbf{k}_2}+[g^{\mathbf{n}_0,0}_{\mathbf{k}_2}(R_{\mathbf{n}_0,0})]^2D^2_{\mathbf{k}_1}}{(\hbar\omega_{\mathbf{k}_1}+\hbar\omega_{\mathbf{k}_2})/2+\hbar\omega_e(R_{\mathbf{n}_0,0})}\right] \\ &= O\left[-\frac{1}{N_xN_y}\sum_{\mathbf{k}_1\leq\mathbf{k_2}}\frac{[g^{\mathbf{n}_0,0}_{\mathbf{k}_1}(R_{\mathbf{n}_0,0})]^2+[g^{\mathbf{n}_0,0}_{\mathbf{k}_2}(R_{\mathbf{n}_0,0})]^2}{(\hbar\omega_{\mathbf{k}_1}+\hbar\omega_{\mathbf{k}_2})/2+\hbar\omega_e(R_{\mathbf{n}_0,0})}\right] \\ &= O\left[-\sum_{\mathbf{k}}\frac{[g^{\mathbf{n}_0,0}_{\mathbf{k}}(R_{\mathbf{n}_0,0})]^2}{\hbar\omega_{\mathbf{k}}+\hbar\omega_e(R_{\mathbf{n}_0,0})}\right] \\ &= O\left(E_{LS}(R_{\mathbf{n}_0,0})\right). \end{aligned} \tag{3.15}$$

In the first line, we used the fact that

$$\langle\mathbf{k}_1,i;\mathbf{k}_2,j|V(R_{\mathbf{n}_0,0})|G(\tilde{\mathbf{0}})\rangle_d \approx [g^{\mathbf{n}_0,0}_{\mathbf{k}_1}(R_{\mathbf{n}_0,0})]^2D^2_{\mathbf{k}_2}+[g^{\mathbf{n}_0,0}_{\mathbf{k}_2}(R_{\mathbf{n}_0,0})]^2D^2_{\mathbf{k}_1}$$

and averaged the Bogoliubov polariton excitation energies. In the second line, assuming that the $\mathbf{k}\gg 0$ values contribute the most, we have $D_{\mathbf{k}}\approx\frac{1}{\sqrt{N_xN_y}}$. Finally, in the third line, we have used the fact that the sum of terms over $\mathbf{k}_1,\mathbf{k}_2$ is roughly equal to N_xN_y times a single sum over $\mathbf{k}$ of terms of the same order. The reason why we are interested in the final approximation is because it corresponds to the Lamb shift of a single isolated molecule, which can be calculated to be $E_{LS}(0)=0.16\,\text{meV}$. Typically, Lamb shift calculations require a cutoff to avoid unphysical divergences [57]; we stress that in our plexciton model, this is not necessary due to the decaying $|g^{\mathbf{n}_0,0}_{\mathbf{k}}(R_{\mathbf{n}_0,0})|$ as a function of $|\mathbf{k}|$. The fact that the corrections $E^{(2)}(R_{\mathbf{n}_0,0},\tilde{\mathbf{0}}')$ have a similar order of magnitude to single-molecule Lamb shifts give a pessimistic conclusion of harnessing USC to control ground-state chemical reactions.

We have, however, from calculations in Fig. 3.4, that there is variability in $E^{(2)}(R_{\mathbf{n}_0,0},\tilde{\mathbf{0}}')$ as a function of molecular density (since density alters the character of the Bogoliubov polaritons), although the resulting values are always close to $E_{LS}(0)$. The molecular density cannot increase without bound, since there exists a minimum molecular contact distance determined by a van der

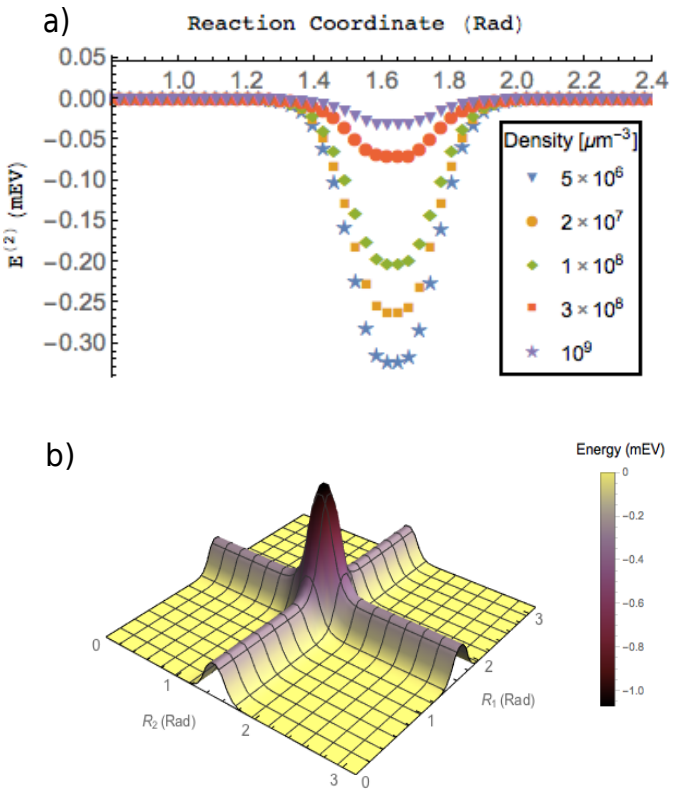

Figure 3.4: (a) Second order energy correction $E^{(2)}(R_{\mathbf{n}_0,0},\tilde{\mathbf{0}}')$ of PES for one molecule isomerizing along the torsional coordinate $R_{\mathbf{n}_0,0}$; the rest of the molecules are fixed at the equilibrium geometry. Calculations are displayed for various densities ρ, keeping $W_z = 120$ nm. Energy corrections are due to SP-exciton (see Eq. 3.13). Note also that the energy scale of this correction is negligible in comparison with the energy barrier of the reaction (see Fig. 3.1a). (b) Same plot as in (a), but for the 2D-ground-isomerization PES of two molecules, keeping the configuration of the other molecules at equilibrium ($E^{(2)}(R_0,R_1,\tilde{\mathbf{0}}')|$); the density $\rho = 3\times10^8$ molecules$/\mu m^3$.

Waals radius of the order of 0.3 nm for organic molecules [58], giving a maximum density of $\rho \approx 10^{10}$ molecules$/\mu m^3$.

The results discussed so far describe the energy profile of the isomerization of a single molecule keeping the rest at equilibrium geometry. It is intriguing to inquire the effects of the SP field in a concerted isomerization of two or more molecules, while keeping the rest fixed at equilibrium geometry. Generalizing Eqs. (3.11)–(3.14) to a two-molecule perturbation $V(R_{\mathbf{n}_0,0},R_{\mathbf{n}_1,0})$, we computed the second order energetic corrections to the 2D-PES that describe the isomerization of two neighbouring molecules at $\mathbf{n}_0$ and at $\mathbf{n}_1 \equiv \mathbf{n}_0 + \Delta_x\hat{\mathbf{x}}$, keeping the other molecules fixed at

$R_{\mathbf{n},s} = 0$. The results are reported in Fig. 3.4 for $\rho = 3 \times 10^8$ molecules/μm^3, although outcomes of the same order of magnitude are obtained for the other densities considered in the one-dimensional case. The two-dimensional PES cross-section $E^{(2)}(R_{\mathbf{n}_0,0}, R_{\mathbf{n}_1,0}, 0, \cdots, 0) \equiv E^{(2)}(R_{\mathbf{n}_0,0}, R_{\mathbf{n}_1,0}, \tilde{\mathbf{0}}')$ shows the existence of an energetic enhancement for the concerted isomerization with respect to two independent isomerizations, *i.e.* $E^{(2)}(R_{\mathbf{n}_0,0} = R^*, R_{\mathbf{n}_1,0} = R^*, \tilde{\mathbf{0}}') \approx 4E^{(2)}(R_{\mathbf{n}_0,0} = R^*, \tilde{\mathbf{0}}')$. This enhacement is due to a constructive interference arising at the amplitude level, $\langle \mathbf{k}_1, i; \mathbf{k}_2, j | V(R_{\mathbf{n}_0,0} = R^*, R_{\mathbf{n}_1,0} = R^*) | G(\tilde{\mathbf{0}}) \rangle_d \approx 2\langle \mathbf{k}_1, i; \mathbf{k}_2, j | V(R_{\mathbf{n}_0,0} = R^*) | G(\tilde{\mathbf{0}}) \rangle_d$ for values of $\mathbf{k}_1, \mathbf{k}_2 \ll \frac{1}{\Delta_x}$, such that the phase difference between the isomerizing molecules is negligible. Interestingly, choosing the neighbouring molecules along the x direction is important for this argument; if instead we consider neighbours along z (molecular positions $\mathbf{n}_0$ and $\mathbf{n}_0 + \Delta_z \hat{\mathbf{z}}$), these interferences vanish and we approximately get the independent molecules result $E^{(2)}(R_{\mathbf{n}_0,0} = R^*, R_{\mathbf{n}_0,1} = R^*, \tilde{\mathbf{0}}') \approx 2E^{(2)}(R_{\mathbf{n}_0,0} = R^*, \tilde{\mathbf{0}}')$.

In light of the nontrivial energetic shift of the two-molecule case, it is pedagogical to consider the SP effects on the cross-section of the concerted isomerization of the whole ensemble, even though it is highly unlikely that this kinetic pathway will be of any relevance, especially considering the large barrier for the isomerization of each molecule. Notice that the conservation of translational symmetry in this scenario allows for the exact (nonperturbative) calculation of the energetic shift $E_0(\tilde{\mathbf{R}}) - N\hbar\omega_g(R)$ by means of Eq. 3.7. Our numerical calculations reveal an energetic stabilization profile, which is displayed in Fig. 3.5 for a molecular ensemble with $\rho = 3 \times 10^8$ molecules μm^{-3}. As expected, we observe a stabilization of reactant and product regions of the ground-state PES. This is a consequence of the transition dipole moment being the strongest at those regions, as opposed to the transition state, see Fig. 3.1b. However, even though these energetic effects are of the order of hundreds of eV, they are negligible in comparison with the total ground-state PES $N\hbar\omega_g(R)$, or more specifically, to the transition barrier $NE_a = N\hbar\omega_g(R^*)$ for the concerted reaction.

Importantly, the change in activation energy per molecule in the concerted isomerization

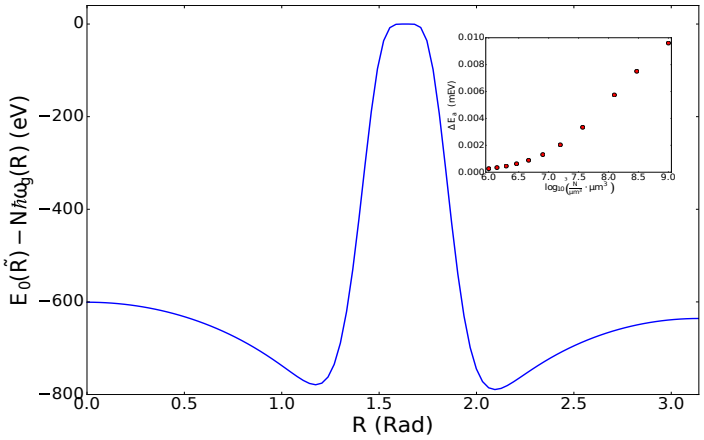

Figure 3.5: *Main:* profile of the energy stabilization of the concerted isomerization ($E_S(R) = E_0(\tilde{\mathbf{R}}) - N\hbar\omega_g(R)$, see Eq. 3.7) of the whole molecular ensemble discussed in the main text, due to the interaction with the plasmonic field. We consider a molecular macroscopic ensemble ($N = 8\times10^7$) with density $\rho = 3\times10^8$ molecules$/\mu m^3$. *Inset:* molecular-density dependence of the the energy shift of the energy barrier per molecule $|\Delta E_a|$ (see main text) due to the plasmonic field, in this concerted scenario.

with respect to the bare case $|\Delta E_a| = \left|\left(\frac{E_0(\tilde{\mathbf{R}}^*)-E_0(\tilde{\mathbf{0}})}{N} - E_a\right)\right| \approx 0.009\,\text{meV}$ is more than one order of magnitude smaller than the corresponding quantity of 0.025 meV for the single-molecule isomerization case, see Fig. 3.4 and inset of Fig. 3.5. We believe that the reason for this trend is that the isomerization of n molecules, $n \ll N$, translates into a perturbation which breaks the original translational symmetry of the molecular ensemble. This symmetry breaking permits the interaction of the molecular vacuum with the polaritonic $\mathbf{k}$-state reservoir without a momentum-conservation restriction. This is reflected in Eq. 3.13, where the sum is carried out over two not necessarily equal momenta. In contrast, in the case of the concerted isomerization of N molecules, the translational symmetry of the system is preserved, which in turn restricts the coupling of the vacuum $|G(\tilde{\mathbf{0}})\rangle_d$ to excited states with $\mathbf{k}_{\text{exc}} = -\mathbf{k}_{\text{phot}}$.

Another intriguing observation is that, for this concerted isomerization, the SP energetic effect per molecule $\frac{E_0(\tilde{\mathbf{R}})}{N}$ diminishes with the width of the slab W_z. This is the case given that the SP quantization length $L_{\mathbf{k}}$ decays quickly with $|\mathbf{k}|$ so that only the closest layers interact strongly with the field. When we divide the total energetic effects due to the SP modes by $N = N_x N_y N_z$,

we obtain that $\frac{E_0(\tilde{\mathbf{R}})}{N} = O(\frac{1}{N_z})$ for large W_z.

The energetic shifts in all the scenarios discussed above are negligible with respect to the corresponding energy barriers and the thermal energy scale at room temperature which, unfortunately, signal the irrelevance of USC to alter ground-state chemical reactivity for this isomerization model. Although there is an overall (extensive) stabilization of the molecular ensemble ground state, this effect is distributed across the ensemble, giving no possibility to alter the chemical reaction kinetics or thermodynamics considerably. However, we highlight the intriguing interferences observed in the concerted isomerization processes. Even though they will likely be irrelevant for this particular reaction, they might be important when dealing with reactions with very low barriers, especially when considering that these concerted pathways are combinatorially more likely to occur than the single-molecule events in the large N limit.

3.3.2 Effects on non-adiabatic dynamics

Finally, we discuss the importance of the nonadiabatic effects afforded by nuclear kinetic energy. Previous works have considered the nonadiabatic effects between polariton states at the level of SC [14, 59]. Alternatively, the consideration of nonadiabatic effects in USC for a single molecule in a cavity was provided in Ref. [60]; here, we address these issues for the many-molecule case and consider both polariton and dark state manifolds. One could expect significantly modified non-adiabatic dynamics about nuclear configurations where the transition dipole moment magnitude $|\mu_{\mathbf{n},s}(R_{\mathbf{n},s})|$ is large, given a reduction in the energy gap between the ground and the lower Bogoliubov polariton state. However, as we show below, this energetic effect is not substantial due to the presence of dark states.

We consider the magnitude of the non-adiabatic couplings (NACs) for the isomerization of a single molecule with reaction coordinate $R_{\mathbf{n}_0,0}$. For a region about $\tilde{\mathbf{R}} = \tilde{\mathbf{0}}$, we estimate the

magnitude of the NAC between $|G(\tilde{\mathbf{0}})\rangle_d$ and a state $|\mathbf{k},i\rangle = \xi^{i\dagger}_{\mathbf{k}}(0)|G(\tilde{\mathbf{0}})\rangle_d$ as:

$$\begin{aligned} |A_{\mathbf{k},i;g}(0)| &= \left|\langle \mathbf{k},i| \frac{\partial}{\partial R_{\mathbf{n}_{0,0}}} \left|G(\tilde{\mathbf{0}})\right\rangle_d\right| \\ &\approx \left|\beta^i_{\mathbf{k}} D_{\mathbf{k}} \left\langle e_{\mathbf{n}_{0,0}}(0) \left| \frac{\partial}{\partial R_{\mathbf{n}_{0,0}}} \right| g_{\mathbf{n}_{0,0}}(0) \right\rangle \right|, \end{aligned} \tag{3.16}$$

where $|g_{\mathbf{n}_{0,0}}(0)\rangle(|e_{\mathbf{n}_{0,0}}(0)\rangle)$ is the ground (excited) adiabatic state of the single molecule under consideration (see Eq. (3.1)) and we have ignored the derivatives of $\beta^i_{\mathbf{k}}$ and $D_{\mathbf{k}}$ with respect to $R_{\mathbf{n}_{0,0}}$, assuming they are small at $\tilde{\mathbf{R}} = \tilde{\mathbf{0}}$, where the chemical character of the Bogoliubov polariton states does not change significantly with respect to nuclear coordinate. This is a consequence of the slowly changing transition dipole moment of the model molecule around $R_{\mathbf{n}_{0,0}} = 0$, see Fig. 3.1b. Notice that we have also assumed $\langle \mathbf{k},i|e_{\mathbf{n}_{0,0}}(0)\rangle \approx \beta^i_{\mathbf{k}} D_{\mathbf{k}}$, where we have used the fact that $\beta^i_{\mathbf{k}} \gg \gamma^i_{\mathbf{k}}$, thus ignoring counterrotating terms, which as we have seen, give negligible contributions. The time-evolution of a nuclear wavepacket in the ground-state will be influenced by the Bogoliubov polariton states, each of which will contribute with a finite probability of transition out of $\left|G(\tilde{\mathbf{0}})\right\rangle_d$. From semiclassical arguments [61], we can estimate the transition probability $|C^i_{\mathbf{k}}(0)|^2$ for a nuclear wavepacket on the ground-state PES at $\tilde{\mathbf{R}} = 0$ to the state $|\mathbf{k},i\rangle$,

$$\begin{aligned} |C^i_{\mathbf{k}}(0)|^2 &\approx \left| \frac{\hbar v_{nuc} A_{\mathbf{k},i;g}(0)}{\hbar\omega_{i,\mathbf{k}}(0) - \hbar\omega_g(0)} \right|^2 \\ &= \left| \frac{\hbar v_{nuc} \beta^i_{\mathbf{k}} D_{\mathbf{k}}}{\hbar\omega_{i,\mathbf{k}}(0) - \hbar\omega_g(0)} \right|^2 \\ &\times \left| \left\langle e_{\mathbf{n}_{0,0}}(0) \left| \frac{\partial}{\partial R_{\mathbf{n}_{0,0}}} \right| g_{\mathbf{n}_{0,0}}(0) \right\rangle \right|^2, \end{aligned} \tag{3.17}$$

v_{nuc} being the expectation value of the nuclear velocity. However, the Bogoliubov polariton $\mathbf{k}$-states are only a small subset of the excited states of the problem. As mentioned right after Eq. 3.3, the plexciton setup contains $N_z - 1$ dark excitonic states for every $\mathbf{k}$ (eigenstates of $H_{\text{dark},\mathbf{k}}(0)$, see discussion right after Eq. 3.3); we ignore the very off-resonant couplings considered in

$H_{\text{unklapp},\mathbf{k}}(0)$. The dark states also couple to $\left|G(\tilde{\mathbf{0}})\right\rangle_d$ non-adiabatically, with the corresponding transition probability out of the ground state being,

$$|C_{\mathbf{k}}^{\text{dark}}(0)|^2 \approx \sum_Q \left| \frac{\hbar v_{nuc} A_{\mathbf{k},Q;g}(0)}{\hbar\Delta(0)} \right|^2 \approx P_{bare}(0) \left(\frac{1}{N_x N_y} - |D_{\mathbf{k}}|^2 \right), \tag{3.18}$$

Here, we have summed over all dark states Q for a given $\mathbf{k}$ and used

$$P_{bare}(0) = \left| \frac{v_{nuc}}{\Delta(0)} \right|^2 \left| \left\langle e_{\mathbf{n}_0,0}(0) \left| \frac{\partial}{\partial R_{\mathbf{n}_{0,0}}} \right| g_{\mathbf{n}_0,0}(0) \right\rangle \right|^2 \tag{3.19}$$

to denote the probability of transition out of the ground state in the absence of coupling to the SP field. In Eq. (3.18) we used the fact that the projection $|e_{\mathbf{n}_0,0}(0)\rangle$ onto the dark $\mathbf{k}$ manifold of exciton states is $\left|\mathbf{P}_{\text{dark},\mathbf{k}}(0)|e_{\mathbf{n}_0,0}(0)\rangle\right|^2 = \langle e_{\mathbf{n}_0,0}(0)|\mathbf{I}_{\text{exc},\mathbf{k}}(0)|e_{\mathbf{n}_0,0}(0)\rangle - |D_{\mathbf{k}}|^2 = \frac{1}{N_x N_y} - |D_{\mathbf{k}}|^2$, with $\mathbf{P}_{\text{dark},\mathbf{k}}(0)$ being the corresponding projector (see Eq. (3.4)). We noticed that when $|\mathbf{k}| \to 0$, the quantization length $L_{\mathbf{k}}$ of the plasmonic field spans all the molecular-ensemble volume resulting in completely delocalized bright and dark exciton states across the different layers of the slab, $\left|\mathbf{P}_{\text{dark},\mathbf{k}}|e_{\mathbf{n}_0,0}(0)\rangle\right|^2 = \frac{N_z-1}{N}$, and the dark states give the major contribution to the nonadiabatic dynamics. On the other hand, when $|\mathbf{k}| \to \infty$, the plasmonic field interacts with the molecular layer at the bottom of the slab only and $\left|\mathbf{P}_{\text{dark},\mathbf{k}}|e_{\mathbf{n}_0,0}(0)\rangle\right|^2 \to 0$. The dark states do not participate, because the molecule located at $\mathbf{n}_0$ only overlaps with the bright state which is concentrated across the first layer of the slab (the dark states, being orthogonal to the bright one, are distributed in the upper layers, and do not overlap with $|e_{\mathbf{n}_0,0}\rangle$). With these results, we can compute the probability of transition out of the ground-state P_{out} as

$$P_{out}(0) = \sum_{\mathbf{k}} \left[\sum_i |C_{\mathbf{k}}^i(0)|^2 + |C_{\mathbf{k}}^{\text{dark}}(0)|^2 \right]. \tag{3.20}$$

In view of the large off-resonant nature of most SP modes with respect to $\hbar\Delta(0)$ (see Fig. 3.3) and Eq. (3.18), we have $\sum_i |C^i_{\mathbf{k}}(0)|^2 \approx P_{bare}(0)|D_{\mathbf{k}}|^2$, such that $P_{out}(0) \approx P_{bare}(0)$. In our model, this is the case, since the plexciton anticrossing occurs at small $|\mathbf{k}|$ and the SP energy quickly increases and reaches an asymptotic value after that point (see Fig. 3.3). Using the parameters in Ref. [48], we obtain $\langle e(R_{\mathbf{n}_0,0})|\frac{\partial}{\partial R_{\mathbf{n}_0,0}}|g(R_{\mathbf{n}_0,0})\rangle \approx 0.01\,\text{Å}^{-1}$, where we have assumed an effective radius of 1 Å for the isomerization mode of the model molecule. We get an estimate of $v_{nuc} \approx 1\text{Å}$ $\omega_{nuc} = 1\text{Å}\sqrt{\frac{k_B T}{m}} = 9\times 10^{10}\,\text{Å s}^{-1}$ using $k_B = 8.62\times 10^{-5}\,\text{eV K}^{-1}$, $T = 298\,\text{K}$ and $m = 2.5\,\text{amu}$ Å^2. Finally, applying $\Delta(0) = 3$ eV gives $P_{bare}(0) \approx 10^{-7}$, which is a negligible quantity. A more pronounced polariton-effect is expected close to the PES avoided crossing. However, the rapid decay of the transition dipole moment in this region (see Fig. 3.1a) precludes the formation of polaritonic states that could have affected the corresponding nonadiabatic dynamics. To summarize this part, even when the USC effects on the nonadiabatic dynamics are negligible for our model, the previous discussion as well as Eq. (3.20) distill the design principle that controls these processes in other polariton systems: the plexciton anticrossings should happen at large $\mathbf{k}$ values to preclude the overwhelming effects of the dark states. This principle will be explored in future work in other molecular systems.

The negligible polariton effect on the NACs, and the magnitude of the energetic effects on the electronic energy landscape are strong evidence to argue that the chemical yields and rates of the isomerization problem in question remain intact with respect to the bare molecular ensemble.

3.4 Conclusions

We showed in this chapter that, for the ground state landscape of a particular isomerization model, there is no relevant collective stabilization effect by USC to SPs which can significantly alter the kinetics or thermodynamics of the reaction, in contrast with previous calculations which show such possibilities in the Bogoliubov polariton landscapes [15, 16]. The negligible energetic

corrections to the ground-state PES per molecule can be approximated and interpreted as Lamb shifts [57] experienced by the molecular states due to the interaction with off-resonant plasmonic modes. The key dimensionless parameter which determines the USC effect on the ground-state PES is the ratio of the individual coupling to the transition frequency $g_{\mathbf{k}}^{\mathbf{n},s}/\hbar\Delta$. This finding is similar to the conclusions of a recent work [14, 62]. In particular, it is shown in Ref. [62]that the rotational and vibrational degrees of freedom of molecules exhibit a self-adaptation which only depends on light-matter coupling at the single-molecule level. Therefore, more remarkable effects are expected in the regime of USC of a single molecule interacting with an electric field. To date, the largest single molecule interaction energy achievable experimentally is around 90 meV [42] in an ultralow nanostructure volume. This coupling strength is almost two orders of magnitude larger that those in our model. Also, previous works have shown [45, 63] that this regime is achievable for systems with transition frequencies on the microwave range. Additionally, the experimental realization of vibrational USC has been carried out recently [47]. The latter also suggests the theoretical exploration of USC effects on chemical reactivity at the rotational or vibrational energy scales, where the energy spacing between levels is significantly lower than typical electronic energy gaps.

We highlighted some intriguing quantum-coherent effects where concerted reactions can feature energetic effects that are not incoherent combinations of the bare molecular processes. These interference effects are unlikely to play an important role in reactions exhibiting high barriers compared to k_BT. However, they might be important for low-barrier processes, where the number of concerted reaction pathways becomes combinatorially more likely than single molecule processes. On the other hand, we also established that, due to the large number of dark states in these many-molecule polariton systems, nonadiabatic effects are not modified in any meaningful way under USC, at least for the model system explored. We provided a rationale behind this conclusion and discussed possibilities of seeing modifications in other systems where the excitonic and the electromagnetic modes anticross at large $\mathbf{k}$ values. To conclude, the present work

highlights the limitations but also possibilities of USC in the context of control of chemical reactions using polaritonic systems.

This chapter, in full, is adapted from the material as it appears in "Can ultrastrong coupling change ground-state chemical reactions?" Martínez-Martínez L. A., Ribeiro R. F., Campos-González-Angulo J. and Yuen-Zhou J. ACS Photonics, 5, 167 (2018). The dissertation author was the primary investigator and author of this material.

Chapter 4

Polariton-assisted Singlet Fission in Acene Aggregates

4.1 Introduction

Singlet fission (SF) is a spin-allowed process undergone by select materials that permits the conversion of a singlet exciton into a triplet-triplet (TT) state with an overall singlet character, which later decoheres and forms two triplet excitons. This process has been used to enhance the efficiency of organic solar cells [21, 64] by allowing a single absorbed photon to produce more than one exciton. This subsequently increases the external quantum yield, which is defined as the number of charge carriers produced per absorbed photon. In this chapter we explore the influence of strong light-matter coupling (SC) on the TT yield of acenes. As discussed in previous chapters, this regime can be achieved at room-temperature, for example, in optical microcavities enclosing densely packed organic dyes. Under these conditions, the energy of interaction between the microcavity photonic modes and the molecular degrees of freedom of the material is larger than their respective linewidths.

By developing a microscopic model for the relevant dynamical processes, we address the

effects of SC on the TT yield in aggregates of acene dyes (tetracene, pentacene and hexacene) and determine the important molecular parameters that rule this yield. Our starting point is a kinetic model based on a Pauli master equation formalism to describe the population dynamics of the states that take part in SF [65]. We then use this model to elucidate the circumstances under which polaritons can enhance SF under realistic dissipative conditions.

4.2 Theoretical model

We consider a simplified one-dimensional acene aggregate comprised of N identical molecules emdedded in a microcavity and strongly interacting with a single electromagnetic mode supported by the latter. The Hamiltonian of the model is given by

$$H = H_S + H_B + H_{S-B} + H_p + H_{p-S} + H_{TT} + H_{TT-B} + H_{TT-S}, \tag{4.1}$$

where H_S (H_{TT}) is the electronic singlet (TT) molecular Hamiltonian of the aggregate given by ($\hbar = 1$)

$$H_S = \sum_n \overline{\omega}_e |n\rangle\langle n|, \tag{4.2a}$$

$$H_{TT} = \sum_{n=0}^{N-1} \overline{\omega}_{TT} |T_n T_{n+1}\rangle\langle T_n T_{n+1}|, \tag{4.2b}$$

where $|n\rangle$ is a localized singlet (Frenkel) exciton [66] at the nth site (molecule), and $|T_n T_{n+1}\rangle$ denotes a TT state delocalized over sites n and $n+1$. Here $\overline{\omega}_e = \omega_e + \sum_i \omega_i \lambda_{S,i}^2$ ($\overline{\omega}_{TT} = \omega_{TT} + 2\sum_i \omega_i \lambda_{T,i}^2$) is the vertical singlet (TT) excitation frequency, where ω_e (ω_{TT}) and $\lambda_{S,i}$ ($\lambda_{T,i}$) are the 0-0 excitation frequency and the square root of the Huang-Rhys factor [20] for the ith vibrational mode coupled to the transition $|G\rangle \to |n\rangle$ ($|G\rangle \to |T_n T_{n+1}\rangle$), respectively, and$|G\rangle$ is the state

corresponding to all molecules in the electronic ground state. $H_B = \sum_{n,i} \omega_i b_{n,i}^\dagger b_{n,i}$ accounts for the vibrational degrees of freedom of the ensemble, where $b_{n,i}^\dagger$ ($b_{n,i}$) is the creation (annihilation) operator of the i-th harmonic vibrational degree of freedom with frequency ω_i on site n. The singlet (TT) vibronic couplings are encoded in H_{S-B} (H_{TT-B}), given by

$$H_{S-B} = \sum_{n,i} |n\rangle\langle n|\omega_i \lambda_{S,i}(b_{n,i} + \text{h.c.}), \tag{4.3a}$$

$$H_{TT-B} = \sum_{n=0}^{N-1} |T_n T_{n+1}\rangle\langle T_n T_{n+1}| \times \sum_i \omega_i \lambda_{T,i}(b_{n,i} + b_{n+1,i} + \text{h.c.}). \tag{4.3b}$$

The singlet-TT electronic coupling is (assuming periodic boundary conditions $|T_{-1}T_0\rangle = |T_{N-1}T_0\rangle$): [67]

$$H_{TT-S} = \frac{V_{TT-S}}{2} \sum_{n=0}^{N-1} \Big[\left(|T_n T_{n+1}\rangle + |T_{n-1}T_n\rangle\right)\langle n| + \text{h.c.}\Big]. \tag{4.4}$$

Finally the photonic degree of freedom is included in $H_p = \omega_{ph} a^\dagger a$ where $a^\dagger(a)$ is the creation (annihilation) operator of the cavity photonic mode. Its interaction with the singlet excitons is described by the light-matter Hamiltonian

$$\begin{aligned} H_{p-S} &= \sum_n g\left(a^\dagger |G\rangle\langle n| + \text{h.c.}\right) \\ &= \sqrt{N} g\left(a^\dagger |G\rangle\langle k=0| + \text{h.c.}\right) \\ &= \frac{\Omega}{2}\left(a^\dagger |G\rangle\langle k=0| + \text{h.c.}\right) \end{aligned} \tag{4.5}$$

where in the second line we have introduced a delocalized Fourier basis for the singlet excitons $|k\rangle = \frac{1}{\sqrt{N}} \sum_n e^{ikn}|n\rangle$ $k = \frac{2\pi m}{N}$, $m = 0, 1, 2, \ldots, N-1$. The $\sqrt{N}g$ term in (4.5) is the collective

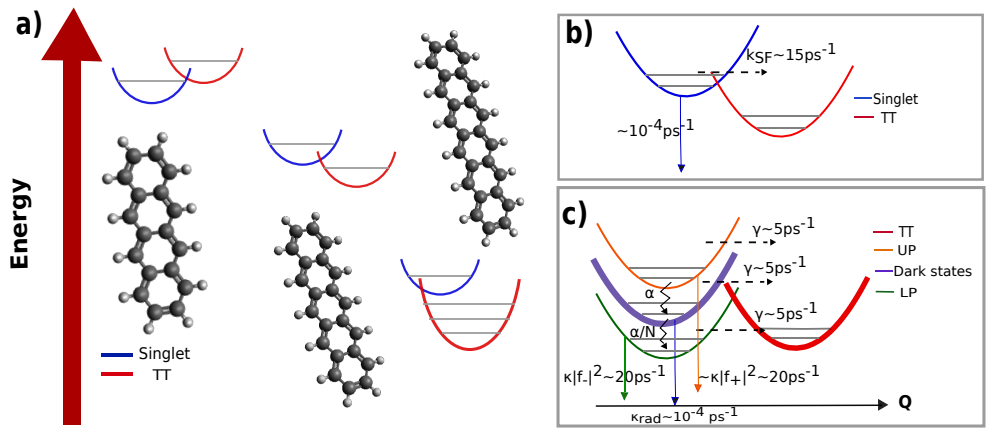

Figure 4.1: a) Bare triplet-triplet (red) and singlet (blue) vibronic energies of the different molecules considered. From left to right: tetracene, pentacene and hexacene. For clarity only the vibrational mode with highest frequency is shown. The SF dynamics is schematically shown for bare case (b) and the SC scenario (c). In (c) the fastest decay constant $\alpha \approx 100$ ps^{-1} is due to vibrational relaxation, γ is the dressed SF rate, κ is the cavity-photon leakage rate and $f_+(f_-)$ is the exciton fraction in the upper (lower) polariton. k_f is the singlet fluorescence decay rate. Continuous arrows denote radiative decay. Thicker lines indicate larger density of states. Approximate SF and relaxation rates for pentacene interacting with a resonant photonic mode are included. The decay timescale for the triplet-triplet state is significantly longer than the timescales considered here.

light-matter coupling and Ω is the so-called Rabi splitting. Importantly, the singlet excitons are optically bright, in contrast to the dark TT states [67]. Because of this property, our model does not feature a TT term analogous to Eq. (4.5).

In our approach we consider the reduced population dynamics of the manifold of TT states ($\{|T_nT_{n+1}\rangle\}$), the two polariton states ($|\pm\rangle$) and the so-called *dark states* ($\{|d\rangle = |k \neq 0\rangle\}$) that emerge from SC (see Fig. 4.1), where

$$|+\rangle = c_{ph}^{+}|G\rangle \otimes |1_{ph}\rangle + c_{ex}^{+}|k=0\rangle \otimes |0_{ph}\rangle, \tag{4.6a}$$

$$|-\rangle = c_{ph}^{-}|G\rangle \otimes |1_{ph}\rangle + c_{ex}^{-}|k=0\rangle \otimes |0_{ph}\rangle. \tag{4.6b}$$

with (zeroth-order) eigenenergies given by

$$\omega_{\pm} = \frac{\overline{\omega}_e + \omega_{ph}}{2} \pm \sqrt{\left(\frac{\overline{\omega}_e - \omega_{ph}}{2}\right)^2 + \left(\sqrt{N}g\right)^2}, \tag{4.7}$$

In Eq. (4.6), $|n_{ph}\rangle$ is the state with n photons in the photonic space and $|+\rangle$ ($|-\rangle$) is the upper (lower) polariton state. Meanwhile, $c_{ph}^{\pm}$ and $c_{ex}^{\pm}$ are the Hopfield coefficients for the photon and exciton components of the polariton states [5]. The reduced dynamics is described by means of a Pauli master equation derived using the Redfield formalism under the secular and Markov approximations [65] (see SI). The kinetic model can be summarized by the following equations,

$$\begin{aligned}\partial_t P_{\pm}(t) = &-f_{\pm}\frac{\alpha(\omega_{\pm D})}{N}(N-1)P_{\pm} + f_{\pm}\frac{\alpha(\omega_{D\pm})}{N}P_D^{total} \\ &- f_{\pm}\frac{\gamma(\omega_{TT,\pm})}{N}(N)P_{\pm} + f_{\pm}\frac{\gamma(\omega_{\pm,TT})}{N}P_{TT}^{total} \\ &- \left(f_{\pm}k_c(\omega_{\pm}) + f_{\pm}^p k_{phot}\right)P_{\pm},\end{aligned} \tag{4.8a}$$

$$\begin{aligned}\partial_t P_D^{total}(t) = &\, f_+\alpha(\omega_{+D})P_+ - f_+\frac{\alpha(\omega_{D+})}{N}P_D^{total} \\ &+ f_-\alpha(\omega_{-D})P_- - f_-\frac{\alpha(\omega_{D-})}{N}P_D^{total} \\ &- \gamma(\omega_{TT,D})P_D^{total} + \gamma(\omega_{D,TT})P_{TT}^{total} \\ &- k_c(\omega_D)P_D^{total},\end{aligned} \tag{4.8b}$$

$$\begin{aligned}\partial_t P_{TT}^{total}(t) = &\, f_+\gamma(\omega_{TT,+})P_+ - f_+\frac{\gamma(\omega_{+,TT})}{N}P_{TT}^{total} \\ &- \gamma(\omega_{D,TT})P_{TT}^{total} + \gamma(\omega_{TT,D})P_D^{total} \\ &+ f_-\gamma(\omega_{TT,-})P_- - f_-\frac{\gamma(\omega_{-,TT})}{N}P_{TT}^{total},\end{aligned} \tag{4.8c}$$

Table 4.1: Summary of bare material-dependent parameters. The values for $\frac{V_{TT-S}}{2}$ and $\Delta G = \omega_{TT} - \omega_e$ were taken from [64]. Based on these, we calculate the bare SF rates k_{SF} and bare TT yields ε_{TT}. Importantly, ε_{TT} is calculated assuming that SF competes with the fast singlet decay process (charge production) $k_{CT} = 17$ ps^{-1}, discussed in the main text.

Molecule	$V_{TT-S}/2$ (meV)	ΔG (meV)	k_{SF} (ps^{-1})	ε_{TT} (%)
Tetracene	41.5	150	0.01	0.01
Pentacene	42	-110	17	100
Hexacene	22	-630	6	48

where $P_+(t)$ ($P_-(t)$) is the population in the $|+\rangle$ ($|-\rangle$) state and P_D^{total} ($P_{TT}^{total}(t)$) is the total population in the dark (TT) state manifold. $f_\pm^p = |c_{ph}^\pm|^2$ and $f_\pm = |c_{ex}^\pm|^2$; $\omega_D = \overline{\omega}_e$ and $\omega_{ab} = \omega_a - \omega_b$. In Eqs. (4.8a)-(4.8c), we phenomenologically introduce the rate constant $k_c(\omega)$ to account for the contribution to the decay rate of the dressed states due to their singlet exciton fraction. $k_c(\omega)$ can be for instance radiative relaxation of the singlet to the ground electronic state via modes that are weakly-coupled to light (e.g. leaky modes or surface plasmon-polaritons in DBR and metal cavities, respectively), non-radiative decay, or its conversion into charges at the interface with charge acceptors, which is the case in donor-acceptor blends used for organic solar cells. The various cases are treated in more detail below.

The $\alpha(\omega)$ transfer rates appearing in Eqs. (4.8a)-(4.8c) are calculated in terms of a spectral density and thermal populations at frequency ω. The $\gamma(\omega)$ rates are computed by means of a Bixon-Jortner-like [68] equation adapted to the SC regime. For sake of simplicity, in the calculation of the latter the vibrational bath is treated by using an effective high (low) frequency $\overline{\omega}_h$ ($\overline{\omega}_l$) that satisfies $\overline{\omega}_h \gg 1/\beta$ ($\overline{\omega}_l \ll 1/\beta$), to which we associate a so-called inner (outer) sphere reorganization energy [69]. We refer the reader to the SI for details of the derivation and other relevant parameters employed in the calculation of $\alpha(\omega)$ and $\gamma(\omega)$. Finally, $\Delta G = \omega_{TT} - \omega_e$, and $V_{TT-S}/2$ are treated as material-dependent; they are taken from Ref. [64] and are summarized in Table 4.1.

4.3 Discussion of results

We first consider the population dynamics of bare (cavity-free) systems containing one of the acene molecules,

$$\frac{dP_S(t)}{dt} = -\big(k_{SF} + k_c(\omega_D)\big)P_S(t) + k_{TF}P_{TT}(t) \tag{4.9a}$$

$$\frac{dP_{TT}(t)}{dt} = k_{SF}P_S(t) - k_{TF}P_{TT}(t) \tag{4.9b}$$

where $P_S(t)$ ($P_{TT}(t)$) is the population of the singlet (TT) electronic state of a given acene, k_{SF} is the bare SF rate, and k_{TF} is the bare triplet fusion rate, which corresponds to the reverse process to SF. k_{SF} and k_{TF} are calculated by means of the Bixon-Jortner equation [68], with the parameters in Table (4.1). For all cases we compute $P_S(t)$ and $P_{TT}(t)$ assuming $P_S(0) = 1$, $P_{TT}(0) = 0$ (see Fig. 4.2). Under these conditions, we define the TT yield

$$\varepsilon_{TT}(t^* \gg 0) = 200\% \times P_{TT}(t^*) \tag{4.10}$$

as the relevant figure of merit for our subsequent analysis where t^* was chosen to reach a stationary $P_{TT}(t)$ value for pentacene and hexacene. We notice that when $k_c(\omega) = k_f = O(10^{-4})$ ps^{-1} (fluorescence rate) pentacene an hexacene are expected to exhibit a 200% TT yield in view of $k_{SF} \gg k_f$ and $k_{TF} = e^{\beta\Delta G}k_{SF} \ll k_{SF}$ (detailed balance, where β is the inverse temperature). This contrasts with tetracene, in view of its higher TT energy compared to the singlet, *i.e.* $\omega_{TT} > \omega_e$, so that $k_{SF} \ll k_{TF}$ and the TT population decays to zero for long t). The experimental TT yield of tetracene is well above zero [70, 71], which is in contrast with our findings (see Fig. 4.2). The reason is that the mechanism that leads to this unexpected yield is not considered in our model and related to entropic gain [72]. We opted to analyze the results that follow from our model, which should be valid in a similar energetic singlet and TT arrangement and in the absence of the

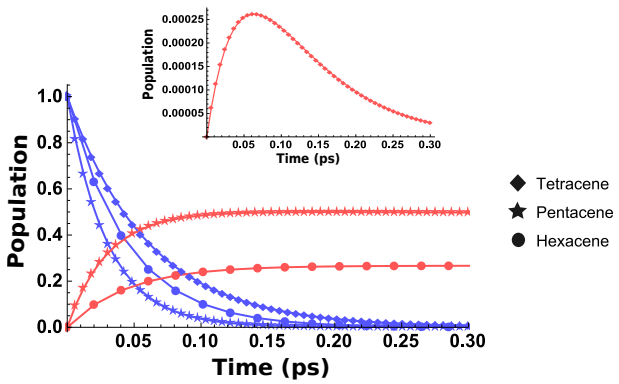

Figure 4.2: Time evolution of populations in the singlet (blue) and TT electronic states (red) of the molecules considered in this chapter in the bare case. We consider the initial conditions that follow from pumping the singlet state at $t = 0$ ($P_S(t = 0) = 1 P_{TT}(t = 0) = 0$), for all the molecules in question. Inset: time evolution of $P_{TT}(t)$ for tetracene.

aforementioned entropic mechanism.

In organic solar cells TT yield is typically below 200% because the processes of singlet migration and charge separation are fast enough to compete with k_{SF} [21]. To consider a similar situation, we assume that the singlet state quickly decays to a charge-transfer state. In our model, this would correspond to a scenario where there is a charge-acceptor next to each of the acene molecules of the chain. For simplicity and for the purpose of showing the possibilities of control of TT yield by polaritonic means, we assume $k_c(\omega) = \delta_{\omega_D,\omega} k_{CT}$, ($\delta_{i,j}$ being the Kronecker delta function) where k_{CT} is equal to the bare pentacene rate $k_{SF} = 17$ ps^{-1}. The form introduced for $k_c(\omega)$ is approximately correct as long as the spectral density describing the singlet-charge-transfer state is peaked around ω_D and decays quickly with ω. The aforementioned k_{CT} value is experimentally reasonable as it has been observed in solar cells with a thin slab of SF material [21].

We use Eq. (4.10) to compute the ε_{TT} values summarized in Table 4.1 in the presence of k_{CT}. Our definition of yield is thus different from that obtained in steady-state, but follows the spirit of many experiments that measure SF using time-domain spectroscopy techniques.

Turning now to the polariton-assisted SF case, the non-trivial dynamics that emerge are due to differences in the density of states (DOS) between the polariton and exciton manifolds, as

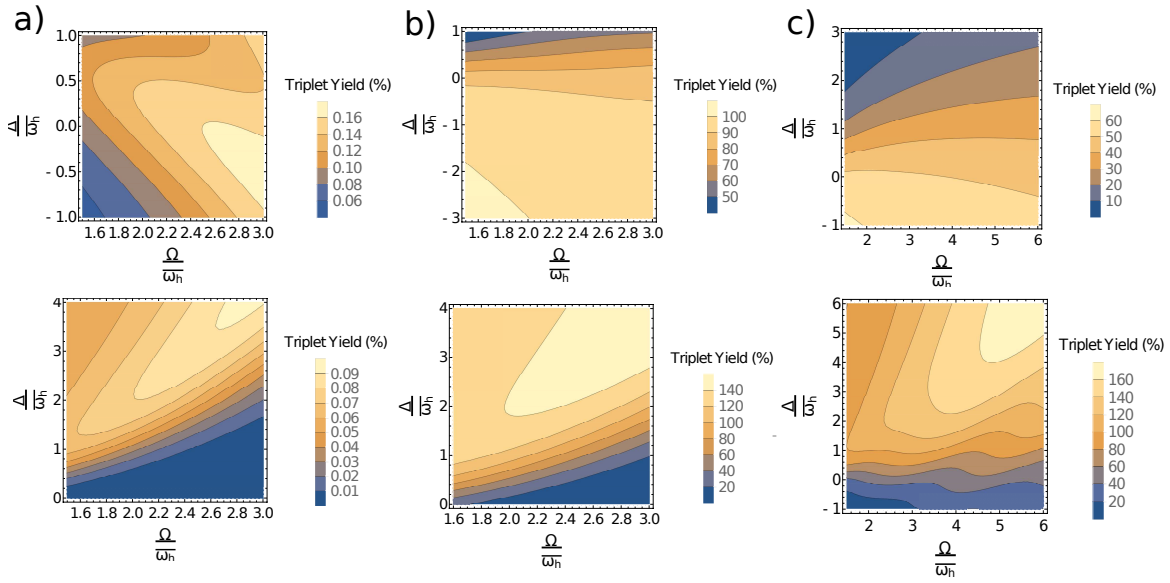

Figure 4.3: TT yield as a function of $\Delta/\overline{\omega}_h = (\omega_{ph} - \omega_e)/\overline{\omega}_h$ and $\Omega/\overline{\omega}_h$ featured by a) tetracene, b) pentacene and c) hexacene. The upper (lower) plot considers the initial conditions of pumping the upper (lower) polariton, *i.e.* $P_+(0) = 1$,$P_{a\neq+}(0) = 0$ ($P_-(0) = 1$, $P_{a\neq-}(0) = 0$) .

well as to the photonic character of each polariton state. These traits are encoded in the prefactors $f_\pm$, $f_\pm^p$, N and $1/N$ in Eqs. (4.8a)-(4.8c). Notably, in the $N \gg 1$ limit, the transfer rates from P_D^{total} and P_{TT}^{total} to the polariton manifold are largely suppressed. This is a consequence of the large DOS of the former (which act like a population sink) and the small DOS of the latter (which is spectrally isolated). The reverse transfers are fast as they have single-molecule relaxation scalings and correspond to going *into* the population sink. Similar findings are reported in Ref. [73], in the context of the dynamics of molecular vibrations under the SC regime and in [12, 13] for exciton polaritons. Therefore, once population reaches the dark and TT states, it is no longer transferred to the polariton manifold, and the subsequent dynamics is determined by transfer rates between dark and TT states. We stress, however, that the suppression of transfer rates between P_D^{total}, P_{TT}^{total} and the polariton manifold is approximate as we are ignoring the polariton bandwidth that emerges from the many photonic modes hosted by the microcavity, which yields non-zero transfer rates between the aforementioned manifolds [9].

We performed numerical simulations of the dynamics of the polariton-assisted scenario by

assuming two different initial conditions: pump of the upper polariton (UP) $\big(P_+(0)=1, P_{a\neq+}(0)\big)$ and of the lower polariton (LP) $\big(P_-(0)=1, P_{a\neq0}(0)\big)$ for all molecules. We denote $\tilde{\varepsilon}_{TT}$ the polariton-assisted TT yields. They were calculated using the same criteria as in Eq. (4.10). From a comparison of ε_{TT} (Table 4.1) and $\tilde{\varepsilon}_{TT}(\Delta,\Omega)$ values (Fig. 4.3), where the detuning $\Delta=\omega_{ph}-\omega_D$, we notice enhancement in the TT yield for hexacene, especially for the pumping of the lower polariton. Under these conditions and high Δ values, the state $|-\rangle$ is almost purely excitonic ($f_-\approx 1$), and the rate of the channel associated to photon leakage is supressed. Moreover, ω_- becomes closer to resonance with the third vibrational state of the TT manifold (with frequency $\overline{\omega}_h$) for a given range of Ω. Thus population transfer $|-\rangle\rightarrow\{|T_nT_{n+1}\rangle\}$ is faster than the bare SF, as the energetic barrier is lower in the former. Finally, there is no competition between the previous transfer process and the decay channel associated to k_c, as $k_c(\omega_-)=0$, under the assumptions of our model. The enhancement considering pumping of the UP for the same molecule is weaker since the fast rate of the transfer $|+\rangle\rightarrow\{|d\rangle\}$ competes with the rate of $|+\rangle\rightarrow\{|T_nT_{n+1}\rangle\}$.

Pentacene shows a similar behavior: when pumping the UP and if $\Delta\approx-\overline{\omega}_h$, then $|+\rangle$ is mainly excitonic and population of the TT states is mainly determined by transfer from the dark state manifold, since $f_+\alpha(\omega_{+D})\gg\gamma(\omega_{TT,+})$ *i.e.* the population from the upper polariton is quickly transferred to dark states before transfer to TT states is carried out. Hence, noting that $\gamma(\omega_{TT,D})\approx k_{SF}$, we recover (the bare) pentacene ε_{TT}. Notice however that for large detunings $\tilde{\varepsilon}_{TT}(\Delta\approx-3\overline{\omega}_h,\Omega\approx1.6\overline{\omega}_h)>\varepsilon_{TT}$ because a phonon blockade prevents fast decay into dark states and also the charge-transfer decay channel is suppressed ($k_c(\omega_+)=0$). On the other hand, for the pump of the LP $\tilde{\varepsilon}_{TT}$ values are higher as a consequence of a slower transfer rate ($\alpha(\omega_{-D})$) to the dark statesrates in such a way that the predominant transfer process is from $|-\rangle$ to TT states.

Tetracene shows a distinct behavior in view of the bare energetic arrangements of its singlet and TT states (see Fig. 4.1). More concretely we have $f_-\gamma(\omega_{TT,-}), f_+\gamma(\omega_{TT,+}), \gamma(\omega_{TT,D})\ll$

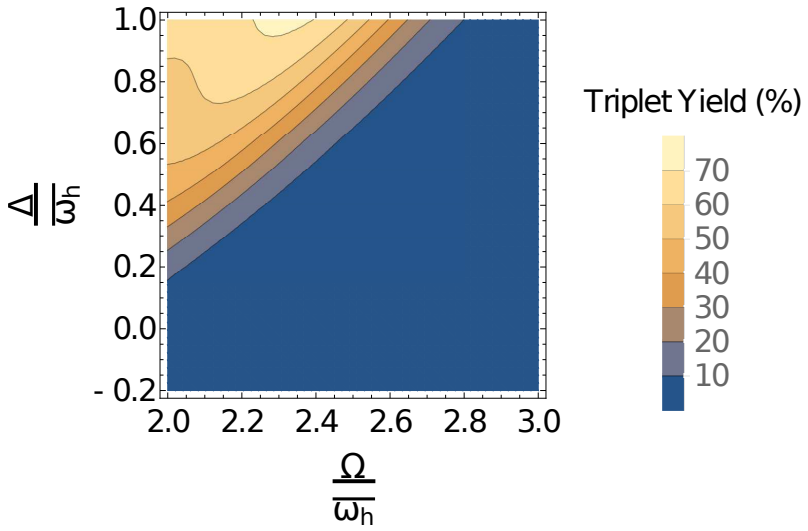

Figure 4.4: TT yield as a function of $\Delta/\overline{\omega}_h = (\omega_{ph} - \omega_e)/\overline{\omega}_h$ and $\Omega/\overline{\omega}_h$ featured by a molecule with $V_{S-TT} = 44$ meV , $\Delta G = -630$ meV, and an outer reorganization energy of 5 meV. We consider the initial conditions of pumping the lower polariton ($P_-(0) = 1$, $P_{a\neq -}(0) = 0$). In this case is that the only competing decay channel with SF is fluorescence.

$\gamma(\omega_{D,TT})$ for most of the explored (Δ,Ω) values. This translates into a rapid depletion of the population of the TT manifold during the considered timescale; which is a consequence of the energy of the TT states lying above the dark state energy, in such a way that the rate of population depletion of TT states towards the dark states outcompetes the rate of the inverse process (in view of detailed balance) as well as rates from the polariton manifold to the TT states. The largest $\tilde{\varepsilon}_{TT}$ values are reached when pumping the UP and parameters (Δ,Ω) which yield a predominant excitonic character to $|+\rangle$ and a sufficiently high rate for $|+\rangle \rightarrow \{|T_nT_{n+1}\rangle\}$ process, such that it can better compete with the rates associated to $|+\rangle \rightarrow \{|d\rangle\}$ and $\{|T_nT_{n+1}\rangle\} \rightarrow \{|d\rangle\}$. Considering the pumping of the LP, the maximal $\tilde{\varepsilon}_{TT}$ values are lower in view of $\omega_{TT} - \omega_- > 0$, which greatly diminishes the rate for the transfer $|-\rangle \rightarrow \{|T_nT_{n+1}\rangle\}$.

So far, we have predicted results on SF materials that feature high TT yields by default in the absence of fast quenching mechanisms. We wonder if anything interesting remains if the latter mechanisms are absent, i.e., if we set $k_c(\omega) = k_f = 2.5 \times 10^{-4}\,\mathrm{ps}^{-1}$ as an approximate fluorescence slow decay rate. To address this, we consider a poor SF material with an outer sphere

reorganization energy of 5 meV, keeping the rest of the parameters as for hexacene. This situation could correspond to hexacene in a solvent that significantly increases the outer sphere SF energy barrier, in which case we find $\varepsilon_{TT} = 18\%$. For this case and the initial conditions that derive from pumping the LP, we observe $\tilde{\varepsilon}_{TT} > \varepsilon_{TT}$ for values (Δ, Ω) (see Fig. 4.4) which correspond to a transfer process $|-\rangle \rightarrow \{|T_n T_{n+1}\rangle\}$ whose rate competes with the rate of $|-\rangle \rightarrow \{|d\rangle\}$. This occurs when ω_- is close to resonance with one of the high-frequency vibronic states of the TT states and $|-\rangle$ is predominantly excitonic. This system would give a straightforward verification of polariton assisted SF in the absence of a fast quenching process.

4.4 Conclusions

To summarize, in this chapter, we have shown that when SF materials are subjected to SC with a microcavity mode, the photonic leakage of the resulting polariton states constitutes an important decay channel that can decrease TT production compared to the bare case. However, the rates associated with this competing decay channel can be tuned by modifying the ratio Δ/Ω (see Fig. 4.3), in such a way that the dynamics are dictated by the energy differences and the DOS of the dressed states involved in SF. Given the large DOS of the dark state manifold and TT states, the TT state must lie lower in energy with respect to the singlet so as to avoid population leakage towards the dark state manifold. Remarkably, while hexacene is a poor SF candidate in the bare case (and in presence of quenchers), it is the material which features the highest enhancement by means of the proposed polaritonic approach and can even outcompete the bare pentacene TT yield under the conditions considered in this work. Similarly, we notice the introduction of TT yield enhancement for pentacene, although the improvements are modest in comparison with those obtained for hexacene. Finally, we have also considered the putative scenario of a SF material with low TT yield, where the SF rate competes with fluorescence. In this case, our model predicts (for acene-like molecules) that $\Delta G \ll 0$ is required to introduce enhancement in TT yields by

polariton methods.

This chapter, in full, is adapted from the material as it appears in "Polariton-Assisted Singlet Fission in Acene Aggregates" Martínez-Martínez L. A., Du M., Ribeiro R. F. and Yuen-Zhou J., J. Phys. Chem. Lett., 9, 1951 (2018). The dissertation author was the primary investigator and author of this material.

Chapter 5

Triplet harvesting in the polaritonic regime: a variational polaron approach

5.1 Introduction

In addition to the applications discussed in the previous chapters, polariton setups have also emerged as promising candidates to boost the efficiency and versatility of light-emitting diodes (LEDs) [74] and organic photodiodes (OPDs) [75]. As a proof of concept, electrical injection of carriers into inorganic polariton architectures has been shown to modulate light-matter coupling [76], thus opening new avenues towards polariton-based optoelectronic switches. Similarly, organic LEDs have been demonstrated utilizing molecular dyes in the ultrastrong coupling regime [77, 78, 79] and it has been recently shown that materials operating in the latter can feature a complete inversion of molecular dark and light-emissive states [80]. These exciting applications prompt the development of theoretical models to account for experimental observations of the molecular SC regime [73, 15, 16, 81], as well as to rationally design new polaritonic setups that could enhance chemical processes of contemporary interest [19].

In this chapter, we explore the triplet electroluminescence efficiency of a microcavity

containing molecules which feature a range of electronic parameters and couplings to the condensed phase vibrational bath. The developed model aims to describe polaritonic OLEDs like those reported in [38, 79], so we consider that (optically dark) triplet excitons are generated upon electrical injection and the latter can transition into fluorescent singlet states that emit light. Our approach relies on a master equation operating in a variationally optimized polaron frame, originally introduced by Silbey and Harris [82, 83] with generalizations due to Pollock [23], Wu [24], and their respective coworkers. The foundation of this method lies on the application of a unitary transformation to the total Hamiltonian which yields renormalized system and system-bath interactions that are weak enough to be perturbatively treated.

The outline of this chapter is summarized as follows. In section 5.2, we introduce our quantum mechanical model and the variational approach to address its dynamics. Next, in section 5.3, we give a formal definition of the triplet electroluminescence efficiency and describe our approach to calculate the time-evolution of populations in the relevant chemical states of the system. Then, in section 5.4, we apply our approach to systems in two regimes of coupling to vibrational degrees of freedom. In section 5.5, we identify the main limitation that must be overcome to reach a polariton-enhanced triplet-harvesting regime and propose an approach to circumvent this drawback. Finally, in section 5.6 we summarize this study and conclude with an outlook of how polaritons could enhance the optoelectronic properties of molecular materials.

5.2 Theory

We consider an ensemble of N identical molecules embedded in an optical microcavity and interacting with the electromagnetic modes supported by the latter; for simplicity, we describe a single photonic mode interacting with the molecular ensemble, a coarse-graining approximation which is based on the much larger density of states (DOS) of the molecular degrees of freedom compared to the photonic ones [73, 84]. Thus, N should not be interpreted as the total number

of molecules in the cavity, but rather as the average number of molecules that couple to a single photon mode.

The Hamiltonian of our model can be written as

$$\begin{aligned} H =& H_S + H_B + H_{S-B} + H_{ph} \\ &+ H_{S-ph} + H_T + H_{T-B} + H_{S-T}. \end{aligned} \tag{5.1}$$

Each molecule is modeled as a three-level electronic system, namely a singlet electronic ground state and two excited states with singlet and triplet spin characters, respectively. The energetics of the latter are correspondingly described by H_S and H_T. Assuming electrical pumping in the linear regime, we can restrict the Hamiltonian to the single excitation manifold such that,

$$H_S = \sum_{n=0}^{N-1} \varepsilon_S |n\rangle\langle n|, \tag{5.2a}$$

$$H_T = \sum_{n=0}^{N-1} \varepsilon_T |T_n\rangle\langle T_n|. \tag{5.2b}$$

Here, $|n\rangle$ ($|T_n\rangle$) denotes a localized singlet (triplet) exciton at the nth molecular site and ε_S (ε_T) is the vertical singlet (triplet) electronic excitation energy, while ($\hbar = 1$)

$$H_B = \sum_{v} \sum_{n=0}^{N-1} \omega_v b_{v,n}^\dagger b_{v,n} \tag{5.3}$$

accounts for the vibrational degrees of freedom in the condensed phase environment, where $b_{v,n}^\dagger$ ($b_{v,n}$) is the creation (annihilation) operator for an excitation in the v-th harmonic mode with frequency ω_v on site n. The mode-dependent singlet (triplet) vibronic couplings $g_S^{(v)}$ ($g_T^{(v)}$) are included in H_{S-B} (H_{T-B}):

$$H_{S-B} = \sum_{v}\sum_{n} |n\rangle\langle n| g_S^{(v)} (b_{v,n} + \text{h.c.}), \tag{5.4a}$$

$$H_{T-B} = \sum_{v}\sum_{n} |T_n\rangle\langle T_n| g_T^{(v)} (b_{v,n} + \text{h.c.}). \tag{5.4b}$$

The singlet-triplet intersystem crossing electronic coupling is given by

$$H_{S-T} = V_{ST} \sum_{n} \left(|n\rangle\langle T_n| + \text{h.c.} \right). \tag{5.5}$$

Finally, the photonic microcavity degree of freedom is encoded in

$$H_{ph} = \omega_{ph} |G, 1_{ph}\rangle\langle G, 1_{ph}|, \tag{5.6}$$

where $|G, 1_{ph}\rangle$ accounts for the state of all molecules in the electronic ground state and one excitation in the photonic mode and its interaction with singlet excitons (in the rotating wave approximation, RWA) is described by

$$H_{S-ph} = \sum_{n} g \left(|G, 1_{ph}\rangle\langle n| + \text{h.c.} \right), \tag{5.7}$$

g being a single-molecule dipolar coupling. To describe the emergent dynamics upon electrical pumping of the optically dark triplet states, we employ a variational polaron transformed master equation. The latter has proven to reproduce reliable quantum dynamics in a wide range of coupling strengths between electronic degrees of freedom and phononic reservoirs [85], while being computationally inexpensive compared to more accurate approaches such as path integral [86, 87], multi-configuration time-dependent Hartree [88, 89], hierarchical equations of motion [90], linearized density matrix evolution [91], surface-hopping [92, 93, 94] and exact factorization [95] formulations. In particular, we consider a similar multi-site approach to the one developed

by Pollock and coworkers [23], who considered a variational polaron transformation to compute population dynamics in exciton networks with local phonon reservoirs. Furthermore, we adapt a generalization introduced by Wu and coworkers [24] who treated the photon-exciton and exciton-vibration on equal footing to describe the photoluminiscence and vibrational dressing in polaritonic setups. As a first step towards the development of a master equation, the Hamiltonian in Eq. (5.1) is transformed to the so-called polaron frame, for which we introduce the unitary transformation e^P, where

$$\begin{aligned} P = &\sum_{n=0}^{N-1}\sum_{v}|n\rangle\langle n|\left[\sum_{l}(b^{\dagger}_{v,n+l}-b_{v,n+l})\frac{f_l^{(v)}}{\omega_v}\right] \\ &+\sum_{n=0}^{N-1}\sum_{v}|G,1_{ph}\rangle\langle G,1_{ph}|\left[(b^{\dagger}_{v,n}-b_{v,n})\frac{h^{(v)}}{\omega_v}\right] \\ &+\sum_{n=0}^{N-1}\sum_{v}|T_n\rangle\langle T_n|(b^{\dagger}_{v,n}-b_{v,n})\frac{f_T^{(v)}}{\omega_v} \\ \equiv &\sum_{n=0}^{N-1}\left[|n\rangle\langle n|\hat{D}_S^{(n)}+|G,1_{ph}\rangle\langle G,1_{ph}|\hat{D}_{ph}+|T_n\rangle\langle T_n|\hat{D}_T^{(n)}\right] \end{aligned} \tag{5.8}$$

is partially based on previous works [24, 96]. According to the ansatz in Eq. (5.8), the electronic and photonic degrees of freedom are dressed with vibrational bath excitations to an extent quantified by the set of parameters $\{f_l^{(v)}, f_T^{(v)}, h^{(v)}\}$ which are variationally determined, as will be explained below. The summation over l in Eq. (5.8) assumes that the vibrational deformation can be extended over all sites in the singlet excited manifold (large polaron limit) as a result of the interaction of all optically bright singlet excitons to the same photon mode. Since the electronic triplet states do not directly interact with the photonic mode, the vibrational deformation of the triplet excited manifold is expected to be more localized (small polaron limit). In the polaron frame we have

$$e^{P}He^{-P} = \tilde{H}_0 + \tilde{H}_I + H_B, \tag{5.9}$$

where

$$\begin{aligned}\tilde{H}_0 =& \sum_n \tilde{\varepsilon}_S |n\rangle\langle n| + \sum_n \tilde{\varepsilon}_T |T_n\rangle\langle T_n| + \tilde{\omega}_{ph} |G,1_{ph}\rangle\langle G,1_{ph}| \\ &+ g\eta_{S-ph} \sum_n \left(|n\rangle\langle G,1_{ph}| + \text{h.c.} \right) \\ &+ V_{ST}\eta_{ST} \sum_n \left(|n\rangle\langle T_n| + \text{h.c.} \right). \\ =& \tilde{H}_{0,k=0} + \sum_{k\neq 0} \tilde{H}_{0,k}\end{aligned} \tag{5.10}$$

and

$$\begin{aligned}\tilde{H}_{0,k=0} =& \tilde{\varepsilon}_S |k=0\rangle\langle k=0| + \tilde{\varepsilon}_T |T_{k=0}\rangle\langle T_{k=0}| \\ &+ \tilde{\omega}_{ph} |G,1_{ph}\rangle\langle G,1_{ph}| \\ &+ \frac{\Omega}{2}\eta_{S-ph} \left(|k=0\rangle\langle G,1_{ph}| + \text{h.c.} \right) \\ &+ V_{ST}\eta_{ST} \left(|k=0\rangle\langle T_{k=0}| + \text{h.c.} \right), \end{aligned} \tag{5.11a}$$

$$\tilde{H}_{0,k\neq 0} = \tilde{\varepsilon}_S |k\rangle\langle k| + \tilde{\varepsilon}_T |T_k\rangle\langle T_k| + V_{ST}\eta_{ST} \left(|k\rangle\langle T_k| + \text{h.c.} \right). \tag{5.11b}$$

In Eqs. (5.10-5.11) we introduced a delocalized Fourier basis for the singlet $|k\rangle = \frac{1}{\sqrt{N}} \sum_n e^{ikn} |n\rangle$ and triplet excitons $|T_k\rangle = \frac{1}{\sqrt{N}} \sum_n e^{ikn} |T_n\rangle$, with $k = \frac{2\pi}{N}$, $m = 0, 1, 2, \ldots, N-1$. In this basis, the state $|k=0\rangle$ couples to the photonic mode with a superradiantly enhanced strength given by $\sqrt{N}g = \Omega/2$. The renormalized on-site energies in (5.10) are given by

$$\tilde{\varepsilon}_S = \varepsilon_S + \sum_v \left(\sum_l \frac{f_l^{(v)2}}{\omega_v} - 2g_S^{(v)} \frac{f_0^{(v)}}{\omega_v} \right) \tag{5.12a}$$

$$\tilde{\varepsilon}_T = \varepsilon_T + \sum_v \left(\frac{f_T^{(v)2}}{\omega_v} - 2g_T^{(v)} \frac{f_0^{(v)}}{\omega_v} \right) \tag{5.12b}$$

$$\tilde{\omega}_{ph} = \omega_{ph} + \sum_v N \frac{h^{(v)2}}{\omega_v} \tag{5.12c}$$

and the renormalization constant η_{ST} (η_{S-ph}) is the thermal average of the relative displacement operator between the singlet and triplet (photonic) harmonic potential energy surfaces,

$$\begin{aligned}
\eta_{S-ph} &= \langle e^{\hat{D}_S^{(n)}} e^{-\hat{D}_{ph}} \rangle \\
&= \exp\left[-\frac{1}{2} \sum_{l,v} \left(\frac{(f_l^{(v)} - h^{(v)})^2}{\omega_v^2} \right) \coth(\beta\omega_v/2) \right], \\
\eta_{ST} &= \langle e^{\hat{D}_S^{(n)}} e^{-\hat{D}_T^{(n)}} \rangle \\
&= \exp\Bigg\{ -\frac{1}{2} \sum_v \Bigg[\frac{(f_0^{(v)} - f_T^{(v)})^2}{\omega_v^2} \\
&\quad + \sum_{l\neq 0} \frac{|f_l^{(v)}|^2}{\omega_v^2} \Bigg] \coth(\beta\omega_v/2) \Bigg\},
\end{aligned}$$

where $\langle A \rangle = \frac{\mathrm{Tr}_B\{Ae^{-\beta H_B}\}}{Z_{H_B}}$, $\mathrm{Tr}_B\{\cdot\}$ denoting a trace over the vibrational degrees of freedom, β being the inverse temperature, and $Z_{H_B} = \mathrm{Tr}_B\{e^{-\beta H_B}\}$ being the vibrational partition function. Notice that by taking $f_l^{(v)} = g_S^{(v)}\delta_{l,0}$ in Eq. (5.12a), we recover the full-polaron transformation for the singlet excitation, and $R_S = -\lambda_S = -\sum_v (g_S^{(v)})^2/\omega_v$, where λ_S is the reorganization energy of the singlet excited state. In Eqs. (5.10)–(5.11), we also introduced a partition of the Hamiltonian into the molecular contribution that is totally symmetric under site permutations $\tilde{H}_{0,k=0}$ and the non-totally-symmetric one $\sum_{k\neq 0} \tilde{H}_{0,k}$. Since $[\tilde{H}_{0,k=0}, \sum_{k\neq 0} \tilde{H}_{0,k}] = 0$, the eigenstates of $\tilde{H}_0$ can be

found by independent diagonalization of each contribution:

$$\tilde{H}_{0,k=0} = \tilde{\varepsilon}_{\mathrm{UP}}|\mathrm{UP}\rangle\langle\mathrm{UP}| + \tilde{\varepsilon}_{\mathrm{MP}}|\mathrm{MP}\rangle\langle\mathrm{MP}| + \tilde{\varepsilon}_{\mathrm{LP}}|\mathrm{LP}\rangle\langle\mathrm{LP}|, \tag{5.14}$$

where we define the upper (UP), middle (MP) and lower (LP) polariton states $|j\rangle = c_S^j|k = 0\rangle + c_T^j|T_{k=0}\rangle + c_{ph}^j|G, 1_{ph}\rangle$, $j = \mathrm{UP}, \mathrm{MP}, \mathrm{LP}$. On the other hand,

$$\sum_{k\neq 0} \tilde{H}_{0,k} = \sum_k \left[\tilde{\varepsilon}_+|k^{(+)}\rangle\langle k^{(+)}| + \tilde{\varepsilon}_-|k^{(-)}\rangle\langle k^{(-)}|\right] \tag{5.15}$$

describes mixed singlet-triplet eigenstates $|k^{(\pm)}\rangle = c_S^{\pm}|k\rangle + c_T^{\pm}|T_k\rangle$ with no photonic component, whose eigenenergies are given by $\tilde{\varepsilon}_{\pm} = \frac{\tilde{\varepsilon}_S+\tilde{\varepsilon}_T}{2} \pm \frac{1}{2}\sqrt{(\tilde{\varepsilon}_S - \tilde{\varepsilon}_T)^2 + 4V_{ST}^2\eta_{ST}^2}$. These states are commonly known as dark or exciton reservoirs [12, 13]. For clarity, we refer to the highest (lowest) energy eigenstates in Eq. (5.15) as the upper (lower) dark states. Notice that since we are ignoring inter-site couplings, we neglect the dispersive character of the exciton in the calculation of the eigenenergies (5.15), a valid assumption in view of the flat exciton dispersion relation compared to the photonic one in the k range of interest. The residual interaction Hamiltonian in Eq. (5.9) is

$$\tilde{H}_I = \tilde{V}_S + \tilde{V}_T + \tilde{V}_{ph} + \tilde{V}_{S-T} + \tilde{V}_{S-ph}, \tag{5.16}$$

which has been written as a sum of different contributions defined as follows,

$$\tilde{V}_S = \sum_v \sum_n |n\rangle\langle n| \Bigg[(g_S^{(v)} - f_0^{(v)})(b_{v,n}^\dagger + b_{v,n}) - \sum_{l\neq 0} f_l^{(v)} (b_{v,n+l}^\dagger + b_{v,n+l}) \Bigg], \tag{5.17a}$$

$$\tilde{V}_T = \sum_v \sum_n |T_n\rangle\langle T_n| \left[(g_T^{(v)} - f_T^{(v)})(b_{v,n}^\dagger + b_{v,n}) \right], \tag{5.17b}$$

$$\tilde{V}_{ph} = -\sum_v h^{(v)} |G, 1_{ph}\rangle\langle G, 1_{ph}| \sum_n \left(b_{v,n}^\dagger + b_{v,n} \right), \tag{5.17c}$$

$$\tilde{V}_{S-T} = \sum_n V_{ST} \left[e^{\hat{D}_S^{(n)} - \hat{D}_T^{(n)}} - \eta_{TS} \right] |n\rangle\langle T_n| + \text{h.c.}, \tag{5.17d}$$

$$\tilde{V}_{S-ph} = \sum_n g \left[e^{\hat{D}_S^{(n)} - \hat{D}_{ph}^{(n)}} - \eta_{S-ph} \right] |n\rangle\langle G, 1_{ph}| + \text{h.c.}. \tag{5.17e}$$

The calculation of the parameters $\{f_l^{(v)}, f_T^{(v)}, h^{(v)}\}$ is carried out by taking advantage of the Feynman-Bogoliubov inequality $F \leq F_0' + \langle \tilde{H}_I \rangle_{\tilde{H}_0'}$ [82, 83], where F (F_0') is the free energy of the system governed by H ($\tilde{H}_0' = \tilde{H}_0 + H_B$) and $\langle A \rangle_{\tilde{H}_0'} = \text{Tr}\{A e^{-\beta \tilde{H}_0'}\}[\text{Tr}\{e^{-\beta \tilde{H}_0'}\}]^{-1}$ where $\text{Tr}\{\cdot\}$ denotes the trace over the eigenstates of $\tilde{H}_0'$. Notice that by construction $\langle \tilde{H}_I \rangle_{\tilde{H}_0'} = 0$, and the leading correction to the exact equilibrium reduced density matrix is $O(\tilde{H}_I^2)$ [85], which justifies the (second order) perturbative treatment in $\tilde{H}_I$. It follows that the parameters $\{f_l^{(v)}, f_T^{(v)}, h^{(v)}\}$ can be found by minimizing $F_0' = -\beta^{-1}\text{Tr}\{e^{-\beta \tilde{H}_0}\}$, which amounts to solving $\frac{\partial F_0'}{\partial f_i^{(v)}} = \frac{\partial F_0'}{\partial h^{(v)}} = 0$. In our calculations, we consider a continuum vibrational bath limit, which is described in terms of the spectral densities $J_i(\omega) = \sum_v |g_v^i|^2 \delta(\omega - \omega_v) = a_i \frac{\omega^3}{\omega_c^2} e^{-\omega/\omega_c}$, $i = S, T$, where ω_c is a cutoff frequency, and a_i is the dimensionless parameter that encodes the strength of coupling between the excited electronic state with character i to the vibrational bath. In the discussion that follows, we focus on the calculation of the population dynamics of the chemically relevant species as well as of the electroluminescence efficiencies.

5.3 Dynamics in the polaron frame and definition of triplet electroluminescence efficiency

The open-quantum system dynamics associated with the Hamiltonian in Eq. (5.1) can be described in terms of the time evolution of the reduced density matrix (RDM) $\rho(t) = \mathrm{Tr}_B\{\rho_{tot}(t)\}$, ($\rho_{tot}(t)$ is the total density matrix), governed by the Liouville equation in the Schrödinger picture

$$\frac{d\rho(t)}{dt} = \mathcal{L}\rho(t) - \{\Gamma_{nrad} + \Gamma_{ph}, \rho(t)\},$$

where $\mathcal{L}\rho(t) = -i\mathrm{Tr}_B\{[H, \rho_{tot}(t)]\}$, and $\{\rho(t), \Gamma_i\} = \rho(t)\Gamma_i + \Gamma_i\rho(t)$; Γ_{rad}, Γ_{nrad}, Γ_{ph} phenomenologically account for the dissipative processes associated with the radiative and nonradiative decay of excitons [97], and photonic leakage, respectively. We define the triplet electroluminescence efficiency

$$\varepsilon = 2\int_0^\infty \mathrm{Tr}\left\{\Gamma_{ph}\rho(\tau)\right\} d\tau, \tag{5.18}$$

where the trace is taken over all the degrees of freedom, namely, the electronic, vibrational, and photonic. Eq. (5.18) is analogous to the integrated probability used to define the efficiency of energy trapping in chromophoric complexes [97], but in the present context, acquires the meaning of the efficiency of emission of a photon. Here, we define $\Gamma_{nrad} = \frac{k^S_{nrad}}{2}\sum_n |n\rangle\langle n| + \frac{k^T_{nrad}}{2}\sum_n |T_n\rangle\langle T_n|$ and $\Gamma_{ph} = \frac{\kappa}{2}|G, 1_{ph}\rangle\langle G, 1_{ph}|$, k^i_{nrad} being the nonradiative decay rate of electronic state $i = S, T$, and κ being the cavity photon leakage rate. Since

$$\begin{aligned}\mathrm{Tr}\{\Gamma_{ph}\rho_{tot}(t)\} =& \mathrm{Tr}\{\Gamma_{ph}e^{-P}\tilde{\rho}_{tot}(t)e^{P}\} \\ =& \mathrm{Tr}\{\Gamma_{ph}\tilde{\rho}_{tot}(t)\},\end{aligned} \tag{5.19}$$

ε is an invariant quantity under the polaron transformation. This last condition permits the computation of Eq. (5.18) in the polaron frame, where the time evolution of the polaron transformed RDM $\tilde{\rho}(t) = \mathrm{Tr}_B\{\tilde{\rho}_{tot}\}$ can be described in terms of second-order perturbation theory on $\tilde{H}_I$ within the secular Born-Markov approximation. This procedure guarantees that the long-time evolution of the polaritonic system properly thermalizes into the reduced equilibrium state due to $\tilde{H}_0$ which, due to the optimization of the variational parameters according to the Feynman-Bogoliubov bound (see Sec. 5.2), provides a good description of the equilibrium state of the full system involving electronic states, vibrations, and photon.

For the calculation of ε, we assume that the initial RDM corresponds to an incoherent mixture of localized excitations in the triplet electronic manifold, *i.e.,* $\sum_n \langle T_n|\tilde{\rho}(0)|T_n\rangle = 1$, $\sum_n \langle T_n|\tilde{\rho}(0)|n\rangle = \sum_n \langle T_n|\tilde{\rho}(0)|G,1_{ph}\rangle = \sum_n \langle n|\tilde{\rho}(0)|n\rangle = \langle G,1_{ph}|\tilde{\rho}(0)|G,1_{ph}\rangle = 0$. Under these assumptions, the initial RDM in the polaron frame can be written as

$$\vec{\tilde{\rho}}(0) \approx \begin{bmatrix} \langle \mathrm{UP}|\tilde{\rho}(0)|\mathrm{UP}\rangle \\ \langle \mathrm{MP}|\tilde{\rho}(0)|\mathrm{MP}\rangle \\ \langle \mathrm{LP}|\tilde{\rho}(0)|\mathrm{LP}\rangle \\ \sum_{k\neq 0}\langle k^+|\tilde{\rho}(0)|k^+\rangle \\ \sum_{k\neq 0}\langle k^-|\tilde{\rho}(0)|k^-\rangle \end{bmatrix} \approx \begin{bmatrix} 0 \\ 0 \\ 0 \\ |c_T^+|^2 \\ |c_T^-|^2 \end{bmatrix}, \tag{5.20}$$

where the approximation is the result of considering a localized initial state, which in the delocalized polaron picture translates into the population distributed uniformly among the dark and polariton states. Since the former feature a larger DOS than the latter, the population is predominantly concentrated in the dark states. We can rewrite Eq. (5.18) as

$$\varepsilon = \int_0^\infty \kappa P_{ph} \cdot \vec{\tilde{\rho}}(\tau) d\tau, \tag{5.21}$$

where the vector

$$P_{ph} = \begin{bmatrix} |c_{ph}^{UP}|^2 & |c_{ph}^{MP}|^2 & |c_{ph}^{LP}|^2 & 0 & 0 \end{bmatrix}$$

accounts for the photonic character of the different chemical species that take part in the population dynamics. The time evolution of $\vec{\tilde{\rho}}(\tau)$ is described in terms of a Pauli master equation in the secular Markovian approximation, where

$$\frac{d\vec{\tilde{\rho}}(t)}{dt} = \mathcal{M}\vec{\tilde{\rho}}(t). \tag{5.22}$$

For simplicity in the calculations and interpretation, we consider the evolution of the total population in the dark state manifolds $\sum_{k\neq 0}\langle k^{\pm}|\tilde{\rho}(t)|k^{\pm}\rangle$ rather than dissected among the individual populations $\{\langle k^{\pm}|\tilde{\rho}(t)|k^{\pm}\rangle\}$. The matrix $\mathcal{M}$ is given by

$$\mathcal{M}_{ij} = \begin{cases} k_{i\leftarrow j} & i \neq j \\ -\sum_{l\neq i} k_{l\leftarrow i} - \kappa_{phot}|\langle i|G,1_{ph}\rangle|^2 & i = j \\ -k_{nrad}^{T}\langle i|\, I_T\, |i\rangle - k_{nrad}^{S}\langle i|\, I_S |i\rangle & \end{cases} \tag{5.23}$$

where $k_{j\leftarrow i}$ is the rate of transfer from the state/manifold $|i\rangle$ to $|j\rangle$, and $I_T = \sum_n |T_n\rangle\langle T_n|$, $I_S = \sum_n |n\rangle\langle n|$. Using Eq. (5.22) together with Eq. (5.21), we have that

$$\varepsilon = -\kappa P_{ph}\mathcal{M}^{-1}\vec{\tilde{\rho}}(0). \tag{5.24}$$

To get further insight into the contributions of the different pathways of population transfer to ε, we consider a Green's function partition approach [97], under which

$$\mathcal{M}^{-1} = \mathcal{M}_{npol}^{-1} - \mathcal{M}_{npol}^{-1}\mathcal{M}_{pol}\mathcal{M}^{-1}, \tag{5.25}$$

where we let $\mathcal{M} = \mathcal{M}_{pol} + \mathcal{M}_{npol}$, $\mathcal{M}_{pol}$ being the rate matrix that accounts for the feed and depletion of polariton states only, which amounts to considering the rates $k_{i\leftarrow j}$ where either i or $j \in \{|UP\rangle, |MP\rangle, |LP\rangle\}$ while setting the other entries of $\mathcal{M}$ to 0. Using Eqs. (5.24) and (5.25),

$$\varepsilon = \varepsilon_{dir} + \varepsilon_{indir}$$

where $\varepsilon_{dir} = \kappa P_{ph} \mathcal{M}_{npol}^{-1} \mathcal{M}_{pol} \mathcal{M}^{-1} \vec{\tilde{\rho}}(0)$, $\varepsilon_{indir} = -\kappa P_{ph} \mathcal{M}_{npol}^{-1} \vec{\tilde{\rho}}(0)$, and ε can be written as a sum of a contribution due to polariton-participating processes and another one where they do not play a role.

5.4 Results and discussion

Based on the approach above, we are particularly interested in the dependence of ε with Rabi energy Ω and detuning between the cavity photon and the vertical singlet energy transition ($\Delta = \omega_{ph} - \varepsilon_S$), considering molecular emitters which feature different regimes of interaction with the vibrational bath degrees of freedom (DOFs). For that purpose, we introduce two cases based on parameters chosen to represent a wide range of organic molecular emitters.

First, we consider (large) strengths of coupling to the vibrational environment $a_S = 10$, $a_T = 15$, and a frequency cutoff $\omega_c = 0.01$ eV. The corresponding reorganization energy of the singlet electronic state is given by $\lambda_S = \int_0^\infty \frac{J_S(\omega)}{\omega} d\omega = 0.2$ eV and the analogous quantity for the triplet is $\lambda_T = \int_0^\infty \frac{J_T(\omega)}{\omega} d\omega = 0.3$ eV. The assumption of a single vibrational reservoir coupled to both the singlet and triplet states allows for the calculation of the reorganization energy of the singlet-triplet transition λ_{ST} , which for this specific case amounts to 0.01 eV. For simplicity, we do not consider high frequency vibrational bath modes (those which feature frequencies $\omega \gg \beta^{-1}$) in our calculations. Furthermore, we assume an energy gap between the equilibrium vibrational configurations of the triplet and singlet $\Delta G = (\varepsilon_T - \lambda_T) - (\varepsilon_S - \lambda_S) = -0.1$ eV and a weak intersystem crossing coupling amplitude $V_{ST} = 2 \times 10^{-5}$ eV. These parameters are typical for

organic molecules that undergo thermally activated delayed fluorescence (TADF) [98, 99, 100], where the population in the dark triplet states transfers to the bright singlets, with a R-ISC rate that depends on a thermal energy barrier between the latter. We also consider a relatively slow nonradiative decay of the triplet $k^T_{nrad} = 2 \times 10^{-7}$ ps^{-1} [99]. Since the characteristic timescale of relaxation of the vibrational environment $\omega_c^{-1} \ll \hbar/|V_{ST}|$, we expect a fast relaxation of the latter into its equilibrium configuration before R-ISC ensues, a scenario termed 'fast bath' in the literature [85]. This is the behaviour expected in the limit $\Omega \to 0$ (small polaron formation before electronic transition) which was confirmed in our numerical calculations.

The second case we considered is the opposite to the previous one, in which the vibrational DOFs of the environment are sluggish in comparison to the R-ISC transition time scale ($V_{ST} \gg \omega_c$), a scenario identified as 'slow bath' [85], which corresponds to molecular emitters with sizable singlet-triplet mixing via spin-orbit coupling or hyperfine interaction. For this case, we also chose large strengths of coupling to the vibrational environment $a_S = 10$, $a_T = 30$, while setting a small cutoff frequency $\omega_c = 5 \times 10^{-3}$ eV (which translate into $\lambda_S = 0.01$ eV, $\lambda_T = 0.03$ eV and $\lambda_{ST} = 0.1$ eV). Furtheremore, we set $V_{ST} = 0.05$ eV and $\Delta G = -0.01$ eV, parameters that are qualitatively aligned with molecules that exhibit fast singlet-fission [64], which exhibit large electronic couplings, comparable to the energy gaps between the singlet and the (two-body) triplet state. For this case, if k^T_{nrad} is small as above, the cavity-free triplet electroluminescence efficiency $\varepsilon \approx 1$ and placing it in the cavity is not productive; hence, we assume that the molecule is such that it features a fast nonradiative triplet decay $k^T_{nrad} = 2 \times 10^{-3}$ ps^{-1} , such that we explore the possibility to outcompete it by cavity-assisted processes. The temperature $T = 300$ K is assumed for both cases.

For reference, we computed electroluminescence efficiencies in the cavity-free (bare molecules) case which are $\varepsilon = 0.027$ for the fast bath case, and $\varepsilon = 0.062$ for the slow one. The latter are calculated using Eq. (5.18), substituting Γ_{ph} with $\Gamma_{rad} = \frac{k^S_{rad}}{2} I_S$, where $k^S_{rad} = 10^{-2}$ ps^{-1}, a typical fluorescence rate for organic molecules.

Upon coupling to a cavity photon mode, the emergent dynamics are changed as a result of the modification of the bare molecular energy landscape and the reorganization energies between the polariton states. In the polaron frame, the former contribution is encoded in the energy spectrum introduced in Eqs. (5.14-5.15), whereas the latter is accounted for in the reorganization energies λ_{i-j}, $i \neq j$, $i,j \in UP, MP, LP, \pm$, where the subindices $\pm$ denote $|k^{\pm}\rangle$ states (in our model, the reorganization energies $\lambda_{i-(\pm)}$ are independent of the momentum of the dark states). The polaron frame picture of the dynamics in both the slow and the fast bath case is schematically illustrated in Fig. 5.1 and the variation of the electroluminescence efficiency with Δ and Ω for the two different molecular emitter cases is shown in Fig. 5.2.

For the discussion in this section, we limit ourselves to the $N = 10^2$ case, postponing the important analysis of larger N values for the next paragraphs.

Fast bath scenario.- For the fast bath molecule, we find that for weak light-matter couplings (Rabi splittings $\Omega \ll \lambda_S$), $\varepsilon(\Delta, \Omega)$ is below the cavity-free scenario (for the resonant case $\Delta = 0$, see inset in Fig. 5.3a). In the polaron frame, this observation can be explained in terms of thermally-activated transfer of population from the triplets to the photonic potential energy surface (PES) via the singlets (see Fig. 5.1a-I). Since this process involves passage through two thermal energy barriers, the time needed to reach the photonic PES is longer that the triplet lifetime and therefore $\varepsilon \ll 1$. On the other hand, when $\Omega/2\lambda_S \approx 2/3$, our calculations predict an abrupt increase in ε (compare inset and main plot in Fig 5.3a). This is a manifestation of polaron decoupling [81, 96] that is expected for sufficiently large Rabi splittings [16, 96], under which the polariton PESs are essentially undisplaced with respect to the electronic ground PES. The intuition behind this decoupling is that the exchange of energy between photon and singlet excitons is much faster than that between vibrations and singlet excitons. Importantly, while this regime was previously predicted for $\Omega \gg \lambda_S$ [101] for a single high-frequency mode, we hereby numerically demonstrate that this stringent condition can be relaxed to smaller Rabi splittings in the case of a continuum of low-frequency modes. In this polaron decoupling regime, our

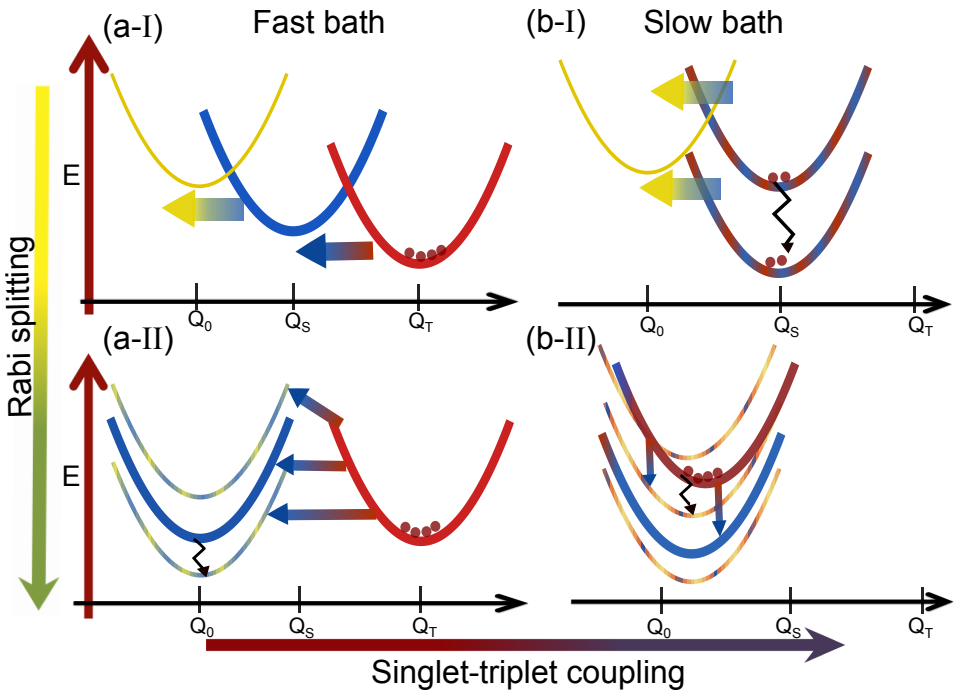

Figure 5.1: Scheme of polaron frame population dynamics which emerge upon injection of optically dark triplet excitons into molecules confined in an optical microcavity. For simplicity, we depict only one vibrational mode and represent its harmonic potential energy E as a function of its coordinate Q, in the photonic state (molecular ground state with one photon, yellow thin curve), and corresponding harmonic potential manifolds for singlet (blue thick curve) and triplet (red thick curve) excited states due to N molecules. We consider molecules which feature (a) fast and (b) slow vibrational environment (see main text), compared to the R-ISC timescale defined by the singlet-triplet coupling $\hbar/V_{ST}$. For each case, we find qualitatively different mechanisms of population transfer among states for (I) weak and (II) strong light-matter coupling. The most significant mechanisms are depicted: multiphonon or Marcus-like processes with straight arrows, and single-phonon or Redfield-like processes with jagged ones.

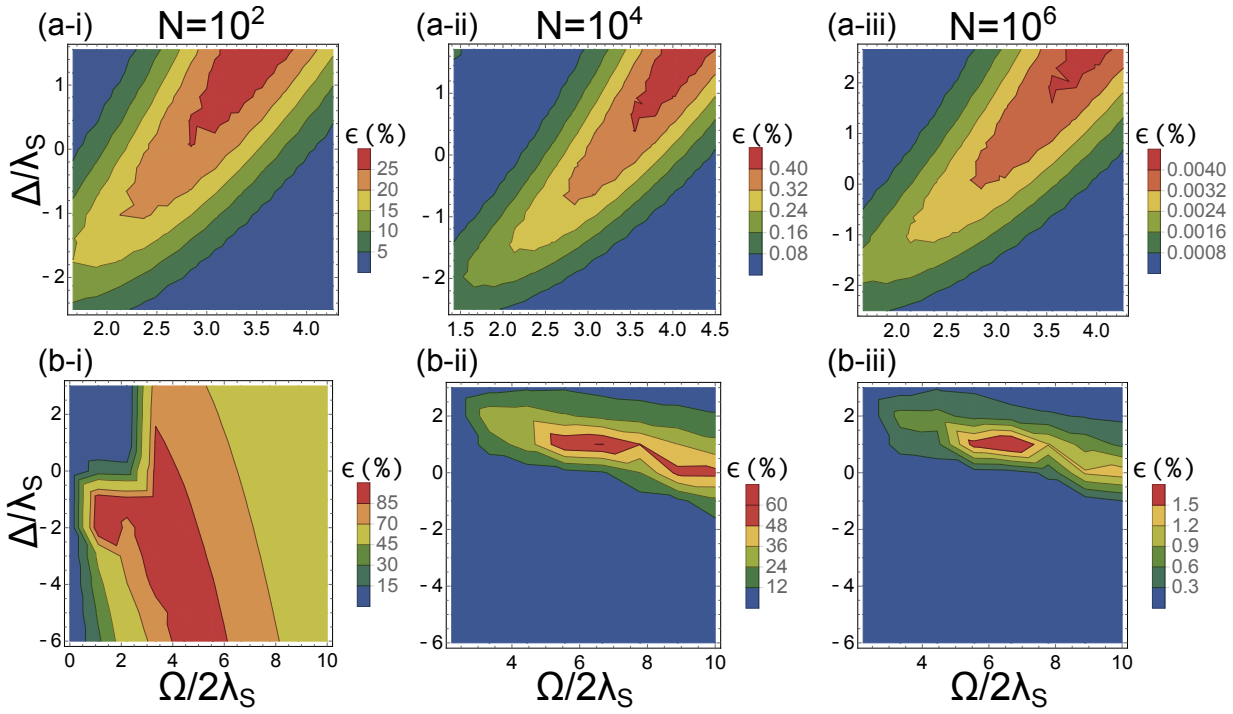

Figure 5.2: Triplet electroluminescence efficiency ε as a function of cavity detuning $\Delta = \omega_{ph} - \varepsilon_S$ and Rabi splitting Ω for (a) the fast bath case, where vibrational equilibration occurs before a slow R-ISC and b) the slow bath case, where the opposite is true (where the emitters feature strong singlet-triplet mixing, see main text). The yields outside of the cavity are (a) $\varepsilon = 0.027$ for the fast bath and (b) $\varepsilon = 0.062$ for the slow one. The effective number of molecules per photon mode is: (i) $N = 10^2$, (ii) $N = 10^4$ and (iii) $N = 10^6$.

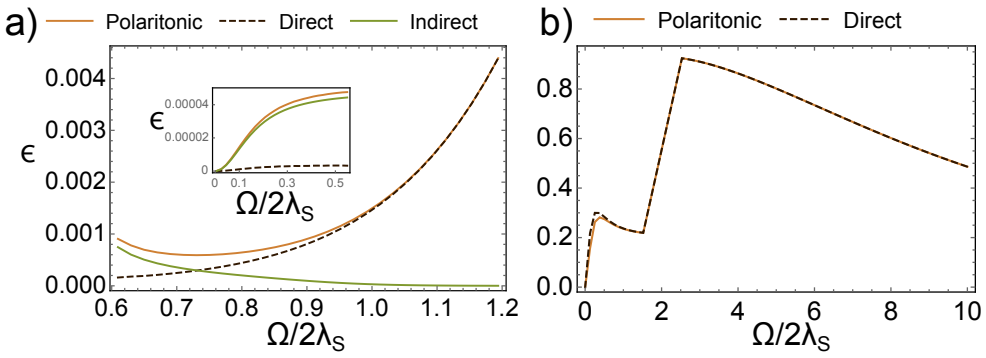

Figure 5.3: Partition of triplet electroluminescence efficiencies as a function of Rabi splitting Ω at light-matter resonance $\omega_{ph} = \varepsilon_S$ (for $\Delta = 0$) for a) a fast bath and b) a slow bath molecule; we show the case for $N = 100$. The triplet electroluminescence efficiency ε (labeled as polaritonic) can be partitioned into a fraction that accounts for the direct and indirect population transfer from dark triplets into polaritons, where indirect means that population passes through other dark states before it reaches the polaritons. In b), we do not explicitly show the indirect contribution since it is negligible for featured Rabi splitting ranges. Inset in (a) zooms into smaller Rabi splitting ranges. For comparison, the yields outside of the cavity are (a) $\varepsilon = 0.027$ for the fast bath and (b) $\varepsilon = 0.062$ for the slow one.

calculations predict that $\lambda_{(-)-UP} = \lambda_{(-)-MP} = \lambda_{(-)-LP} = \lambda_{(+)-(-)} > \lambda_{ST}$ [where the equality among the previous quantities is a result of the ansatz in Eq. (5.8), which for $\Omega/2\lambda_S > 2/3$, corresponds to $f_l^{(v)} = f^{(v)} = O(\frac{g_S^{(v)}}{N})$, for all l. In other words, the singlet exciton PESs are negligibly displaced with respect to the ground state PES when N is large]. As a consequence, the R-ISC energy barrier can either decrease or increase with respect to the bare molecules by tuning the Rabi splitting. In fact, we notice that as Ω increases (see Figs. 5.2a-i and 5.1a-II), ε increases and then decreases with respect to the cavity-free value, given that the smallest R-ISC to polariton energy barrier decreases and then increases as this rate goes from normal to inverted Marcus regimes. Notice that Fig. 5.3a only shows an increasing behavior in ε because the plotted range of Rabi splittings is small.

Slow bath scenario.- For the slow bath case, we observe a significantly different $\varepsilon(\Delta, \Omega)$. In Fig. [5.2b-i], we show that there is no need to invoke Rabi splittings beyond the reorganization energy to observe an enhancement in electroluminescence efficiency.

Similarly to the previous fast bath scenario, our calculations reveal two qualitatively

different pictures of the population dynamics in the polaron frame depending on the magnitude of Ω. For sufficiently weak light-matter coupling, the initial state is comprised of approximately equally populated lower and upper dark state manifolds since $|c_S^+|^2 \approx |c_S^-|^2$ [see Eq. (5.20) and Fig. 5.1b-I], a consequence of the prevalence of the electronic coupling V_{ST} over the weak coupling of the R-ISC transition to the phonon environment. In this regime, ε can be explained in terms of a Marcus picture where the photonic PES receives population from the upper and lower dark-state manifolds with a rate proportional to a diabatic coupling of order $|g|^2$, corresponding to single-molecule light-matter coupling [see Eq. (5.17e) and Fig. 5.1b-I]. High and small R-ISC energy barriers can be obtained by scanning across Δ, thus decreasing and increasing ε, respectively; for the computed range of Δ values, the dominant R-ISC pathway is the one starting from the upper dark states (they are closer in energy to the photonic PES, see Fig. 5.1b-I). In fact, for sufficiently small increase in Ω, the triplet electroluminescence efficiency ε also rises because $|g|^2$ increases; see Fig. 5.3b, which shows a cut of ε at light-matter resonance $\Delta = 0$. In this plot, this mechanism is operative up to a first maximum in ε at $\Omega \approx \lambda$, upon which light-matter coupling changes from weak to moderate and ε decreases. This effect can be understood as follows: as Ω increases, it can compete with V_{ST}, thus reducing the magnitude of the dressed $\tilde{V}_{ST}$, and concomitantly reducing the mixing between singlets and triplets. The result is that the lower and upper dark states become more triplet and singlet-like, respectively. Therefore, the initial triplet population has more probability of residing in the lower dark states, but these feature a much larger energy barrier to the photonic mode, thus leading to slower R-ISC and lower ε.

Keeping our discussion around Fig. 5.3b, our model predicts a sharp change in the dynamics under strong light-matter coupling starting at $\Omega \approx 4\lambda_S$, with ε increasing with Ω, featuring a second maximum in ε at $\Omega \approx 6\lambda_S$, and then decreasing for larger Ω. An intriguing feature of this regime is that, for the chosen parameters, the upper and lower dark states have largely triplet and singlet characters, respectively; that is, the configuration of minimal energy of the vibrational DOFs coupled to the singlet and triplet states in the polaron frame is such

that their energy ordering is inverted with respect to that in the original frame (Fig. 5.1b-II) where $\varepsilon_S - \lambda_S > \varepsilon_T - \lambda_T$. This effect is due to the slow relaxation of the bath that renders the vibrational dressing of the states at nonequilibrium nuclear configurations close to those accessed by vertical transitions from the ground state. Under these circumstances, population is primarily initialized in the upper dark states and transfers to the MP (Fig. 5.1b-II) which is closer in energy than the other polaritons or dark states. Notice that in contrast to the weak light-matter coupling case, MP has significant singlet, triplet, and photonic characters and the population transfer mechanism can be essentially dissected into sizable contributions from multiphonon (a Marcus-like contribution due to displacement between the upper dark states and MP harmonic potentials) and one-phonon (Redfield-like) processes. In our example, a steady boost in ε is given by the Redfield processes which dominate over the Marcus-like ones, given the large activation energy barriers to be surmounted in the latter. These Redfield processes are primarily due to the triplet character in both upper dark states and MP. After the second maximum in ε, further increase of Ω leads to a phonon blockade and a concomitant decrease in ε: the MP energy keeps lowering but no one-phonon process is available to mediate the transfer from the upper dark states (the vibrational DOS decreases exponentially as a function of frequency in our chosen spectral density).

5.5 The large N issue

So far, we have addressed the $N = 100$ case in detail. In fact, strong light-matter coupling with such small number of molecular emitters has been reported using plasmonic nanoparticle environments [102, 103]. However, most microcavity systems have much larger N values. We thus proceed to comment on the ε behavior for increasing values of N, while keeping Rabi splittings Ω fixed (and hence energy barriers and energy differences between states, see Fig. 5.2). For weak light-matter coupling, both fast (a) and slow (b) baths yield insensitive changes of ε

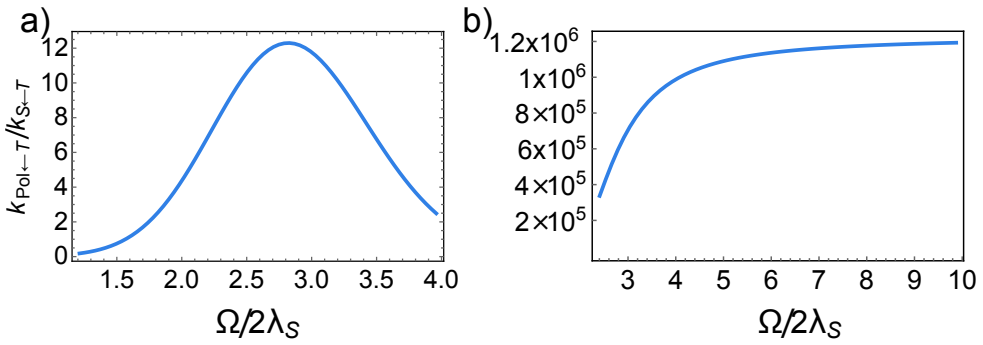

Figure 5.4: Relative R-ISC rates from triplet manifold to polariton states (at light-matter resonance $\omega_{ph} = \varepsilon_s$) in the polaron frame with respect to the cavity-free case, for (a) the fast bath scenario and (b) the slow bath case, as a function of Rabi splitting, considering $N = 10^2$. The profile observed in (a) (where the bare R-ISC rate is $k_{S\leftarrow T} = 5.4 \times 10^{-9}$ ps^{-1}), can be explained in terms of a multiphonon Marcus theory process from triplets to singlets (see Fig. 5.1a-II), where the lowest activation barrier between triplets and polaritons decreases (normal regime) and then increases (inverted regime). In (b) (where the bare R-ISC rate is $k_{S\leftarrow T} = 4.6 \times 10^{-6}$ ps^{-1}), the trend is different since the dominant R-ISC channel is a one-phonon process from triplets to the MP state (see Fig. 5.1b-II) and significantly depends on the triplet character of the latter. The asymptotic behavior of the rate reflects the increase in triplet character of the (MP) polariton state with Rabi splitting and the suppression of the energy gap between the latter and the triplet states. However, in this asymptotic limit, the photonic component of the MP vanishes and this channel does not longer contribute to the cavity electroluminescence efficiency. Finally, since the $k_{Pol\leftarrow T}$ rates shown here scale as $1/N$, the rates expected at different N can be calculated by scaling the values displayed accordingly.

to increase of N. This is due to the fact that changing N does not alter the energy barriers to be surmounted in the R-ISC process.

For strong light-matter coupling, the overall electroluminescence efficiency is damped as a result of the ratio of triplet to polariton states increasing. For the fast bath case (a), since both dark and polariton states feature the same reorganization energies in the polaron frame, ε is determined by the competition between the nonradiative triplet decay and transfer to the polariton state closer in energy, that is because the latter channel features a lower activation energy barrier compared to the dark states [see Fig. 5.1a-II)]. However, at light-matter resonance, the R-ISC rate to the final polariton state scales as $\frac{1}{N}$, given that the polariton is delocalized across N singlets and only one of them can undergo coupling to a given triplet. Importantly, for $N \geq 10^4$ the rate of transfer to the polaritons falls below the cavity-free R-ISC rate for the entire (Δ, ω) range displayed (see Fig. 5.2 top panels and 5.4a). The conclusion is similar for the slow bath case (b). While for small N values, high efficiencies are obtained (see Fig. 5.2b-i and 5.2b-ii), the assistance of polariton modes decreases with increasing N. This is because the ratio of rates (dark states $\rightarrow$ polariton)/(polariton$\rightarrow$ dark states) scales as $\frac{1}{N}$ given the delocalization of the polariton state; this implies that the backward process polariton$\rightarrow$ dark states becomes more relevant as N increases, an effect which is detrimental to ε. Finally, the decrease of photon character in the MP for $\Delta < 0$ [see Fig. 5.1b-II)] together with a fast back transfer to the denser manifold of upper dark states for larger N, explains the drop of ε at $\Delta < 0$, specially for $N > 10^4$ (see Fig. 5.2 lower panels and 5.4b).

Based on the discussion above, a pressing question is the characterization of an optimal scenario that overcomes the deleterious effects of cavity R-ISC rates as N increases, the latter being as large as 10^7 [84]. Here, we propose a case where the energy tunability of the polaritons introduces an increase of many orders of magnitude relative to the cavity-free R-ISC rate, and this enhancement can outcompete the suppression due to the low polariton DOS. The scenario is built upon the fast bath case studied above, but assuming a sufficiently large singlet-triplet

energy gap and weak couplings of the electronic states to the bath (small a_S and a_T parameters). Under these conditions, the reduced dynamics of transfer in the polaron frame in the cavity-free scenario corresponds to the inverted-Marcus regime (for the singlet to triplet transition), where the population of the triplet manifold needs to overcome an enormous energy barrier to reach the singlet state (see Fig. 5.5). Upon confinement to a microcavity, the emergent lower polariton could introduce a much smaller energy barrier from the triplet states. Our results and the precise parameters used in our calculations are shown in Fig. 5.5, which show that polariton-assistance introduces four orders of magnitude enhancement relative to the bare R-ISC rate.

On the other hand, we note that the polariton-assisted R-ISC rate is upper-bounded by $\frac{V_{ST}^2}{N}\sqrt{\frac{\pi\beta}{\lambda_{T-pol}}}$, which must be higher than k_{nrad}^T to lead to harvesting of triplets. If we take $N = 10^6$, and use the parameters above for the fast bath scenario ($k_{nrad} = 2\times10^{-7}$ ps^{-1}), we need a very small $\lambda_{T-pol} = 10^{-17}$ eV. Therefore, in order to obtain a sizable ε, emitters with negligible couplings to a vibrational environment are required (small reorganization energies λ_{ST} and λ_S); that is, poor R-ISC molecules (*i.e.*, the opposite of TADF materials) will obtain most benefit from polaritonic effects.

For the slow bath case, there is no possibility to enhance electroluminescence for large N because the associated R-ISC processes via polaritons happen via one-phonon vibrational relaxation (Redfield) processes, rather than multiphonon (Marcus) processes that exhibit exponential sensitivity on energy barriers. Hence, the only option for enhancement of electroluminescence for that case is to use samples with small N values.

5.6 Conclusions

In this chapter, we have developed a variational model for the prediction of electroluminescence efficiency of molecular emitters interacting with a photonic mode of a microcavity. The latter can describe the emergent dynamics on a range of Rabi splittings that extend from the weak

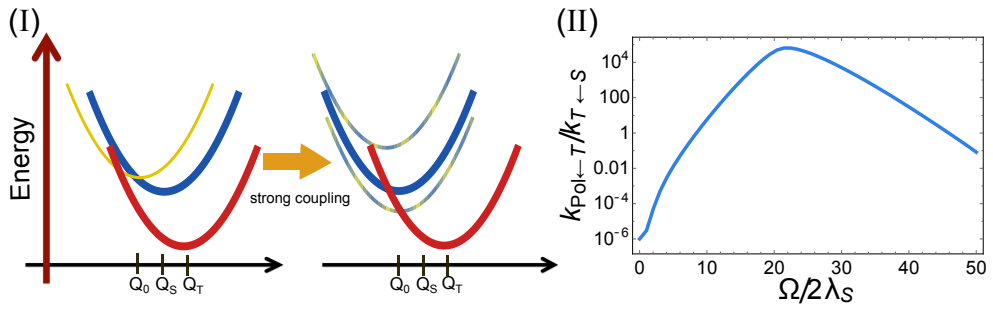

Figure 5.5: Ideal case to maximize the rate of transfer from the triplet state manifold (blue thick curve) to polariton states, with respect to the cavity free triplet-to-singlet (R-ISC) transfer rate. (I) Energy diagrams in the polaron frame. Left: a molecular emitter in which the singlet (blue) and triplet (red) states have similar equilibrium nuclear configurations and the dynamics between them falls within the Marcus inverted regime. (I) Right: upon strong coupling to a photon mode and in the polaron frame, the energy barrier between the triplet states and the lower polariton (in this case, the lower polariton) quickly decreases with Rabi splitting, giving rise to orders of magnitude increase in the $k_{T\rightarrow \mathrm{LP}}$ rate, thus avoiding the wash-out effect of delocalization of the singlet of interest among N molecules. (II) Cavity mediated R-ISC enhancement $k_{T\rightarrow \mathrm{LP}}/k_{T\rightarrow S}$. Note that the cavity provides a realization of the various regimes of Marcus theory, from normal to inverted, as a function of Rabi splitting. The specific parameters for the vibrational bath are $a_S = 0.5$, $a_T = 1$ and $\omega_c = 0.01$ eV (see section 5.2), which accounts for a singlet reorganization energy $\lambda_S = 0.01$ eV and $\lambda_T = 0.02$ eV. We also assumed that the number of molecules per photon mode is $N = 10^6$, $\Delta G = (\varepsilon_S - \lambda_S) - (\varepsilon_T - \lambda_T) = 0.2$ eV, where we recall that ε_S (ε_T) is the vertical singlet (triplet) transition energy; and the singlet-triplet electronic coupling $V_{TS} = 1 \times 10^{-5}$ eV.

to the the strong coupling regime.

Our calculations indicate that the main limitation to polariton-assist the electroluminescence process is the delocalized character of polaritons: the probability of a triplet state to R-ISC into the latter is strongly suppressed by a $\frac{1}{N}$ factor, similarly to results discussed in previous works [19, 9, 80]. There are two approaches that could overcome the detrimental delocalization effect and therefore introduce a polariton-enhanced electroluminescence with respect to the cavity-free scenario: 1) for fast and slow bath cases (*i.e.* for chromophores with weak and strong singlet-triplet mixing), as Figs. 5.2a-i and 5.2b-i show, strong coupling with a small number of molecules per photonic mode N introduces significant electroluminescence yield enhancements with respect to the bare molecular case. This regime should be feasible in the context of plasmonic nanoparticles coated with organic dyes, where N can be more than 3 orders of magnitude smaller than those needed in a microcavity to attain the strong coupling regime [102, 103, 104]. 2) The second approach only works for the fast bath case and consists on tuning of polariton energies and taking advantage of the exponential sensitivity of R-ISC rates with respect to energy barriers. Therefore, a high thermal energy barrier for the R-ISC transition in the bare molecular case translates into the possibility of its partial or total reduction via a triplet to polariton R-ISC transition, thus potentially outcompeting the delocalization effect, and introducing a net electroluminescence enhancement. For a molecular emitter the previous requirement is equivalent to an inverted Marcus regime for the singlet→triplet ISC transition. This mechanism is also reminiscent to a recently proposed catalysis of thermally-activated reactions under vibrational strong coupling, where a sufficient decrease in activation energy can outcompete the large activation entropy of the dark states [105]. An inverted Marcus regime being the ideal scenario to introduce polariton assistance has also been found in [19] for singlet fission and in [106], the latter in the context of a single-molecule charge transfer process assisted by a photon mode.

On the other hand, for the scenario of a slow vibrational bath, the efficiencies are largely determined by the energetic proximity of the polariton and dark state resonances. The increase

of Rabi splitting in this case diminishes the rate of transition of the triplet to the polariton state closer in energy, because the vibrational DOS that can assist the transition decreases exponentially with the energy gap betwen them. Therefore, for the slow phonon bath scenario considered in this work, approach 1) is the only alternative to minimize the polariton-delocalization effect on efficiencies.

This chapter, in full, is adapted from the material as it appears in "Triplet harvesting in the polaritonic regime: A variational polaron approach" Martínez-Martínez L. A., Eizner E., Kéna-Cohen S. and Joel Yuen-Zhou, J. Chem. Phys., 151, 054106 (2019). The dissertation author was the primary investigator and author of this material.

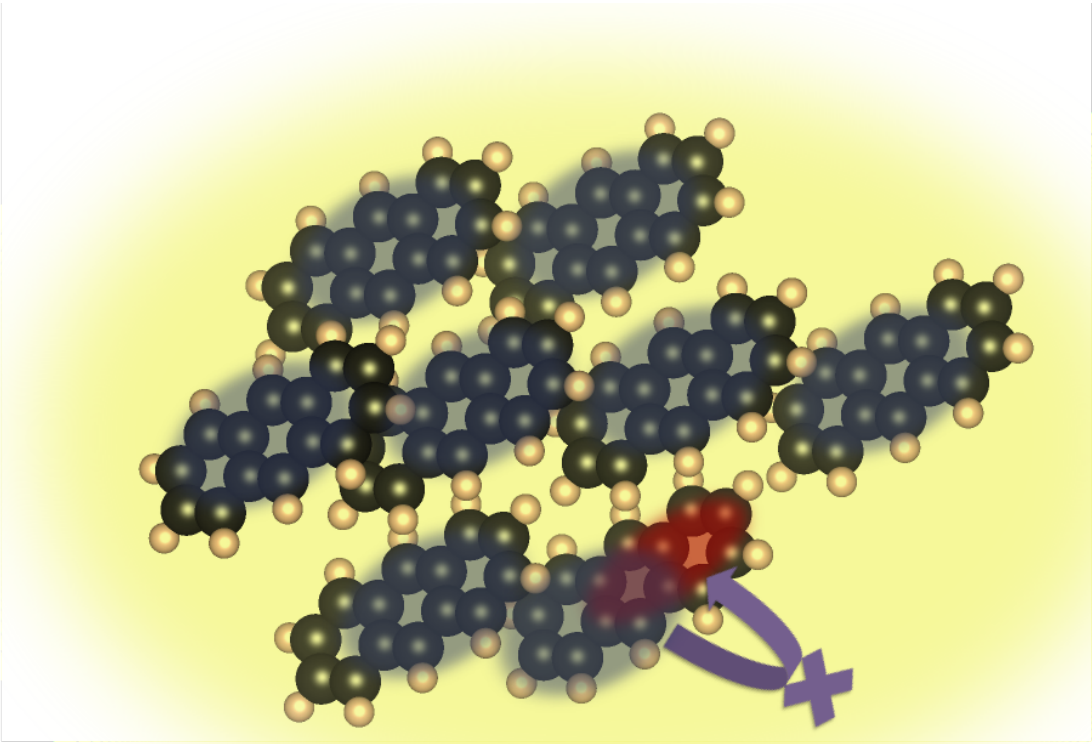

Figure 5.6: Scheme that illustrates the delocalization of a singlet electronic excitation (denoted as a faint blue on N molecules) in a polariton mode under strong coupling to a confined electromagnetic environment (denoted as yellow). The localized nature of a triplet state (red) precludes a fast transfer to the polariton modes, in view of the local character of R-ISC and the dilution of probability of the R-ISC transition among N molecules. As elaborated in section 5.5 of this chapter, this rate suppression can be overcome by 1) coupling fewer molecular emitters to each photon mode while preserving strong light-matter coupling (using e.g. plasmon nanoparticle systems); and/or ii) harnessing strong coupling of molecules with singlet→triplet transition in the Marcus inverted regime, which feature very large R-ISC energy barriers, such that introduction of a polariton channel may decrease this barrier and possibly compete effectively against the many dark-state channels.

Chapter 6

Conclusions

This dissertation presents effective coarse-grained models that provide insight on the dynamical nuclear and electronic processes of molecules when confined in a spatially localized electromagnetic environment.

One of the first works to explore chemical reactivity *in the dark* under the ultrastrong light-matter coupling (USC) regime reached in plasmonic setups, is presented in Chapter 3. It is shown that for the adiabatic ground state nuclear energy landscape of a particular isomerization model, there is no significant modification that could alter the kinetics or thermodynamics of the reaction. As was highlighted in Chapter 1 of this dissertation, vacuum fluctuations of the electromagnetic field induce (small) renormalization of molecular transition energies, known as Lamb shifts. It is therefore shown that the changes of the isomerization potential energy landscape experienced by the nuclei upon confinement in a plasmonic field can be understood as (nuclear-position dependent) Lamb shifts [57].

Furthermore, it is shown that the adiabatic nuclear energy barrier for isomerization, albeit slightly changed, decrease rather than the opposite. An increase of the barrier would be the more intuitive conjecture based on the fact that reactants feature a non-vanishing dipole moment in contrast with the transition geometry (see Fig. 3.1). This observation can be understood as

follows: the potential energy corresponding to a single molecule (i.e. local) isomerization process at its transition geometry corresponds to $N-1$ molecules coupled to the plasmonic EM field (N being the total number of molecules in the ensemble) and one molecule uncoupled to the former. This leads to a slight energy increase of the global plasmonic-molecular system (compared to that of all molecules in their reactant geometry) that translates into a reduction of the energy barrier. In spite of the negligible tunability of this type of reactions in the ultrastrong coupling regime, it is highlighted the existence of quantum-coherent effects where concerted reactions occur. These interference effects are unlikely to play an important role in reactions exhibiting high energy barriers compared to k_BT. However, they might be important for low-barrier processes, where the number of concerted reaction pathways becomes combinatorially more likely than single molecule processes.

This dissertation was also focused on two photophysical processes of technological importance. On one hand it is shown that when singlet-fission (SF) materials are subjected to a strong coupling with a microcavity mode, the photonic leakage of the resulting polariton states constitutes an important decay channel that can decrease the production of triplets when compared to the bare case. In order to counteract this deleterious dissipation channel, it is proposed that the the competition between SF and the photon leakage rate could be tuned by modifying the ratio between the detuning (frequency difference of the singlet molecular transition and the cavity photon mode) and the collective light-matter coupling. When this approach is implemented, it is shown the possibility to favor the material character of the polariton modes and the subsequent suppression of photonic leakage. Remarkably, it is shown that hexacene is a poor SF candidate in a cavity-free scenario (and in presence of quenchers), but it is the material (among the ones considered in this dissertation, see Chapter 4) which features the highest enhancement by means of the proposed polaritonic approach and can even outcompete the bare pentacene TT yield under the conditions considered in this work. One question of significance is: what are the ideal features a molecule must posses in order to boost the efficiency of SF transitions when confined in a

microcavity? Based on the findings explained in Chapter 4, it is shown that the ideal material would feature a highly exergonic SF process together with a low reorganization energy associated to the low-frequency mode of the SF transition.

On the the other hand, similar queries were addressed for the related photophysical process known as Reverse Intersystem Crossing (R-ISC), which is the main ingredient for electroluminescence of organic materials. More specifically, the degree of tunability of the electroluminescence by means of microcavity devices is considered. In order to treat the problem with the same footing from the weak through the strong light-matter interaction regime, a variational model for the dynamics of transitions between the singlet and triplet electronic states was developed.

The calculations suggest that the main limitation to polariton-assist the electroluminescence process is the delocalized character of polaritons: the probability of a triplet state to R-ISC into the latter is strongly suppressed by a $\frac{1}{N}$ factor, similarly to results discussed in previous works [19, 9, 80].

To overcome the detrimental delocalization effect and therefore introduce a polariton-enhanced electroluminescence with respect to the cavity-free scenario and for typical organic molecules it is proven the need of the R-ISC transition to be in the so-called inverted Marcus regime, where it is shown that when this is the case, there is a possibility for the direct triplet-lower polariton kinetic channel to outcompete the rate transfer to the dense density-of-states manifold of the dark states.

To conclude, even though the presence of dark states and short cavity photon lifetimes render the control of molecular processes inside microcavities difficult, there is still room to cavity-assist the funneling of energy from molecular processes, as it was shown recently in Ref. [107].

To further advance our understanding of molecular polariton dynamics, the development of theoretical tools to aid the interpretation of nonlinear spectroscopy of polariton setups is of

high relevance. Molecular cavity-induced phase-transition possibilities, as well as theoretical perspectives on molecular dynamics in extreme regimes of light-matter intraction are also fertile ground for exploration of novel phenomena that microcavities and other platforms could offer.

Bibliography

[1] Moshe Shapiro and Paul Brumer. *Principles of the quantum control of molecular processes*. 2003.

[2] Herbert Walther, Benjamin TH Varcoe, Berthold-Georg Englert, and Thomas Becker. Cavity quantum electrodynamics. *Rep. Prog. Phys.*, 69(5):1325, 2006.

[3] H. B. G. Casimir and D. Polder. The influence of retardation on the london-van der waals forces. *Phys. Rev.*, 73:360–372, Feb 1948.

[4] C. M. Wilson, G. Johansson, A. Pourkabirian, M. Simoen, J. R. Johansson, T. Duty, F. Nori, and P. Delsing. Observation of the dynamical casimir effect in a superconducting circuit. *Nature*, 479(7373):376–379, 11 2011.

[5] J. J. Hopfield. Theory of the contribution of excitons to the complex dielectric constant of crystals. *Phys. Rev.*, 112:1555–1567, December 1958.

[6] James A. Hutchison, Tal Schwartz, Cyriaque Genet, Eloïse Devaux, and Thomas W. Ebbesen. Modifying chemical landscapes by coupling to vacuum fields. *Angew. Chem. Int. Ed.*, 51:1592–1596, 2012.

[7] Anoop Thomas, Jino George, Atef Shalabney, Marian Dryzhakov, Sreejith J. Varma, Joseph Moran, Thibault Chervy, Xiaolan Zhong, Eloïse Devaux, Cyriaque Genet, James A. Hutchison, and Thomas W. Ebbesen. Ground-State Chemical Reactivity under Vibrational Coupling to the Vacuum Electromagnetic Field. *Angew. Chem. Int. Ed.*, 128(38):11634–11638, 2016.

[8] Xiaolan Zhong, Thibault Chervy, Shaojun Wang, Jino George, Anoop Thomas, James A. Hutchison, Eloise Devaux, Cyriaque Genet, and Thomas W. Ebbesen. Non-radiative energy transfer mediated by hybrid light-matter states. *Angew. Chem. Int. Ed.*, 55(21):6202–6206, 2016.

[9] Matthew Du, Luis A. Martínez-Martínez, Raphael F. Ribeiro, Zixuan Hu, Vinod M. Menon, and Joel Yuen-Zhou. Theory for polariton-assisted remote energy transfer. *Chem. Sci.*, 9:6659–6669, 2018.

[10] Joel Yuen-Zhou and Vinod M Menon. Polariton chemistry: Thinking inside the (photon) box. *Proc. Natl. Acad. Sci. U.S.A.*, 116(12):5214–5216, 2019.

[11] Raphael F. Ribeiro, Luis A. Martínez-Martínez, Matthew Du, Jorge Campos-Gonzalez-Angulo, and Joel Yuen-Zhou. Polariton chemistry: controlling molecular dynamics with optical cavities. *Chem. Sci.*, 9:6325–6339, 2018.

[12] Vladimir M. Agranovich, Marina Litinskaya, and David G. Lidzey. Cavity polaritons in microcavities containing disordered organic semiconductors. *Phys. Rev. B*, 67:085311, 2003.

[13] Marina Litinskaya, Peter Reineker, and Vladimir M. Agranovich. Fast polariton relaxation in strongly coupled organic microcavities. *J. Lumin.*, 110(4):364–372, 2004.

[14] Javier Galego, Francisco J. Garcia-Vidal, and Johannes Feist. Cavity-induced modifications of molecular structure in the strong-coupling regime. *Phys. Rev. X*, 5:041022, November 2015.

[15] Javier Galego, Francisco J Garcia-Vidal, and Johannes Feist. Suppressing photochemical reactions with quantized light fields. *Nat. Commun.*, 7:13841, 2016.

[16] Felipe Herrera and Frank C. Spano. Cavity-controlled chemistry in molecular ensembles. *Phys. Rev. Lett.*, 116:238301, June 2016.

[17] Alexey Kavokin, Jeremy J Baumberg, Guillaume Malpuech, and Fabrice P Laussy. *Microcavities*. Oxford university press, 2017.

[18] Javier del Pino, Johannes Feist, and Francisco J Garcia-Vidal. Quantum theory of collective strong coupling of molecular vibrations with a microcavity mode. *New J. Phys.*, 17(5):053040, 2015.

[19] Luis A. Martínez-Martínez, Matthew Du, Raphael F. Ribeiro, Stéphane Kéna-Cohen, and Joel Yuen-Zhou. Polariton-assisted singlet fission in acene aggregates. *J. Phy. Chem. Lett.*, 9(8):1951–1957, 2018.

[20] Volkhard May and Oliver Khün. *Charge and energy transfer dynamics in molecular systems*. John Wiley & Sons, Berlin, 2008.

[21] Daniel N. Congreve, Jiye Lee, Nicholas J. Thompson, Eric Hontz, Shane R. Yost, Philip D. Reusswig, Matthias E. Bahlke, Sebastian Reineke, Troy Van Voorhis, and Marc A. Baldo. External quantum efficiency above 100% in a singlet-exciton-fission–based organic photovoltaic cell. *Science*, 340(6130):334–337, 2013.

[22] Heinz-Peter Breuer, Francesco Petruccione, et al. *The theory of open quantum systems*. Oxford University Press on Demand, 2002.

[23] Felix A Pollock, Dara PS McCutcheon, Brendon W Lovett, Erik M Gauger, and Ahsan Nazir. A multi-site variational master equation approach to dissipative energy transfer. *New J. Phys.*, 15(7):075018, 2013.

[24] Ning Wu, Johannes Feist, and Francisco J Garcia-Vidal. When polarons meet polaritons: Exciton-vibration interactions in organic molecules strongly coupled to confined light fields. *Phys. Rev. B*, 94(19):195409, 2016.

[25] Kerry J Vahala. Optical microcavities. *Nature*, 424(6950):839–846, 2003.

[26] Mark S Tame, KR McEnery, ŞK Özdemir, Jinhyoung Lee, Stefan A Maier, and MS Kim. Quantum plasmonics. *Nat. Phys.*, 9(6):329–340, 2013.

[27] Dominik Lentrodt and Jörg Evers. Ab initio few-mode theory for quantum potential scattering problems. *Phys. Rev. X*, 10(1):011008, 2020.

[28] W Domcke. Projection-operator approach to potential scattering. *Phys. Rev. A*, 28(5):2777, 1983.

[29] Notes on the algebraic structure of wave equations. `http:https://math.mit.edu/~stevenj/18.369/wave-equations.pdf`. Accessed: 2021-02-17.

[30] Shaul Mukamel. *Principles of nonlinear optical spectroscopy*. Number 6. Oxford University Press on Demand, 1999.

[31] Javier Galego, Clàudia Climent, Francisco J. Garcia-Vidal, and Johannes Feist. Cavity casimir-polder forces and their effects in ground-state chemical reactivity. *Phys. Rev. X*, 9:021057, Jun 2019.

[32] Myung-Ki Kim, Hongchul Sim, Seung Ju Yoon, Su-Hyun Gong, Chi Won Ahn, Yong-Hoon Cho, and Yong-Hee Lee. Squeezing photons into a point-like space. *Nano Lett.*, 15(6):4102–4107, 2015.

[33] Carlos Gonzalez-Ballestero, Johannes Feist, Esteban Moreno, and Francisco J. Garcia-Vidal. Harvesting excitons through plasmonic strong coupling. *Phys. Rev. B*, 92:121402, September 2015.

[34] Johannes Feist and Francisco J. Garcia-Vidal. Extraordinary exciton conductance induced by strong coupling. *Phys. Rev. Lett.*, 114:196402, May 2015.

[35] Jacek Kasprzak, M Richard, S Kundermann, A Baas, P Jeambrun, JMJ Keeling, FM Marchetti, MH Szymańska, R Andre, JL Staehli, V Savona, PB Littlewood, B Deveaud, and L S Dang. Bose–einstein condensation of exciton polaritons. *Nature*, 443(7110):409–414, 2006.

[36] Dario Gerace and Iacopo Carusotto. Analog hawking radiation from an acoustic black hole in a flowing polariton superfluid. *Phys. Rev. B*, 86:144505, October 2012.

[37] H. S. Nguyen, D. Gerace, I. Carusotto, D. Sanvitto, E. Galopin, A. Lemaître, I. Sagnes, J. Bloch, and A. Amo. Acoustic black hole in a stationary hydrodynamic flow of microcavity polaritons. *Phys. Rev. Lett.*, 114:036402, January 2015.

[38] Jonathan R. Tischler, M. Scott Bradley, Vladimir Bulović, Jung Hoon Song, and Arto Nurmikko. Strong coupling in a microcavity led. *Phys. Rev. Lett.*, 95:036401, July 2005.

[39] P. A. Hobson, W. L. Barnes, D. G. Lidzey, G. A. Gehring, D. M. Whittaker, M. S. Skolnick, and S. Walker. Strong exciton-photon coupling in a low-q all-metal mirror microcavity. *Appl. Phys. Lett.*, 81(19):3519–3521, 2002.

[40] J. Bellessa, C. Bonnand, J. C. Plenet, and J. Mugnier. Strong coupling between surface plasmons and excitons in an organic semiconductor. *Phys. Rev. Lett.*, 93:036404, July 2004.

[41] Adi Salomon, Cyriaque Genet, and Thomas W. Ebbesen. Molecule-light complex: Dynamics of hybrid molecule-surface plasmon states. *Angew. Chem. Int. Ed.*, 48(46):8748–8751, 2009.

[42] Rohit Chikkaraddy, Bart de Nijs, Felix Benz, Steven J Barrow, Oren a Scherman, Edina Rosta, Angela Demetriadou, Peter Fox, Ortwin Hess, and Jeremy J Baumberg. Single-molecule strong coupling at room temperature in plasmonic nanocavities. *Nature*, 535(7610):127–130, 2016.

[43] Alexander Moroz. A hidden analytic structure of the rabi model. *Ann. Phys.*, 340(1):252–266, 2014.

[44] R. Stassi, A. Ridolfo, O. Di Stefano, M. J. Hartmann, and S. Savasta. Spontaneous conversion from virtual to real photons in the ultrastrong-coupling regime. *Phys. Rev. Lett.*, 110:243601, June 2013.

[45] T. Niemczyk, F. Deppe, H. Huebl, E. P. Menzel, F. Hocke, M. J. Schwarz, J. J. Garcia-Ripoll, D. Zueco, T. Hümmer, E. Solano, A. Marx, and R. Gross. Circuit quantum electrodynamics in the ultrastrong-coupling regime. *Nat. Phys.*, 6(10):772, 2010.

[46] T. Schwartz, J. A. Hutchison, C. Genet, and T. W. Ebbesen. Reversible switching of ultrastrong light-molecule coupling. *Phys. Rev. Lett.*, 106:196405, May 2011.

[47] Jino George, Thibault Chervy, Atef Shalabney, Eloïse Devaux, Hidefumi Hiura, Cyriaque Genet, and Thomas W Ebbesen. Multiple rabi splittings under ultrastrong vibrational coupling. *Phys. Rev. Lett.*, 117(15):153601, 2016.

[48] Kunihito Hoki and Paul Brumer. Dissipation effects on laser control of cis/trans isomerization. *Chem. Phys. Lett.*, 468(1-3):23–27, 2009.

[49] Joel Yuen-Zhou, Semion K. Saikin, Tony H. Zhu, Mehmet C. Onbasli, Caroline A. Ross, Vladimir Bulovic, and Marc A. Baldo. Plexcitons: Dirac points and topological modes. *Nat. Commun.*, 7:11783, 2016.

[50] A. González-Tudela, P. A. Huidobro, L. Martín-Moreno, C. Tejedor, and F. J. García-Vidal. Theory of strong coupling between quantum emitters and propagating surface plasmons. *Phys. Rev. Lett.*, 110(March):126801, 2013.

[51] Barry M Garraway. The dicke model in quantum optics: Dicke model revisited. *Phil. Trans. R. Soc. A*, 369(1939):1137–1155, 2011.

[52] Alexandre Archambault, Fran çois Marquier, Jean-Jacques Greffet, and Christophe Arnold. Quantum theory of spontaneous and stimulated emission of surface plasmons. *Phys. Rev. B*, 82:035411, July 2010.

[53] Marlan O Scully and M Suhail Zubairy. *Quantum optics*. Cambridge University Press, Cambridge,UK, 1 edition, 1997.

[54] Cristiano Ciuti, Gérald Bastard, and Iacopo Carusotto. Quantum vacuum properties of the intersubband cavity polariton field. *Phys. Rev. B*, 72:115303, September 2005.

[55] F. Tassone and Y. Yamamoto. Exciton-exciton scattering dynamics in a semiconductor microcavity and stimulated scattering into polaritons. *Phys. Rev. B*, 59(16):10830–10842, 1999.

[56] P Törmä and W L Barnes. Strong coupling between surface plasmon polaritons and emitters: a review. *Rep. Prog. Phys.*, 78:013901, 2015.

[57] H. A. Bethe, L. M. Brown, and J. R. Stehn. Numerical value of the lamb shift. *Phys. Rev.*, 77:370–374, February 1950.

[58] R Scott Rowland and Robin Taylor. Intermolecular nonbonded contact distances in organic crystal structures: Comparison with distances expected from van der waals radii. *J. Phys. Chem*, 100(18):7384–7391, 1996.

[59] Markus Kowalewski, Kochise Bennett, and Shaul Mukamel. Cavity Femtochemistry: Manipulating Nonadiabatic Dynamics at Avoided Crossings. *J. Phys. Chem. Lett.*, 7:2050–2054, 2016.

[60] Kochise Bennett, Markus Kowalewski, and S Mukamel. Novel Photochemistry of Molecular Polaritons in Optical Cavities. *Farad. Discuss.*, 194:259–282, 2016.

[61] A. Bohm, A. Mostafadeh, H. Koizumi, Q. Niu, and J. Zwanziger. *The Geometric Phase in Quantum Systems*. Springer, New York, 1 edition, 2003.

[62] Justyna A. Ćwik, Peter Kirton, Simone De Liberato, and Jonathan Keeling. Excitonic spectral features in strongly coupled organic polaritons. *Phys. Rev. A*, 93:033840, March 2016.

[63] Mark Jenkins, Thomas Hümmer, María José Martínez-Pérez, Juanjo García-Ripoll, David Zueco, and Fernando Luis. Coupling single-molecule magnets to quantum circuits. *New J. Phys.*, 15(9):095007, 2013.

[64] Shane R. Yost, Jiye Lee, Mark WB. Wilson, Tony Wu, David P. McMahon, Rebecca R. Parkhurst, Nicholas J. Thompson, Daniel N. Congreve, Akshay Rao, Kerr Johnson, Matthew Y. Sfeir, Moungi G. Bawendi, Timothy M. Swager, Richard H. Friend, Marc A. Baldo, and Troy Van Voorhis. A transferable model for singlet-fission kinetics. *Nat. Chem.*, 6(6):492, 2014.

[65] Abraham Nitzan. *Chemical dynamics in condensed phases: relaxation, transfer and reactions in condensed molecular systems*. Oxford university press, New York, 2006.

[66] J. Frenkel. On the Transformation of light into Heat in Solids. I. *Phys. Rev.*, 37:17–44, January 1931.

[67] Paul E. Teichen and Joel D. Eaves. Collective aspects of singlet fission in molecular crystals. *J. Chem. Phys.*, 143(4):044118, 2015.

[68] Joshua Jortner and Mordechai Bixon. Intramolecular vibrational excitations accompanying solvent–controlled electron transfer reactions. *J. Chem. Phys.*, 88(1):167–170, 1988.

[69] Joshua Jortner. Temperature dependent activation energy for electron transfer between biological molecules. *J. Chem. Phys.*, 64(12):4860–4867, 1976.

[70] Jonathan J. Burdett, Astrid M. Muller, David Gosztola, and Christopher J. Bardeen. Excited state dynamics in solid and monomeric tetracene: The roles of superradiance and exciton fission. *J. Chem. Phys.*, 133(14):144506, 2010.

[71] Tong Zhu, Yan Wan, Zhi Guo, Justin Johnson, and Libai Huang. Two birds with one stone: Tailoring singlet fission for both triplet yield and exciton diffusion length. *Adv. Mater.*, 28(34):7539–7547, 2016.

[72] Wai-Lun Chan, Manuel Ligges, and XY Zhu. The energy barrier in singlet fission can be overcome through coherent coupling and entropic gain. *Nat. Chem.*, 4(10):840–845, 2012.

[73] Javier del Pino, Johannes Feist, and F. J. Garcia-Vidal. Signatures of vibrational strong coupling in raman scattering. *J. Phys. Chem. C*, 119(52):29132–29137, 2015.

[74] Daniele Bajoni, Elizaveta Semenova, Aristide Lemaître, Sophie Bouchoule, Esther Wertz, Pascale Senellart, and Jacqueline Bloch. Polariton light-emitting diode in a gaas-based microcavity. *Phys. Rev. B*, 77:113303, 2008.

[75] Elad Eizner, Julien Brodeur, Fábio Barachati, Aravindan Sridharan, and Stéphane Kéna-Cohen. Organic photodiodes with an extended responsivity using ultrastrong light–matter coupling. *ACS Photonics*, 5(7):2921–2927, 2018.

[76] Biswanath Chakraborty, Jie Gu, Zheng Sun, Mandeep Khatoniar, Rezlind Bushati, Alexandra L. Boehmke, Rian Koots, and Vinod M. Menon. Control of strong light–matter interaction in monolayer ws2 through electric field gating. *Nano Lett.*, 18(10):6455–6460, 2018.

[77] Christopher R Gubbin, Stefan A Maier, and Stéphane Kéna-Cohen. Low-voltage polariton electroluminescence from an ultrastrongly coupled organic light-emitting diode. *Appl. Phys. Lett.*, 104(23):233302, 2014.

[78] M Mazzeo, A Genco, S Gambino, D Ballarini, F Mangione, O Di Stefano, S Patanè, S Savasta, D Sanvitto, and G Gigli. Ultrastrong light-matter coupling in electrically doped microcavity organic light emitting diodes. *Appl. Phys. Lett.*, 104(23):233303, 2014.

[79] Armando Genco, Alessandro Ridolfo, Salvatore Savasta, Salvatore Patané, Giuseppe Gigli, and Marco Mazzeo. Bright polariton coumarin-based oleds operating in the ultrastrong coupling regime. *Adv. Opt. Mat.*, 6(17):1800364, 2018.

[80] Elad Eizner, Luis A Martínez-Martínez, Joel Yuen-Zhou, and Stéphane Kéna-Cohen. Inverting singlet and triplet excited states using strong light-matter coupling. *Sci. Adv.*, 5(12):eaax4482, 2019.

[81] Felipe Herrera and Frank C. Spano. Dark vibronic polaritons and the spectroscopy of organic microcavities. *Phys. Rev. Lett.*, 118:223601, 2017.

[82] R Silbey. Variational calculation of the dynamics of a two level system interacting with a bath. *J. Chem. Phys.*, 80:2615, 1984.

[83] Robert A Harris and Robert Silbey. Variational calculation of the tunneling system interacting with a heat bath. ii. dynamics of an asymmetric tunneling system. *J. Chem. Phys*, 83(3):1069–1074, 1985.

[84] Konstantinos S Daskalakis, Stefan A Maier, and Stéphane Kéna-Cohen. Polariton condensation in organic semiconductors. In *Quantum Plasmonics*, pages 151–163. Springer, 2017.

[85] Chee Kong Lee, Jeremy Moix, and Jianshu Cao. Accuracy of second order perturbation theory in the polaron and variational polaron frames. *J. Chem. Phys*, 136(20):204120, 2012.

[86] Nancy Makri and Dmitrii E Makarov. Tensor propagator for iterative quantum time evolution of reduced density matrices. i. theory. *J. Chem. Phys*, 102(11):4600–4610, 1995.

[87] Nancy Makri and Dmitrii E Makarov. Tensor propagator for iterative quantum time evolution of reduced density matrices. ii. numerical methodology. *J. Chem. Phys*, 102(11):4611–4618, 1995.

[88] H-D Meyer, Uwe Manthe, and Lorenz S Cederbaum. The multi-configurational time-dependent hartree approach. *Chem. Phys. Lett.*, 165(1):73–78, 1990.

[89] Michael H Beck, Andreas Jäckle, GA Worth, and H-D Meyer. The multiconfiguration time-dependent hartree (mctdh) method: a highly efficient algorithm for propagating wavepackets. *Phys. Rep.*, 324(1):1–105, 2000.

[90] Akihito Ishizaki and Graham R Fleming. Unified treatment of quantum coherent and incoherent hopping dynamics in electronic energy transfer: Reduced hierarchy equation approach. *J. Chem. Phys.*, 130(23):234111, 2009.

[91] Pengfei Huo and David F Coker. Communication: Partial linearized density matrix dynamics for dissipative, non-adiabatic quantum evolution. *J. Chem. Phys.*, 135(20):201101, 2011.

[92] John C Tully. Molecular dynamics with electronic transitions. *J. Chem. Phys.*, 93(2):1061, 1990.

[93] Oleg V Prezhdo and Peter J Rossky. Mean-field molecular dynamics with surface hopping. *J. Chem. Phys.*, 107(3):825–834, 1997.

[94] Joseph E. Subotnik, Amber Jain, Brian Landry, Andrew Petit, Wenjun Ouyang, and Nicole Bellonzi. Understanding the surface hopping view of electronic transitions and decoherence. *Annu. Rev. Phys. Chem.*, 67(1):387–417, 2016.

[95] Norah M Hoffmann, Heiko Appel, Angel Rubio, and Neepa T Maitra. Light-matter interactions via the exact factorization approach. *Eur. Phys. J. B*, 91(8):180, 2018.

[96] M. Ahsan Zeb, Peter G. Kirton, and Jonathan Keeling. Exact states and spectra of vibrationally dressed polaritons. *ACS Photonics*, 5(1):249–257, 2018.

[97] Patrick Rebentrost, Masoud Mohseni, and Alán Aspuru-Guzik. Role of quantum coherence and environmental fluctuations in chromophoric energy transport. *J. Phys. Chem. B*, 113(29):9942–9947, 2009.

[98] Xian-Kai Chen, Shou-Feng Zhang, Jian-Xun Fan, and Ai-Min Ren. Nature of highly efficient thermally activated delayed fluorescence in organic light-emitting diode emitters: nonadiabatic effect between excited states. *J. Phys. Chem. C*, 119(18):9728–9733, 2015.

[99] Z. Yang, Z. Mao, Z. Xie, Y. Zhang, S. Liu, J. Zhao, J. Xu, Z. Chi, and M. P. Aldred. Recent advances in organic thermally activated delayed fluorescence materials. *Chem. Soc. Rev.*, 46(3):915–1016, 2017.

[100] Qian Peng, Di Fan, Ruihong Duan, Yuanping Yi, Yingli Niu, Dong Wang, and Zhigang Shuai. Theoretical study of conversion and decay processes of excited triplet and singlet states in a thermally activated delayed fluorescence molecule. *J. Phys. Chem. C*, 121(25):13448–13456, 2017.

[101] Felipe Herrera and Frank C. Spano. Theory of nanoscale organic cavities: The essential role of vibration-photon dressed states. *ACS Photonics*, 5(1):65–79, 2018.

[102] N. T. Fofang, N. K. Grady, Z. Fan, A. O. Govorov, and N. J. Halas. Plexciton dynamics: Exciton-plasmon coupling in a j-aggregate-au nanoshell complex provides a mechanism for nonlinearity. *Nano Lett.*, 11(4):1556–1560, 2011.

[103] Ankit Bisht, Jorge Cuadra, Martin Wersäll, Adriana Canales, Tomasz J Antosiewicz, and Timur Shegai. Collective strong light-matter coupling in hierarchical microcavity–plasmon–exciton systems. *Nano Lett.*, 19(1):189–196, 2018.

[104] Battulga Munkhbat, Martin Wersäll, Denis G Baranov, Tomasz J Antosiewicz, and Timur Shegai. Suppression of photo-oxidation of organic chromophores by strong coupling to plasmonic nanoantennas. *Sci. Adv.*, 4(7):eaas9552, 2018.

[105] Jorge A Campos-Gonzalez-Angulo, Raphael F Ribeiro, and Joel Yuen-Zhou. Resonant catalysis of thermally activated chemical reactions with vibrational polaritons. *Nat. Commun.*, 10(1):1–8, 2019.

[106] Alexander Semenov and Abraham Nitzan. Electron transfer in confined electromagnetic fields. *J. Chem. Phys.*, 150(17):174122, 2019.

[107] Daniel Polak, Rahul Jayaprakash, Thomas P Lyons, Luis Á Martínez-Martínez, Anastasia Leventis, Kealan J Fallon, Harriet Coulthard, David G Bossanyi, Kyriacos Georgiou, Anthony J Petty, H Bronstein, J Yuen-Zhou, A I Tartakovskii, J Clark, and A J Musser. Manipulating molecules with strong coupling: harvesting triplet excitons in organic exciton microcavities. *Chem. Sci.*, 11(2):343–354, 2020.